Max-Planck-Institut
für Meteorologie

MAX-PLANCK-GESELLSCHAFT

International Max Planck Research School
on Earth System Modelling

A two Turbulence Kinetic Energy Model for the Scale Adaptive Treatment of the Planetary Boundary Layer

Ritthik Bhattacharya

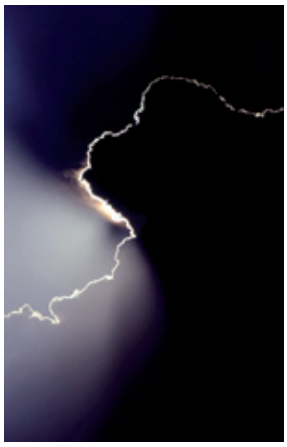

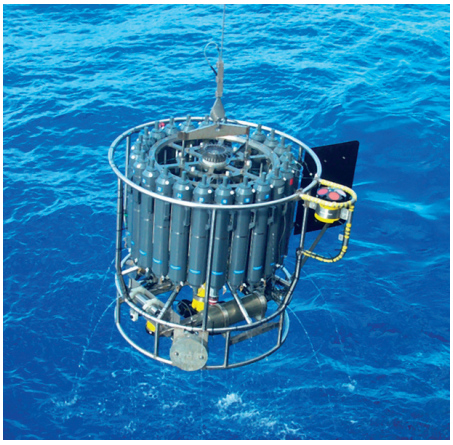

Berichte zur Erdsystemforschung 154
2014

Reports on Earth System Science

Hinweis

Die Berichte zur Erdsystemforschung werden vom Max-Planck-Institut für Meteorologie in Hamburg in unregelmäßiger Abfolge herausgegeben.

Sie enthalten wissenschaftliche und technische Beiträge, inklusive Dissertationen.

Die Beiträge geben nicht notwendigerweise die Auffassung des Instituts wieder.

Die "Berichte zur Erdsystemforschung" führen die vorherigen Reihen "Reports" und "Examensarbeiten" weiter.

Notice

The Reports on Earth System Science are published by the Max Planck Institute for Meteorology in Hamburg. They appear in irregular intervals.

They contain scientific and technical contributions, including Ph. D. theses.

The Reports do not necessarily reflect the opinion of the Institute.

The "Reports on Earth System Science" continue the former "Reports" and "Examensarbeiten" of the Max Planck Institute.

Anschrift / Address

Max-Planck-Institut für Meteorologie
Bundesstrasse 53
20146 Hamburg
Deutschland

Tel.: +49-(0)40-4 11 73-0
Fax: +49-(0)40-4 11 73-298
Web: www.mpimet.mpg.de

Layout:

Bettina Diallo, PR & Grafik

Titelfotos:
vorne:
Christian Klepp - Jochem Marotzke - Christian Klepp
hinten:
Clotilde Dubois - Christian Klepp - Katsumasa Tanaka

Berichte zur Erdsystemforschung 154/2014

A two Turbulence Kinetic Energy Model for the Scale Adaptive Treatment of the Planetary Boundary Layer

Ritthik Bhattacharya

Kolkata, India

Hamburg 2014

Reports on Earth System Science 154/2014

ISSN 1614-1199

Ritthik Bhattacharya
Max-Planck-Institut für Meteorologie
Bundesstrasse 53
20146 Hamburg

Als Dissertation angenommen
vom Fachbereich Geowissenschaften der Universität Hamburg

auf Grund der Gutachten von
Prof. Dr. Bjorn Stevens
und
Dr. Cathy Hohenegger

Hamburg, den 5. Juni 2014
Professor Dr. Christian Betzler
Leiter des Departments Geowissenschaften

ISSN 1614-1199

A two Turbulence Kinetic Energy Model for the Scale Adaptive Treatment of the Planetary Boundary Layer

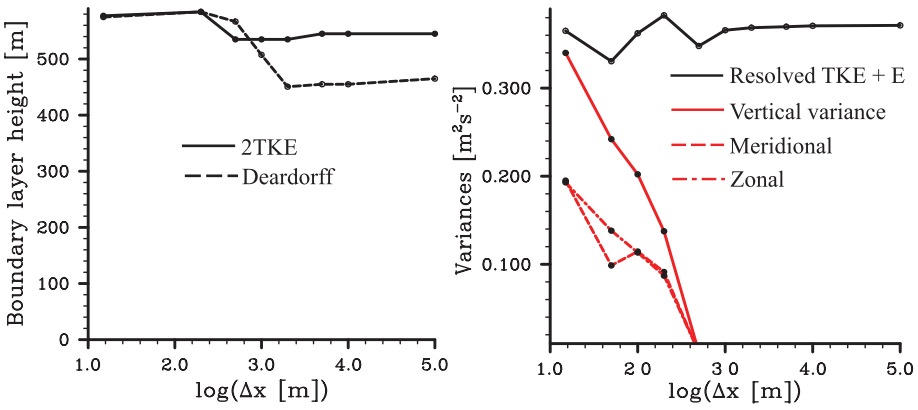

Ritthik Bhattacharya

Hamburg 2014

Abstract

I present a newly-developed two Turbulence Kinetic Energy (2TKE) model, which allows for an improved representation of the dry atmospheric boundary layer for Numerical Weather Prediction and Climate model applications irrespective of the grid of the underlying model (scale adaptive model). The 2TKE model is derived from the Large Eddy Simulation (LES) set of equations for isotropic grid with size of the order of the vertical grid of the large-scale model. The LES equations include evolution equations for the LES-resolved quantities (potential temperature and mean winds) as well as an evolution equation for the LES-unresolved subgrid scale TKE. A Reynolds filter with size of order of the large-scale model horizontal grid size is applied to this set. This leads to governing equations for the large-scale resolved quantities and for two energies: one is a Reynolds average of LES subgrid TKE and the other is the TKE of eddies whose size range from the boundary layer scale to the vertical grid scale. The two energies are used to model the mixing in the boundary layer as two separate processes, both using the eddy diffusivity approximation.

The use of two energies working at different scales allows us, in principle, to work across a range of horizontal resolutions. This means, on one hand, when the entire boundary layer is unresolved (as in current models) the large boundary layer scale eddies (modeled by large TKE) do most of the mixing. On the other hand, with increase in computational power, as the grid size approaches the size of the current LES grids the boundary layer scale eddies are resolved and hence only the smaller isotropic eddies of size of order of the LES grid size that remain subgrid (modeled by the small scale TKE) perform the subgrid mixing. The two TKEs contribute differently to mixing throughout the boundary layer even in the limit of large grid sizes: the large-scale TKE determines the bulk of mixing inside the mixed layer (ML), while the small-scale TKE contributes substantially at the sites of higher gradients (which are the surface layer and the interfacial layer).

I have developed a single column model for testing this new 2TKE model in idealized scenarios. This testing brings out the desirable properties of the 2TKE model in the large-scale limit of horizontal grid sizes, the properties in intermediate and fine horizontal grid sizes being studied next to that (in a three dimensional setup). In the single column, the 2TKE model is seen to make the numerical model solutions fairly independent of the vertical grid size, since the grid dependency (with some numerical corrections) is physically incorporated via mixing by the small scale TKE. This is a very desirable property since excessive vertical grid dependence is a problem with many current models. The physical properties of the boundary layer are well represented:

mean and flux profiles, the growth rate of the boundary layer, as well as fluxes at the surface and the top of the boundary layer. The physical nature of the model implies a smoother transition from convective to stable boundary layer regimes without the need to use different schemes for different stability conditions or use stability functions in the outer layer of the boundary layer as some current models do.

I have then incorporated this 2TKE model in the UCLA-LES model (a three dimensional model), such that the LES behaves reasonably for idealized dry convective boundary layer cases and the behavior of the 2TKE model in intermediate and fine horizontal grid sizes can be studied. In the limit that the horizontal grid size of the model is large compared to the boundary layer height, it has been benchmarked with the 2TKE implementation in a single column model. In the other limit, wherein the grid of the model is nearly isotropic and much smaller compared to the boundary layer height, the 2TKE model has been benchmarked against standard subgrid models that are used at this regime of grid sizes (the Smagorinsky and the Deardorff models). A blending function approach has then been looked into such that the transition between solutions from these two limits can be achieved smoothly in the intermediate range of horizontal grid sizes. This blending function modifies the source terms of the large TKE and the length over which it acts, in this range. It is a continuous and monotonic function of the grid size that assumes a normal (in physical and spectral space) distribution of boundary layer integrated buoyancy and momentum fluxes. The 2TKE model with blending is also designed to take into account the fact that the small TKE should be independent of the horizontal grid spacing and its mixing length should approach the standard Deardorff TKE mixing length in the limit of fine grids.

Simulations with the 2TKE model show a convergent behavior throughout the intermediate range of grid sizes. This is identified by similar boundary layer growth rates as well as similar behavior of the normalized-higher-moments of the resolved scales, irrespective of the grid size. It is seen that the role of the large-scale energy is performed progressively by the resolved scales as the grid gets finer. Thus, in this thesis I develop a boundary layer model that incorporates the idea of two scales operating within the boundary layer and use physical reasoning of the properties of these two scales as well as numerical simulations (in a single column and in a 3-D setup) to make the model solution independent of the numerical grid in which it acts.

Contents

Chapter 1

Introduction

The planetary boundary layer is a thin layer of the atmosphere near the surface of the earth that mediates the influence of the surface on the atmosphere. Thermodynamics and turbulence interact in the stably stratified atmosphere to create this layer that interacts with the rest of the troposphere through an inversion at its top. The planetary boundary layer has different structures during the day and night. During daytime, when large buoyant plumes rise from the surface (the boundary layer in this regime is called the convective boundary layer, e.g. Deardorff (1979)), the boundary layer exhibits a three layer structure. This consists of an unstable layer of approximately 15% of the boundary layer height where the turbulent plumes are generated (the surface layer), a mixed layer on top of the surface layer of approximately 60% of the height where the plumes mix all the atmospheric variables into a well-mixed profile, and an entrainment zone atop the mixed layer that is approximately 25% of the height. In this zone the convective plumes from the surface and the local turbulence entrain the warm quiescent free tropospheric air into the boundary layer. The height of the boundary layer is approximately of the order of a kilometer at its peak value around noon. At night the boundary layer (called the stable boundary layer, see for example Wyngaard (1985)) is much shallower (of the order of a couple of hundred meters) and exhibits a different structure: an inversion near the surface and the presence of nocturnal jets. A boundary layer model (or parameterization) is used in the weather prediction/ climate models to represent the bulk properties of the boundary layer which influence the large scale dynamics of the atmospheric flows. Modeling of the boundary layer involves solving for the mean thermodynamic and momentum profiles, their fluxes and the depth of the boundary layer.

For large scale models, the boundary layer parameterizations have historically been designed in such a way that the entirety of boundary-layer processes are subgrid (al-

though the vertical structure of the boundary-layer mean profiles might be resolved, at least away from the entrainment and surface layers). Large-eddy simulations (LES), on the other hand, resolve much of the energy-containing boundary-layer-scale eddies and model the locally-homogeneous isotropic-turbulence that remains unresolved, via the LES subgrid schemes. With increasing computational power, the grid size of operational large scale models are becoming smaller. This means that the operational models are beginning to resolve some of the boundary-layer-scale processes but yet not to the degree of LES models. Wyngaard (2004) referred to this intermediate scale, wherein boundary-layer-turbulence is not well resolved, but nor is that grid scale so large that it allows one to use Reynolds-averaged approximations, as "Terra incognita". Others refer to this as the "grey-zone" and this is the nomenclature that will be used throughout the thesis. Modeling of partially resolved boundary layer features requires parameterizations that are aware of the size of the scales they resolve, as well as the depth of the boundary layer (or free-turbulent layer) as a whole. This allows the parameterization to "know" which part of the processes are resolved and which part is still sub grid for a given grid size. In this thesis, I present the derivation and implementation of a model which is aware of two scales within the boundary layer: the boundary layer depth and the vertical grid size. I design this model to work in two limits: large-scale limit of contemporary global models, which resolves only eddies that are much larger than the boundary layer height, as well as the LES-limit of grid sizes, which at least for convective cases, resolve eddies on scales much smaller than the boundary layer height and of the order of the vertical grid size (for isotropic grids). I then implement this model in an LES model to approach the "grey-zone" in such a way that eddies with sizes of the scale of the boundary layer depth have a progressively lesser contribution to mixing as the horizontal grid gets finer, while the eddies of the scale of the vertical grid size have similar contribution to the mixing irrespective of the horizontal grid size.

Traditionally, models of the planetary boundary layer adopt a single (or master) length scale which is assumed to play the dominant role inside the boundary layer. For example, many current PBL models represent the vertical fluxes inside the boundary layer as:

$$\overline{\Theta' w'} = -K_h \left(\frac{\partial \overline{\Theta}}{\partial z} - \gamma \right), \tag{1.1}$$

Θ and w are the potential temperature and the vertical wind velocity respectively ($\overline{\Theta}$ and Θ' are the Reynolds mean and fluctuations thereof of the potential temperature field, as described in details in Section 2.1). K_h, on the rhs, represents the eddy

diffusivity and γ offers the possibility of modeling fluxes not proportional to the local gradient, e.g. Troen and Mahrt (1986). The eddy diffusivity is generally computed as a product of a single velocity scale and a single length scale, both of which are chosen to be representative of the dominant scale performing the mixing. This approach makes use of the assumption that the entirety of the boundary layer processes are subgrid.

Two approaches for selecting the constituent elements of K_h can be identified. A *local* approach e.g Bretherton and Park (2009) or Brinkop and Roeckner (1995) uses a velocity scale that is proportional to the square root of the turbulence kinetic energy (TKE) at any given height. This approach uses a length scale which grows linearly (Blackadar (1962)) or super-linearly (Grenier and Bretherton (2001)) near the surface to asymptotically reach a prescribed value above a certain height from the surface (sometimes the length scale formulation may include modifications to account for changes in the local stability). The *non-local* description of the eddy diffusivity (viscosity) specifies a predetermined shape for the profile of K based on the height above the surface (Troen and Mahrt (1986), see also Large et al. (1994)) non-dimensionalized by the boundary-layer height (henceforth called the K-profile parameterization, KPP). Hence the major properties of the K_h profile are governed by the global properties of the boundary layer, such as the convective velocity and the boundary layer height. In general, the *local* description works well for stable to near-neutral boundary layers which have smaller turbulent-structures that are more influenced by local stability, whereas the *non-local* models often perform better in convective conditions with larger boundary-layer-scale turbulent structures (Lock et al. (2000)). The parameter γ allows the model to take into account the strength of thermals from the surface penetrating the stable region near and at the boundary layer top and also works on the scale of the boundary layer height. This term has the effect of ventilating the surface layer and thus indirectly affecting the diagnosis of the boundary layer depth in many models (Stevens (2000)). Regardless of the details, within the mixed layer (ML) and the entrainment zone (EZ), most boundary layer models use a single length scale that is larger than the vertical grid size (even when the energy/velocity scale being used is local), and thus assume that the entire spectrum of boundary-layer-scale-eddies active in the mixing are subgrid.

At the surface, a separate length scale is often implicit in the treatment of the surface boundary condition. These boundary conditions relate surface fluxes to mean gradients inside the surface layer, usually using some variation of the Monin-Obukhov theory (Louis (1979), Dyer (1974) and Högström (1988)). This improves the representation of the surface layer but is not free of issues. In particular Zhang and Zheng (2004) show that the use of similar coupling (including length scales) of momentum and heat

inside the surface layer can misrepresent the mixing of momentum as compared to heat, and this is another motivation for a more comprehensive treatment of scales inside the boundary layer.

Recently, Siebesma et al. (2007) introduced a model that, at least in principle, recognizes two different scales. Their approach was a hybrid one, which combined aspects of the eddy-diffusivity approach used to model turbulent-boundary layers, and the mass flux approach used to model large convective plumes, of the type clouds are often associated with. They called their model the Eddy-Diffusivity-Mass-Flux (EDMF) model. The mass-flux part of the model, which assumes that the area-fraction occupied by the updraft is small compared to the grid size of the large-scale model, models the fluxes as a product of a convective velocity scale and the area-fraction. The small scale turbulent part of the fluxes, on the other hand, are sometimes modeled by a local-stability based diffusion term and sometimes by a K-profile like scheme. However EDMF schemes by themselves are not scale adaptive: since in intermediate grid sizes, the assumption of small area-fraction of strong updrafts does not hold (Honnert et al. (2011)) and neither is the sample size of updrafts inside the grid box enough to draw conclusions about its distribution. Nonetheless, the present approach is motivated by the ideas in the EDMF approach, wherein the boundary layer processes are represented by eddies of two range of scales whose respective weights are used to address the "grey-zone"

In this backdrop, I develop my two Turbulence Kinetic Energy (2TKE) model which formalizes the idea of two scales of eddies acting inside the boundary layer. The first, which are eddies representing the large-boundary-layer-scale plumes (in a convective boundary layer) perform most of the mixing in the normal range of horizontal grid size of weather-prediction/climate models. The second scale of eddies that scale with the vertical grid size of these models predominantly perform mixing only at the interfaces for these horizontal grid sizes. However in the "grey-zone" the first scale of eddies contribute progressively lesser to the subgrid mixing (since they are resolved by the numerical grid) while the second scale of eddies continue to act similarly irrespective of the horizontal grid size. Finally, since the theory of turbulence suggests that the larger eddies create local instabilities that causes them to break up into smaller eddies, these two scales of eddies are energetically linked.

I construct this model to reproduce LES results in the limit of LES grid sizes while, at the same time, represent the boundary layer with physical accuracy in large scale model applications. Hence, I adopt the approach to start from the LES equations and apply boundary layer simplifications used in current large scale models to this

equation set. The idea is that such a model working in these two limits can be tuned with physical motivations to work in the range of grid sizes in between. The approach that is adopted is to derive two energies: one representing the energy of all eddies from the boundary layer scale to the LES grid scale, and the other representing the large scale average of the LES subgrid energy. The first, or larger-scale TKE, reduces as the large-scale model grid is refined and ultimately vanishes if the grid sizes allow for a resolved representation of PBL eddies, as in the original LES equations. The small scale TKE is nearly invariant of the grid size and converges to LES subgrid TKE in the limit of fine LES grids. In the large-scale limit, mixing throughout the ML is predominantly represented in terms of the large scale energy with the exception of the interfacial layers at the top and bottom of the turbulent layer, where the small scale energy contributes substantially. The large energy for very-large-horizontal grid sizes works on a length scale proportional to the boundary layer height and hence is responsible for the mean structure and fluxes inside the boundary layer. This changes as the horizontal grid size is reduced and thus the length scale of mixing by the large scale TKE is designed to be proportional to the amount of large energy at any given grid size. The small TKE works on a scale proportional to the depth of the interfacial layer and the vertical grid size irrespective of the horizontal grid size and hence models fluxes within the EZ and near the surface. The resultant equations, when reverted back to the LES limit result in the original LES equation set with one formal difference: in the present derivation I don't allow for horizontal exchanges, which should emerge as the grid-scale is refined. These horizontal terms, in the full LES equation set, act as fluxes for the potential temperature and the momentum and as fluxes and production terms for the LES subgrid TKE.

To develop this 2TKE model I went through six steps (shown schematically in Fig. 1.1), which are listed as follows:

1. Developing a single column setup as a framework to model the turbulent boundary layer and to test the different tubulence models (existing ones as well as the new 2TKE model).

2. Implementing the *local* TKE (ECHAM) boundary layer model (Brinkop and Roeckner (1995)) in the single column setup and exploring its physical and numerical properties as well as comparing it with the *non-local* K profile parameterization (Troen and Mahrt (1986)).

3. Deriving the 2TKE model: which is a set of PBL equations starting with the LES set of equations, applying the Reynolds averaging on it and then modeling the subgrid fluxes.

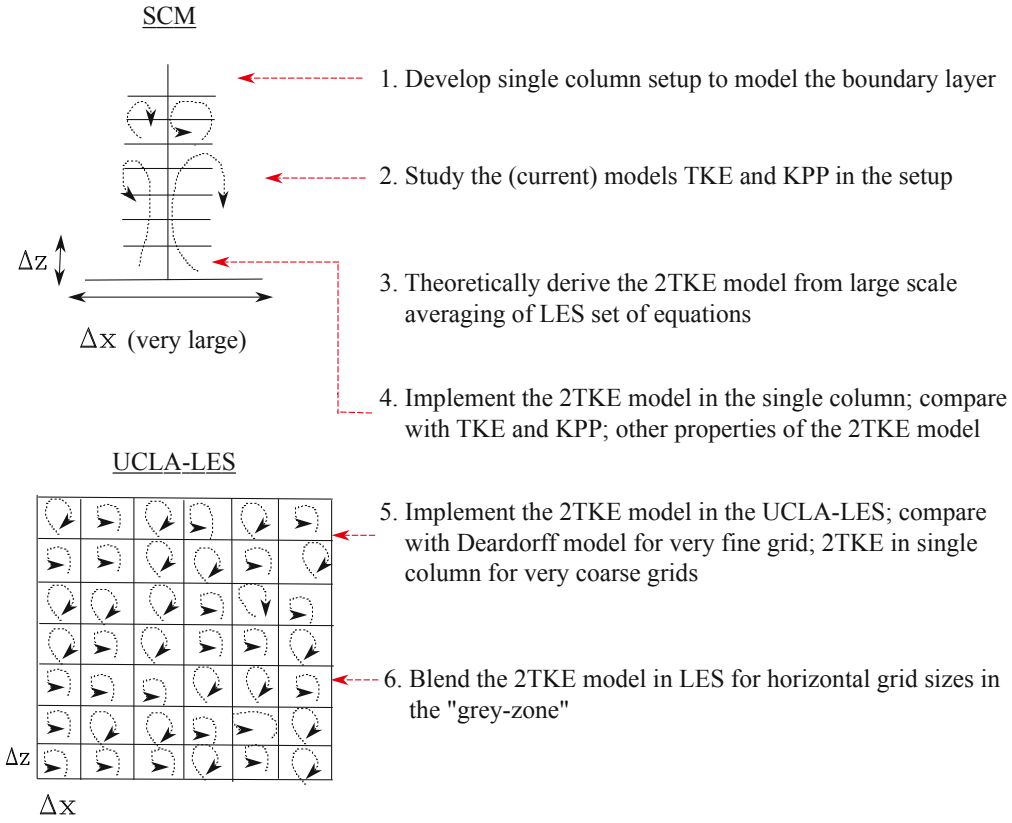

Figure 1.1: Illustration of steps to develop the 2TKE model. The solid lines represent the model grids, the dotted lines with arrows for the subgrid eddies that are modeled. SCM is the single column model and the UCLA-LES is the LES model where we implement the 2TKE model in Chapter 4. Note the UCLA-LES is a 3-dimensional model of which just the x-z plane is shown for clarity.

4. Implementing the 2TKE model in the single column setup, comparing it with the TKE (ECHAM) model and the KPP and exploring its unique properties.

5. Implementing the 2TKE model in the UCLA-LES (an LES model), and benchmarking the implementation by studying its properties in two limits: very large and very small horizontal grid sizes.

6. Exploring the "grey-zone" with the 2TKE model by making physically motivated assumptions about the large and the small energies in the "grey-zone" thus getting a model that provides convergent results irrespective of the grid size.

The chapters, thus, are ordered as follows: Chapter 2, which covers Steps 1 and 2, explains the development of the single column model: the grid, the boundary conditions,

as well as specific test cases I study. I then explain and implement the TKE (ECHAM) model in the single column and study its representation of the dry convective boundary layer, its numerical properties, and how it compares to the KPP. Finally I explore the stable boundary layer with the TKE model.

Steps 3 and 4 are taken up in Chapter 3. Here I explain the derivation of the 2TKE model from the set of LES equations. This includes the idea of two turbulence kinetic energies acting in two different ranges of scales and how the corresponding contribution to the subgrid fluxes are modeled. In this chapter, I also compare the 2TKE model with the TKE and the KPP in the single column setup and bring out its desirable properties: its remarkable independence from the vertical grid of the single column (as compared to the KPP for example) and its applicability in both convective and stable regimes.

Finally, Chapter 4 elaborates on the implementation of the 2TKE model in the UCLA-LES and how the model is used to explore the "grey-zone": the last two steps. This required implementing the Deardorff subgrid model in the UCLA-LES and then implementing the 2TKE model using that backdrop. The 2TKE model is then benchmarked in two limits of horizontal grid sizes: in the very large grid size limit, to the 2TKE model implementation in the single column and in the very small grid size limit, to the Deardorff model. Upon benchmarking, the 2TKE model is applied in the "grey-zone" where physically motivated assumptions on the large and the small TKE, their sources and their mixing length scale are used to make the model applicable in the "grey-zone" in a manner that no current model is applicable there.

Chapter 5 concludes the thesis and here I revisit the six steps mentioned above. What I learn in each step and how that helped in approaching the next step is succinctly presented. I also briefly re-examine the properties of the full 2TKE model and talk about the scope for the further development of the model and the issues involved in its implementation in weather-prediction/climate models.

Chapter 2

Modeling Turbulent Boundary Layers in A Single Column

2.1 Introduction

This chapter describes the single column model (SCM) we have developed for studying the presently-used boundary layer models as well as the 2TKE model (the 2TKE model is covered in the next chapter). This aids us in understanding the general delicacies involved in modeling of the turbulent atmospheric boundary layer with the currently-used boundary-layer models in a single column. Properties of idealized boundary layers, such as the convective and the stable boundary layer with constant surface fluxes, are well documented in numerous books in the field of boundary-layer meteorology, for example Stull (1988) and Garratt (1992). This allows us to use these idealized cases to focus on the study as well as development of the boundary layer models themselves in detail.

The single column model is described first (Section. 2.2). This begins with the description of the grid and of the numerical discretization techniques used to solve for the boundary layer equations. We then describe the types of boundary conditions which can be implemented in the model. The various types of boundary -layer-depth-diagnosis schemes which have been tested is then focused on. A brief description of what established theory says about simple boundary layers with standard boundary conditions follows next. Finally, the section ends with a description of the cases we look into throughout the thesis.

Implementation of the *local* TKE model, as used in ECHAM (Brinkop and Roeckner (1995)), is then described (Section. 2.3). This brings out the properties of the

SCM as well as that of the TKE-model itself in some details, including the numerical properties of the model solutions. The ECHAM TKE model is then compared with a *non-local* model called the KPP (Troen and Mahrt (1986)) to compare the main issues of modeling the boundary layer *locally* vs. those when it is modeled *non-locally* (the qualitative features of *local* and *non-local* models have been discussed in Chapter 1). All the discussion above has been done for different cases of the convective boundary layer (CBL), so a stable boundary layer (SBL) case has been looked into in the end and it can be noted that the ECHAM TKE model, being a *local* model, fares reasonably well in SBL cases, as opposed to the CBL case. At the end of the chapter, we have a numerical setup which we understand fairly well as well as an understanding of the current boundary layer models. This guides us in the derivation and the implementation of our 2TKE model, which we do in the next chapter.

2.2 The Single Column Model

2.2.1 Grid

The single column model has a one-dimensional vertical grid which discretizes the vertical height coordinate, z (Fig. 2.1). M is the number of model levels in which, within the first level (that is always assumed to lie within the surface layer), the model variables are assumed to have a logarithmic distribution with height. Above the first level, a linear profile is assumed. The solid horizontal lines are the model levels, where the model variable values, $\overline{U}, \overline{V}, \overline{\Theta}$, are specified, while the dashed horizontal lines represent the half levels, where the fluxes and the diffusivities (K_h) are defined. Specifying the variables in this manner simplifies the spatial discretization as described next.

The nonlinear diffusion equation, describing the evolution of the potential temperature, can be written as (neglecting the counter-gradient term in Eq. 1.1 in Chapter 1 for now. We come back to this issue later):

$$\frac{\partial \overline{\Theta}}{\partial t} = -\frac{\partial \overline{\Theta' w'}}{\partial z} = \frac{\partial}{\partial z}\left(K_h \frac{\partial \overline{\Theta}}{\partial z}\right) \ . \tag{2.1}$$

This is solved using second order central differencing (CD-2) in space and semi implicit time differencing.

$$\frac{\Theta_i^{n+1} - \Theta_i^n}{\Delta t} = \frac{K_{i+1/2}^n \left(\frac{\Theta_{i+1}^{n+1} - \Theta_i^{n+1}}{\Delta z_{i+1}}\right) - K_{i-1/2}^n \left(\frac{\Theta_i^{n+1} - \Theta_{i-1}^{n+1}}{\Delta z_i}\right)}{\frac{1}{2}(\Delta z_{i+1} + \Delta z_i)} \ , \tag{2.2}$$

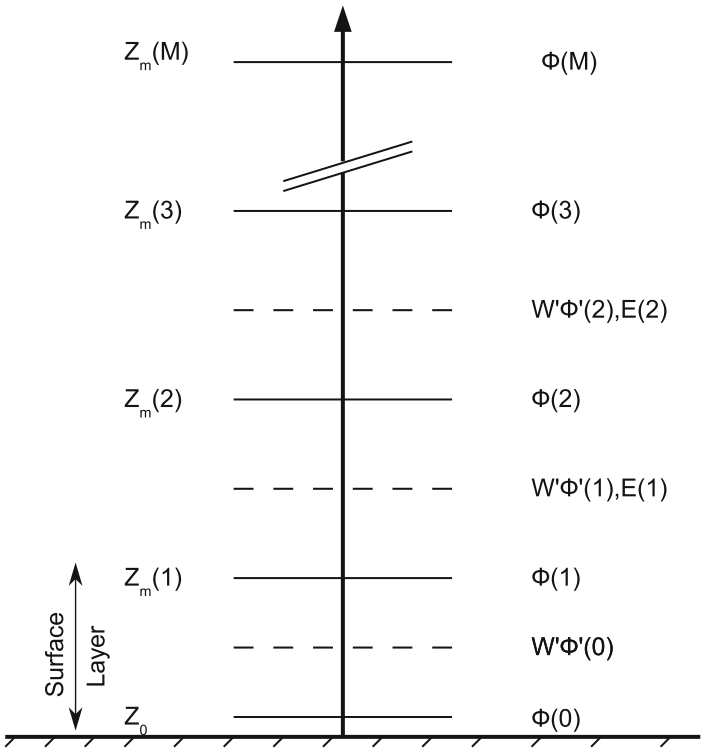

Figure 2.1: Grid used in the single column model

where the superscript denotes the time level and the subscript denotes the height level (K is used instead of K_h for notational simplicity, in this one instance). In addition we explore the impact of an alternative temporal discretization introduced by Troen and Mahrt (1986). This discretization, known as the Chapeau function approach, is based on ideas taken from finite element methods. Using this approach the numerator in the lhs of Eq. 2.2 is replaced by the following expression while the rhs remains unchanged,

$$\frac{{\Theta_{i+1}}^{n+1} + 4{\Theta_i}^{n+1} + {\Theta_{i-1}}^{n+1}}{6} - \frac{{\Theta_{i+1}}^{n} + 4{\Theta_i}^{n} + {\Theta_{i-1}}^{n}}{6} \; . \tag{2.3}$$

The different temporal discretization techniques (Eq. 2.2 and Eq. 2.3) are found to not

yield any substantial difference in the model solutions, at least in the range of temporal and spatial resolutions that have been explored.

The evolution equation for zonal wind that is solved is:

$$\frac{\partial \overline{U}}{\partial t} = \frac{\partial}{\partial z}\left(K_m \frac{\partial \overline{U}}{\partial z}\right) + f(V - V_g) \ , \tag{2.4}$$

which means that the vertical flux of the wind is treated similar to the vertical flux of the potential temperature with K_m being the eddy viscosity. The second term in the rhs is the Coriolis contribution to mean zonal acceleration with f being the Coriolis parameter and V_g being the geostrophic wind in the meridional direction. The equation is solved similar to that of the potential temperature (lhs = the first term in the rhs) and the Coriolis contribution is added explicitly in time to the tendency obtained from the first balance. The evolution equation for the meridional wind component has a similar form and is solved similar to the evolution equation of the zonal wind velocity.

2.2.2 Boundary Conditions

The surface fluxes of buoyancy and momentum are the boundary conditions to the model (the fluxes at the top of the domain are assumed to be zero). Two types of surface flux formulations have been looked into. In the first case, a constant surface flux is specified. This helps in comparing the model solutions to the theoretical solutions as well as in tuning model parameters. The other is the specification of constant surface temperature at the roughness length (velocity being zero at roughness length) and calculating the fluxes from the difference between values at the surface and values at the first model level. This is a more realistic boundary condition since it limits the heat uptake by the boundary layer and helps in quantifying the interaction between the surface model and the boundary layer model. The fluxes are calculated (Φ being a generic variable) following a bulk approach, such that:

$$\overline{w'\Phi'}(0) = -C_\Phi |V(1)|(\overline{\Phi}(1) - \overline{\Phi}(0)). \tag{2.5}$$

Here $V(1)$ is the wind speed at the first model level and C_ϕ is the surface transfer coefficient for the variable Φ.

The transfer coefficient (C_ϕ) in the surface layer is obtained from the Monin-Obukhov similarity theory by integrating the flux profile over the lowest model level, following the analytical expressions derived by Louis (1979) for momentum,(m)and heat and other scalars (h). The major details of the implementation of the surface

scheme (further details in Roeckner (2003)) is presented next. Thus:

$$C_{m,h} = C_N f_{m,h}(Ri_B, z_0, z_L) \ , \tag{2.6}$$

where,

$$C_N = \frac{\kappa^2}{(ln\frac{z_m(1)}{z_0})^2} \tag{2.7}$$

is the neutral transfer coefficient, κ is the Von Kármán constant (taken to be .41), $z_m(1)$ is the height of the lowest model level and z_0 is the surface roughness length that is taken constant and set to the same value for both heat and momentum. Ri_B is the bulk Richardson number of the surface layer. The functions that describe the stability corrections to the neutral transfer coefficient are given by :

$$f_{m,h} = 1 - \frac{bRi_B}{1 + c|Ri_B|^{1/2}} \ , \tag{2.8}$$

in the unstable surface layer and

$$f_{m,h} = \frac{1}{(1 + b'Ri_B)^2} \ , \tag{2.9}$$

in the stable surface layer. The constants b and b' are taken to be 9.4 and 4.7 respectively which satisfies a continuity relation of the derivative of f (the function, not the Coriolis constant) between the stable and unstable cases and c is obtained as :

$$c = C_* {C_N}^2 b \left(\frac{z_L}{z_0}\right)^{1/2} , \tag{2.10}$$

with $C_* = 7.4$. A positive surface heat (potential temperature) flux implies heating from the surface and leads to the growth of the convective boundary layer (situation during daytime), whereas negative surface heat flux implies surface cooling, so that the shear production of turbulence is required to maintain a turbulent boundary layer (night time scenario).

2.2.3 Boundary layer height diagnosis schemes

How the boundary layer height is diagnosed is important for the boundary layer models. This is because it is within this height that the boundary layer models contribute to mixing (though *local* models, with much smaller diffusivities, are used above the

boundary layer too in most weather prediction/climate models). This depth diagnosis is also, implicitly (in *local* models) and explicitly (in *non-local* models, tied to the value of eddy diffusivity (viscosity) used in mixing.

Two boundary layer depth diagnosis procedures have been used. The first one, called the gradient method, is used when a purely convective boundary layer without shear has been studied. This method calculates the depth of the boundary layer as the height where the slope of the potential temperature profile is maximum. This means:

$$h = z, \text{ where } \frac{\partial \overline{\Theta}(z)}{\partial z} \text{ is maximum.} \tag{2.11}$$

The gradient method is often used in large eddy simulations of atmospheric flows (see for instance Sullivan et al. (1998)).

In the presence of shear, another method, called the parcel method, has been used (following Troen and Mahrt (1986)) and has been found to give better height diagnosis over longer simulation times (it can also be argued that this method is more inclusive of the entirety of the phenomenon inside the boundary layer to calculate the depth than just the local temperature gradient at each height level). The method starts by calculating an initial estimate of the boundary layer height, such that a parcel of air having the same properties as the surface exceeds a certain critical bulk Richardson number (Ri_{cr}) at that height. This initial estimate allows the calculation of a convective velocity scale, which along with the surface friction velocity gives an estimate of the velocity scale for the plumes at the surface, w_s. This velocity scale allows the introduction of the temperature excess ($\Delta\Theta$), such that:

$$\Delta\Theta = \frac{D\overline{w'\Theta'}(0)}{w_s} \ . \tag{2.12}$$

The (new) boundary layer height is then calculated as the height where a parcel with temperature of the first model level (that is, $\Theta(1)$) plus $\Delta\Theta$ exceeds Ri_{cr}.

2.2.4 Theoretical growth of the boundary layer

The background stratification of potential temperature over which the boundary layer grows is specified as an initial condition for the model. A constant lapse rate is assumed for simplicity. A larger lapse rate implies a larger jump of potential temperature at the top of the boundary layer and hence a slower growth rate of the boundary layer(see Deardorff (1974) for example). For a convective boundary layer (assuming the flux at

the top is a constant fraction of the surface flux):

$$h^2(t_1) \;\propto\; 2\frac{\int_0^{t_1}\overline{w'\Theta'}_0 dt}{\gamma} \;. \tag{2.13}$$

For a stable boundary layer, a steady state height is reached that is governed by the shear generated growth of the turbulent structures, so that :

$$h_e = \gamma_c\sqrt{u_\tau L_{MO}/|f|} \tag{2.14}$$

γ_c is a constant which is obtained from the balance of shear production of turbulence and the buoyant destruction of turbulence in steady state. For horizontal terrain, γ_c is taken to be 0.4 (Garratt (1992)). u_τ is the surface friction velocity, L_{MO} is the Monin-Obukhov length,

$$L_{MO} = -\frac{{u_\tau}^3\Theta(0)}{g\kappa\overline{w'\Theta'}(0)} \;, \tag{2.15}$$

and f is the Coriolis frequency. Since the surface friction velocity and hence the Monin-Obukhov length scale varies (for generalized stable boundary layers) as the profile changes in time, an average value is taken to provide a rough estimate of h_e

$$\frac{\partial h}{\partial t} = \frac{(h_e - h)}{T_{\text{relax}}}, \tag{2.16}$$

with h being the instantaneous boundary layer height and T_{relax} is the relaxation time which is given by the difference between the potential temperature of the surface and the top of the stable layer divided by the surface cooling rate. The solution to the relaxation equation is a logarithmic growth of h with time, eventually reaching h_e on the timescale of T_{relax}.

2.2.5 Case Description

This section presents the cases we consider throughout the thesis to bring out the properties of the TKE, the KPP and the 2TKE models. The initial temperature profile consists of a stably stratified column from surface to 3 km height. The potential temperature near the surface is set at 299 K and the initial lapse rate at 6 K km^{-1}, unless otherwise specified. For the purpose of this discussion, we use results from our model for four different boundary conditions, although two further boundary conditions, that simulate the diurnal variability of surface fluxes, have also been used to more fully explore the model's properties. The first (Case: CBL1) is a constant-surface-heat-flux boundary condition in which a constant flux of .05 K m s^{-1} is applied at the surface.

The initial wind profile is set at a constant value of 10 m s^{-1} over the entire domain and assumed to be the same in magnitude and direction as the geostrophic wind. A no-slip condition is applied at the surface and the parcel method is used to diagnose the boundary layer height. Next, to bring out the properties of the two energies in a pure CBL case for our 2TKE model (in Chapter 3), a case similar to CBL1, but without any wind profile, is used, where the boundary layer height is calculated using the gradient method (case: CBL2). Another CBL case (case: CBL3) has been considered in this chapter in which the boundary layer is heated up from the surface with a prescribed surface temperature of 305 K (the same wind profile as CBL1 is taken) to consider the impact of surface models (Section.2.2.2) and limited heat uptake in our single column model.

Two stable boundary layer (SBL) scenarios have been considered. In this chapter, an SBL (case: SBL1) scenario similar to the GABLS stable boundary layer case 1 (Cuxart et al. (2005)), has been used with the initial profile starting from 265.753 K at the first model level (at height 10 m) and having a lapse rate of 7.83 K Km^{-1} to study the behavior of the TKE model for realistic SBL scenarios. The profile is cooled from the surface, the temperature of which is set at 265 K. The initial zonal wind is set to be constant with height at 10 m s^{-1} and the meridional wind is set to zero (same as the geostrophic wind velocity). In the other SBL scenario (case:SBL2) used in Chapter 3, the surface shear (same wind profile as CBL1) drives the turbulence while the surface temperature is set at 293 K which cools and puts a cap on the boundary layer growth. This scenario is used to compare the role of buoyancy and shear in the flux profiles and the respective contribution to the two TKEs by these two mechanisms. In both SBL scenarios, the parcel method is used to determine the boundary layer height. The five cases have been summarized in Table. 2.1.

The simulations are run with a Coriolis parameter of $3.4643.10^{-5}$ s^{-1}, which is consistent with the Coriolis parameter at 14° north. The surface roughness length for momentum and for heat are taken to be the same at 5.10^{-4} m. It is noted that the solutions approach a self-similar state within a large eddy turnover time (of the order of 10 mins). The vertical grid size is varied in the range of fine (uniform) grid of size 3 m to coarse grids of size 100 m so as to study the behavior of the solutions as well as the different parameters of the model over a range of grid sizes.

Table 2.1: Case Description (SHF: Surface heat flux, ST:Surface Temperature, LR:Lapse Rate, WS:Wind speed)

Case	Boundary Condition	Initial condition	Boundary layer height diagnosis
CBL1	1. SHF =.05 K.m s^{-1} $\approx$ 60 W m^{-2} 2. Full slip condition	1. LR = 6 K Km $^{-1}$ starting at 299 K near surface 2.WS = 10 m s^{-1}= Geostrophoic wind	Parcel method
CBL2	SHF = .05 K m s^{-1}	1. LR = 6 K km^{-1} starting at 299 K near surface 2. No wind	Gradient method
CBL3	1. ST = 305 K 2. No slip condition 3.Fluxes computed	1. LR = 6 K km^{-1} starting at 299 K near surface 2.WS = 10 m s^{-1}= Geostrophoic wind	Parcel method
SBL1	1. ST = 265 K 2. No slip condition 3.Fluxes computed	1. LR = 7.83 K Km^{-1} starting at 265.753 K near surface 2. WS = 10 ms^{-1} = Geostrophic wind	Parcel method
SBL2	1. ST = 293 K 2. No slip condition 3.Fluxes computed	1. LR = 6 K Km^{-1} starting at 299 K near surface 2. WS = 10 m s^{-1} = Geostrophic wind	Parcel method

2.3 Properties of currently used models

2.3.1 The TKE (ECHAM) model

Inside the boundary layer, that is above the surface layer, Eq. 2.1 is used to calculate for the fluxes (and hence the tendencies). This requires the evaluation of eddy diffusivity/viscosity at the half levels (Fig. 2.1). The eddy diffusivity/viscosity are calculated as a product of a length scale and a velocity scale. In the TKE model used in ECHAM (Brinkop and Roeckner (1995)), this velocity scale is taken to be the square root of the total Turbulence Kinetic Energy (TKE):

$$K_{m,h} = \Lambda_{m,h}\sqrt{E}. \tag{2.17}$$

The subscript m refers to the momentum and h, in this context, to potential temperature and other scalars (if applicable). $\Lambda_{m,h}$ is the length scale of mixing. This is

calculated as the product of a neutral length scale (that is the mixing length wherever inside the boundary layer the stability is neutral, for example in the mixed layer) and stability function that takes into account the profile stability at a given height. The neutral length scale follows the log law of wall near the surface and asymptotically reaches a constant value with height (Blackadar (1962)). The stability function (Mellor and Yamada (1982)) accounts for the fact that in grid points with unstable profiles (that is, roughly speaking, more energetic air below less energetic air) there is more mixing than in neutral profiles and in stable profiles there is lesser mixing. E, in this chapter, is the TKE defined at each half level. The TKE has the evolution equation,

$$\frac{\partial E}{\partial t} = -\overline{w'u'}\frac{\partial u}{\partial z} - \overline{w'v'}\frac{\partial v}{\partial z} + \frac{g}{\theta_v}\overline{w'\theta'_v} - (S_{Nm}^{-3}l)^{-1}E^{3/2} - \frac{\partial \overline{w'E}}{\partial z} \ . \tag{2.18}$$

The first and second terms in the rhs represents the production of TKE by wind-shear in zonal and meridional directions respectively. The third term is the effect of buoyancy production/suppression on the TKE. The fourth term in the rhs represents the cascade of TKE to smaller scales i.e to viscous dissipation. The final term in the rhs is the vertical transport of TKE which is treated diffusively with the same eddy viscosity (that is, K_m) as diffusion of momentum.

The boundary values required for this initial boundary value problem have been taken from ECHAM documentation (Roeckner (2003)). Since the model variables are at the model levels and the TKE needs to be calculated at the half levels, the derivatives in the first three terms of the rhs can be effectively calculated numerically. Eq. 2.18 is solved in two steps. The first step involves solving for the partial tendency of the TKE using the balance between the lhs and just the first four terms of the rhs. This allows us to compute a tentative TKE for the next time step by adding this tendency to the TKE for the present time step. A diffusion equation for this tentative TKE is then solved semi-implicitly (like that for the potential temperature) such that the actual TKE for the next time step can be obtained. Having solved for the TKE at each half level, the values of the eddy diffusivity/viscocity can be calculated there using Eq. 2.17 which is used to compute the fluxes using Eq. 2.1.

2.3.2 CBL: Temperature and shear profiles

Upon implementation of the TKE model in the single column, we simulate the case CBL1 using the setup. Idealized convective boundary layers with constant surface flux have been studies extensively (Stull (1988), Garratt (1992), and Deardorff (1974) for

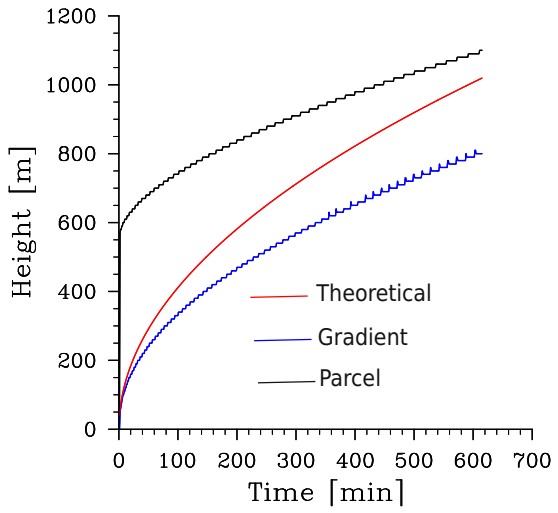

Figure 2.2: Boundary Layer growth from different formulations compared to the theoretical value

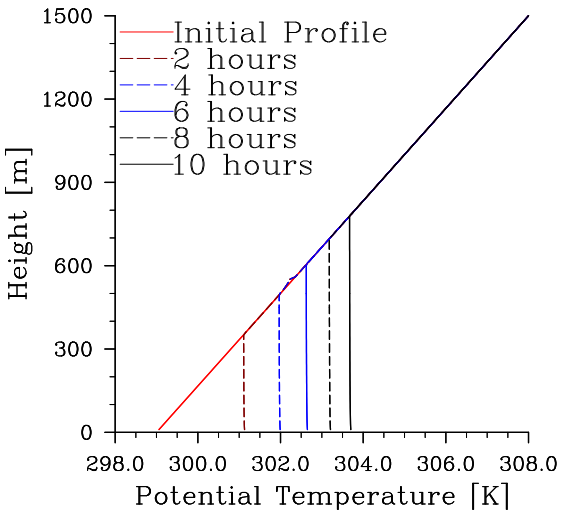

Figure 2.3: Growth of the convective boundary layer with time

example). This means we know the generic properties of the temperature, flux and velocity fields which allows us to analyze the TKE model in its ability to reproduce those features. This brings out the successes and shortcomings of the model as well as allows us to compare it with the KPP.

Influence of the boundary layer height diagnosis schemes

The boundary layer evolution for the two different height specification model have been compared with an estimate of the theoretical value of the boundary layer height (Eq. 2.13), the formulation for which has been explained in, for example Stull (1988). Fig. 2.2 shows that both the models show a boundary layer growth rate slightly less than the theoretical growth rate which is proportional to the square root of time of simulation. It can be noted that the parcel method gives a more accurate representation of the boundary layer growth for larger simulation times. The gradient method is accurate enough for calculating the encroachment depth, but fails to take the entrainment zone, that is atop the encroachment layer, into account. This is an expected result since the parcel method takes into account both the surface flux as well as the boundary layer properties (both temperature and wind), while the gradient method

takes into account just the boundary layer structure of potential temperature. Since the parcel method shows a better behavior, it is being used here on for the depth diagnosis unless for case CBL2 (used in later chapters) where there is no wind shear (rendering the parcel method invalid) and hence the gradient method is used.

Temperature and Shear profiles

The growth of profiles of potential temperature and the wind velocity is studied next. Fig. 2.3 shows that the TKE model creates a boundary layer that is well mixed throughout (since the model is down gradient the profile is slightly unstable as this is required to maintain the down gradient flux). Thus there is no entrainment zone at the upper quarter of the boundary layer.

The reasons for such a behavior are two fold. Firstly this is due to the fact that since the surface-flux is prescribed to be a constant, the temperature-excess ($\Delta\Theta$ in Eq. 2.12) at the first model level decreases with time (this is different for other surface-boundary conditions, as described in Section. 2.3.4). The second reason for this behavior can be noted in the profiles of eddy diffusivity (viscosity) the TKE model generates (Fig. 2.5). The figure shows that on the one hand values of both the diffusivity and the viscosity are large in general in the mixed layer (of the order of 1000 m^2s^{-1}). The values near the surface are smaller than in the mixed layer but still substantial. On the other hand, towards the upper one third of the boundary layer (of height 1100 m), the values reduce to close to zero (suppression of mixing by stability function). This explains the well-mixed nature of the variables (very slightly unstable) even near the surface and almost no mixing or entrainment zone near the top of the boundary layer. This is unphysical and even upon the removal of stability functions, it is found that the entrainment is not correctly predicted and neither are the surface layer properties. The growth of the shear layer can be seen in Fig. 2.4. Here too the suppression of mixing at the boundary layer top can be evidenced from the absence of wind turning, which is a feature of shear layers (see, for example, Deardorff (1974)).

2.3.3 Numerical Analysis of the TKE model in the model

The numerical analysis of the TKE model in the single column elucidates on the correct implementation of the model as well as on the numerical properties of the single column itself. It involves the following steps:

1. Checking for conservation property of the implementation.

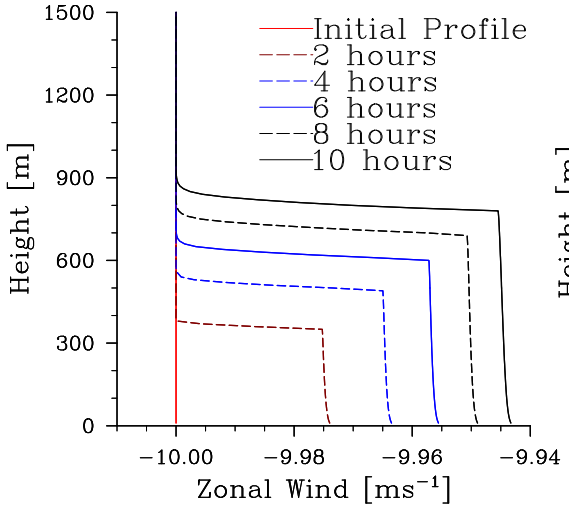

Figure 2.4: Growth of the convective boundary layer zonal wind profile with time

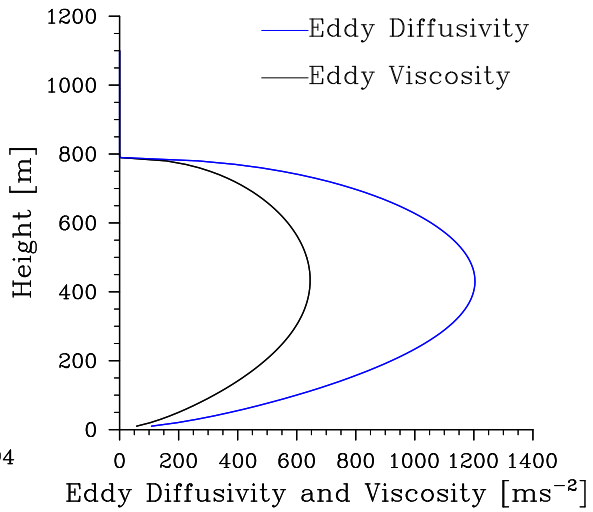

Figure 2.5: Profiles of eddy diffusivity and viscosity

2. Exploring the consistency and convergence of the numerical solution and determining if the code solves the equations with the same accuracy as the numerical model it is supposed to represent.

3. Determining the error bound of the numerical solution. and approaching a higher-order more accurate solution from lower-order accurate solutions on multiple grids.

4. Studying model behavior for stretched grids.

The equations used in the analysis presented in this section are explained in greater details in any advanced book on computational methods in fluid dynamics, such as Ferziger and Peric (1996).

Conservation

The equations being solved are conservative, which means that in the absence of sources and sinks the weighted integral of the variables like potential temperature (weighted by the difference between half levels they represent) within the domain should remain constant with time. If there are sources or sinks or boundary fluxes, then the weighted

integral should change exactly by the integral of the fluxes over time. This can be easily checked for case CBL1 (prescribed surface flux) and the variables are found out to be conservative within the machine accuracy.

Consistency and Convergence

This section talks about how we test that in the limit that the grid of the numerical setup is fine enough, the solution to the discretized set of equation, we solve, not only reaches a limit (consistency) but does so to the solution of the actual differential equation, the discretized set represents (convergence).

Since the discretized equations (represented as L_h for a grid spacing of h) represents approximations to the differential equations (Λ), the exact solution to the latter (Φ) does not satisfy the difference equations. This imbalance, which is due to the truncation of the Taylor series, is called the truncation error. For a grid spacing of h, the truncation error, τ_h, is thus defined as:

$$\tau_h = \Lambda(\Phi) - L_h(\Phi) \ . \tag{2.19}$$

Now since the solution to the difference equation, denoted by ϕ_h satisfies:

$$L_h(\phi_h) = 0 \ , \tag{2.20}$$

there is a difference between Φ and ϕ_h, which is called the discretization error.

$$\Phi = \phi_h + {\epsilon_h}^d \tag{2.21}$$

Consistency implies that the truncation error (τ_h) should tend to zero as the spatial and temporal grid size tend to zero.

But consistency alone does not imply that the numerical solution will converge to the "correct" solution in the limit of small grid size (convergence), which is what we want to achieve (that is ${\epsilon_h}^d$ to tend to zero for as the resolution increases). That requires the additional consideration of stability, which means that the numerical solution should remain bounded. Stability is very hard to verify for nonlinear problems with boundary conditions. So it is analyzed for a corresponding linear problem without boundary conditions by freezing the coefficient to a constant value. An analysis of stability for linearized diffusion problem yields the answer that upon the usage of implicit time stepping and central differencing in space, the numerical model is unconditionally stable (see for example Ferziger and Peric (1996)). This result is assumed to be reasonable for the boundary layer equations (which are nonlinear diffusion equations, Eq. 2.1

for example) too, within a range of time and space grid sizes (the range comes into play primarily because of the presence of boundary condition, as well as non linearity due to the dependence of the diffusivity itself on the grid size and height above surface).

The model has been tested for consistency by calculating the L_2-error of the variables like potential temperature, after the run time of 10 hours for different uniform grid spacings close to the finest possible uniform grid. This verifies the choice of the finest possible grid used, as optimum to gain convergence (if the errors from a particular grid is monotonically decreasing with "closeness" to the grid and the magnitude of this error is small compared to the value, the grid is taken to be optimal). The L_2-error for a variable ϕ is defined as:

$$\sqrt{\frac{\sum_{j/i=1}^{M/i} (\phi_{j/i,ih} - \phi_{j,h})^2}{(M/i)}}, \tag{2.22}$$

the summation is performed over all of the variable values for the coarsest grid whose number is given by M/i. h, in this context, is the finest grid spacing used and i is the multiplicative factor for the coarser grid. The first term in the subscript of ϕ i.e j (for fine grid) or j/i (for coarse grid) is the grid point (height level) the value at which is being used for the calculation. The finest grid used in this presentation is of uniform 10 m size, the coarser grids are of uniform sizes 20 m and 40 m respectively. This error as a function of time step is shown in Fig. 2.6. From the figure it can be inferred that the error growth with time for any grid size is small within a range of small temporal spacings (See also Fig. 2.7). It is also observed from the figure that the growth of error with different spatial grid spacings is of the same order as of the differences in grid spacing themselves. Considering that this is a global error (i.e integrated over the grid), and that global error is one order of magnitude lower than the local error (the local error is the error in estimation at coarser grids with respect to the fine grid at each grid point), the conclusion can be reached that the local error is second order in space. This property has been used to verify that the code is indeed a faithful representation of a central-difference (of order 2) in space (rhs in Eq. 2.2) system. Finally, the magnitude of the error, for any grid size, is found to be of the order of .01 K which is much lesser than the mean value of the variable (which is of the order of 300 K). This allows us to conclude that the numerical model is sufficiently convergent for a grid size of 10 m.

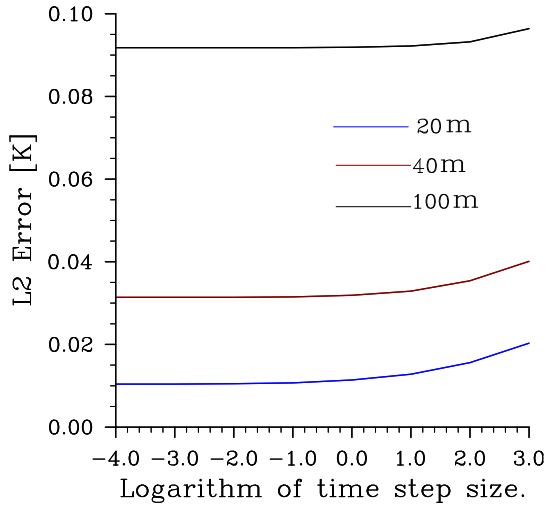

Figure 2.6: L2 error with respect to the finest grid resolution of 10 m

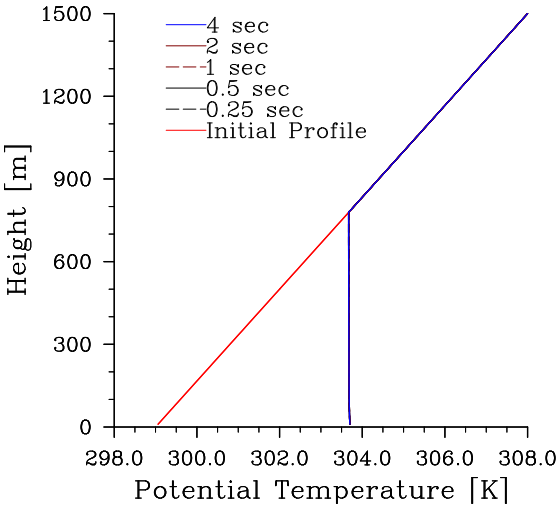

Figure 2.7: Effect of decreasing temporal resolution

Error analysis

In this section we focus our attention on the solution of the discretized set of equation for a given grid size (which is not fine enough) and on methods to estimate its deviation from the "actual" solution of the differential equation. The idea we employ is to use the error information to approach a more accurate solution for a given grid size.

For linear set of equation (Λ and its discretized version L_h), Eq. 2.19 and Eq. 2.21 imply:

$$L_h({\epsilon_h}^d) = -\tau_h \ , \tag{2.23}$$

which means that the truncation error is the source of the discretization error which is diffused and convected by the linear operator L_h. Even for non-linear problems, like the boundary layer equations, this property is assumed if the error is small enough (which is the case for these simulations, as shown in the last section). Now since the exact solution (Φ) is not known for the problem, the truncation error cannot be known precisely. Hence an estimation of the truncation error is done by using the solutions (and hence the discretization error) from different grid sizes. The assumption is that for sufficiently fine grids, both the truncation error and the discretization error are

proportional to the leading term in the Taylor series. Therefore:

$$\epsilon_h{}^d = \alpha h^p + H \ , \tag{2.24}$$

where α is a constant and H consists of the higher order terms. Thus:

$$\Phi = \phi_h + \alpha h^p + H = \phi_{2h} + \alpha(2h)^p + H = \phi_{4h} + \alpha(4h)^p + H \ , \tag{2.25}$$

where p is the order of the model which may be used for code checking (that the code being used is indeed of the same order as the numerical discretization it is supposed to represent, a fact we have established differently in the last section). We have used the L_2 -error as described above, as a surrogate for the difference of the values obtained using different grids. For example for a specified flux as the boundary condition, the single column model has an order of 1.94 for both the Chapeau function method and the standard numerics which are numbers close to 2. This is used to check that the SCM solves the equation with approximately the same order as the CD-2 model in space, which it represents. On the other hand, in case CBL3 which we explore in more details in Section. 2.3.4, where the surface model variable is specified at the roughness length and the fluxes are calculated and then applied as boundary condition to the first model level, the order of the model reduces to approximately 1.3 which should be traced back to the inaccuracy originating from the surface flux formulation.

Once the order of the model has been established, the error may be estimated as:

$$\epsilon_h{}^d = \frac{\phi_h - \phi_{2h}}{2^p - 1} \ . \tag{2.26}$$

An accurate estimation of the true solution can be made by adding this error to the solution from the finest grid possible, if the convergence is found to be monotonic. Again for the test case with constant specified flux (CBL1), this has been checked to give a very accurate solution. This process, which is called Richardson extrapolation, can be summarized as follows (for solutions from two grid sizes): let ϕ_{h1} be the solution for grid size $h1$ and ϕ_{h2} be the solution for grid size $h2$. Then:

$$\phi_{h1} = \Phi + \alpha(h1)^2 + H \ , \tag{2.27}$$

and

$$\phi_{h2} = \Phi + \alpha(h2)^2 + H \ . \tag{2.28}$$

Multiplying Eq. 2.27 by $(h_2)^2$ and Eq. 2.28 by $(h_1)^2$, subtracting the resulting equations

from each other, and solving for Φ we arrive at:

$$\Phi = \frac{(h2)^2\phi_{h1} - (h1)^2\phi_{h2}}{(h2)^2 - (h1)^2} + H \ . \tag{2.29}$$

In this equation, Hrepresents higher order terms, which for CD-2 in space should be of at least the fourth order (Ferziger and Peric (1996). The value of the potential temperature at a grid point (at height 600 m for case CBL1) using this corrected value (that uses the original grid value and value at another grid double the size of the former grid) and the original value obtained from the code is shown in Fig. 2.8. The figure shows how upon using this extrapolation, solutions much closer to the fine grid solution can be achieved even upon the usage of coarser grids (provided we also have the solution from another grid double (or some other integral times) the size the coarser grid).

The benefit of the method is if the process can be applied, it is usually computationally cheaper than either solving the same numerical model for a finer grid or solving a higher order (fourth order central difference, for example) on the same grid. Hence it can be applied with sufficient confidence in the Dirichlet boundary condition (surface temperature specified) case too, provided the grid sizes concerned are sufficiently fine and the solutions are found to be converging monotonically with finer grid spacing. However the solutions from this method does not retain conservativeness, which limits its usability. What this means is that the method is better used to estimate the error in the solution for a given grid than to approach the "correct" solution using that information.

Effects of grid stretching

The behavior of solutions to the discretized equations in grids with nonuniform grid spacings (like those in operational models) can be very different from that of the solution in uniform fine or coarse meshes which we explored till now. To fully understand the numerical properties of the TKE (ECHAM) model in a single column that mimics operational models, that is the issue we explore next.

Height levels within the first three kilometers of height from the one of the operational versions of ECHAM, ECMWF and the COSMO models are implemented in our single column model. They have 10, 21 and 18 levels within the first three kilometers respectively (Table.2.2), each starting from fine grid spacing near the surface (since the surface exhibits finer structures and steeper gradients which need to be vertically resolved) to increasingly coarser spacing with height. An issue with using stretched

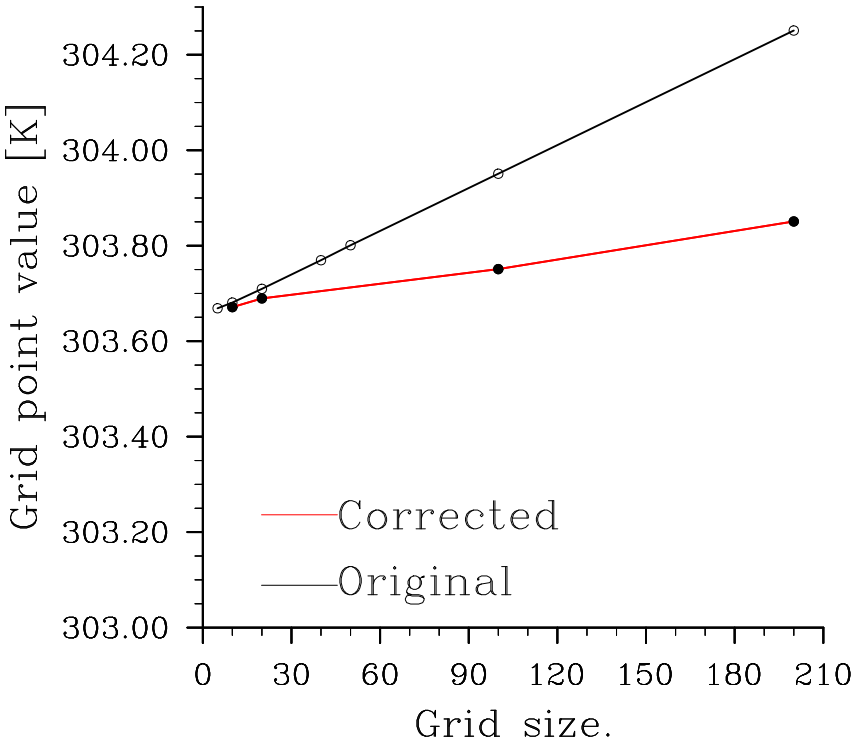

Figure 2.8: Reduced grid dependence upon Richardson extrapolation

grids is that it inadvertently leads to a misrepresentation of the boundary-layer depth and entrainment-zone processes owing to poor resolution of the boundary-layer top profiles. This is one of the issues we address with the development of the 2TKE model, in the next chapter.

In this section we discuss the different types of grid stretching used operationally (using the three grids mentioned above) and their corresponding impacts on the solution to the boundary layer equations (that uses the TKE (ECHAM) model). Rigorously it can be shown that with stretched grids,the truncation error has a leading term which

Table 2.2: Height levels (approximately within the first three kilometers of height), where the mean potential temperature and wind velocity are specified, for the ECHAM, the ECMWF and the COSMO grids. The fluxes and the diffusivities are specified at the center of these levels and the difference between any two height levels gives the corresponding grid spacing.

ECHAM	ECMWF	COSMO
33.34	10.23	20
150.85	35.03	49
359.59	69.47	89
642.10	114.88	143
987.41	171.27	214
1387.64	237.83	303
1834.36	316.04	412
2320.14	408.43	542
2838.73	515.60	695
3388.17	637.49	870
− − −	776.22	1070
− − −	930.93	1295
− − −	1103	1545
− − −	1294.79	1820
− − −	1506.79	2125
− − −	1737.67	2455
− − −	1987.29	2815
− − −	2255.31	3200
− − −	2541.456	− − −
− − −	2845.72	− − −
− − −	3168.05	− − −

is an order less than that for uniform grids for the same CD-2 discretization. For stretched grid, the truncation error is:

$$\epsilon = -\frac{(\Delta z_{i+1})^2 - (\Delta z_i)^2}{2(\Delta z_{i+1} + \Delta z_i)}(\frac{\partial^2 \phi}{\partial z^2})_i - \frac{(\Delta z_{i+1})^3 + (\Delta z_i)^3}{6(\Delta z_{i+1} + \Delta z_i)}(\frac{\partial^3 \phi}{\partial z^3})_i \ , \tag{2.30}$$

where $\Delta z_i = z_i - z_{i-1}$. Two different kinds of grid stretching (ECHAM vs. the ECMWF/COSMO) lead to two different kinds of behavior of this truncation error, as presented next.

It can be noted from the analysis of the ECHAM grid that the stretched grid has an expansion ratio($r_e = \frac{\Delta(z_{i+1})}{\Delta(z_i)}$) of approximately 1.2 within the usual boundary layer height (of 1 km). Thus the leading truncation error term can be written as:

$$\frac{(1 - r_e)\Delta z_i}{2}(\frac{\partial^2 \phi}{\partial z^2})_i \ , \tag{2.31}$$

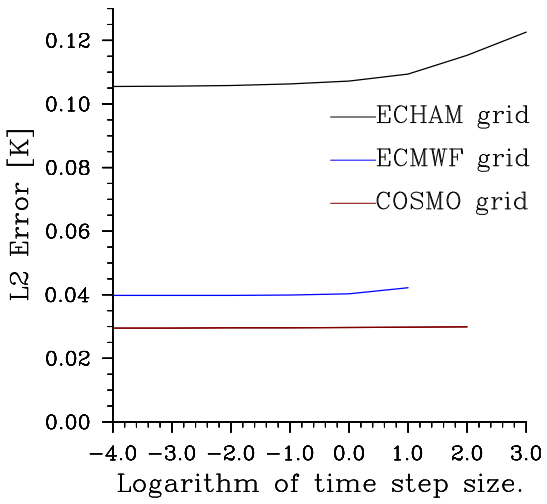

Figure 2.9: L2 error for stretched grids with respect to finest resolution

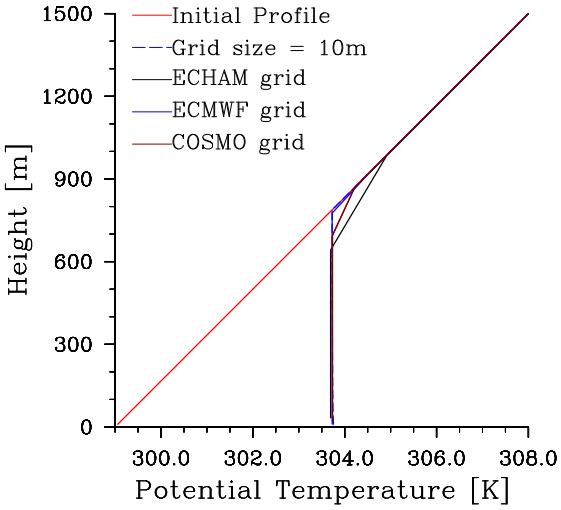

Figure 2.10: Potential temperature profile after 10 hours for different grids

which is linear in the grid spacing.

On the other hand, for the ECMWF and the COSMO grids, the differences in the grid spacings $(\Delta(z_{i+1}) - \Delta(z_i))$ is nearly a constant within the boundary layer. So, upon defining d as $\Delta z_{i+1} = \Delta z_i + d$, the coefficient of the second derivative in Eq.(2.30) becomes:

$$\frac{d^2 + 2(\Delta z_i)d}{4\Delta z_i + 2d}. \tag{2.32}$$

Now since $\Delta z_i \geq d$ for these grids, the coefficient becomes approximately equal to $d/2$ which is independent of the first order of Δz_i. This means that the leading truncation error remains almost quadratic in the grid spacing, like for the uniform grid spacings. Hence with the ECMWF/COSMO grids, i.e grids having a constant increase in grid stretching with height, the simulations show a very similar behavior to those when the grid spacing itself is very fine and uniform. The results can be seen in the Fig. 2.9. The L_2-error is seen to be of the same order as that when the uniform grid is expanded (Fig. 2.6) and hence much smaller than the modeled variable (potential temperature in this case). Fig. 2.9 shows that the error is much less when the grid spacings are in nearly an arithmetic progression with the differences being much less than the grid spacing themselves, than when the grid with an almost constant grid expansion factor is used. On the other side, larger grid spacing of ECHAM implies

stability of the model even upon the usage of larger temporal grid spacings. The profiles of potential temperature after a simulation time of 10 hours for the different grids are shown in Figure 2.10. It shows that even for stretched grid, the convergence is monotonic. The coarsest grid (ECHAM grid) has the farthest deviation from the fine grid solution, both due to its coarseness as well as due to its almost constant grid expansion factor, as explained above. However monotonicity implies that using solutions of two coarse grids (for example ECHAM and COSMO grid), the fine grid solution can be approached. This involves a slight delicacy since the grid sizes are not in any particular ratio. However, the inverse of the ratio of the number of grid points within the given height for the two grids can be taken as an approximation for the ratio of the grid sizes. This is found out to be a reasonable approximation and is used to approach the fine grid solution. As an example, for the constant temperature boundary condition (surface temperature kept constant at 305 K, case CBL3, in Section. 2.3.4), whose results shows considerable variability with grid spacing (Fig. 2.13), the value obtained from the ECHAM and the COSMO grids for a particular grid point (at height of 600 m) were 303.52 K and 303.65 K respectively. Using Eq. 2.29 and replacing $h1$ and $h2$ by the average grid spacing of both grids, we arrive at a solution value of 303.71 K for that grid point which is much closer to the fine grid solution (uniform grid of size 10 m) of 303.74 K.

2.3.4 The role of Boundary Conditions in the model

After testing with the flux boundary condition (case CBL1) the model is tested using the Dirichlet boundary condition (case CBL3) to understand the role of different boundary conditions upon the model solutions. A different behavior of the boundary layer growth, the development of the potential temperature and that of the shear profiles is seen. Fig. 2.11 shows the growth of the boundary layer with time. It can be observed that in contrast to Fig. 2.2, the gradient and the parcel formulations of the boundary layer height give closer values after long enough simulation times. This is due to the fact that the heat uptake by the boundary layer is limited by the prescribed surface temperature. Thus, beyond a time of rapid growth of the boundary layer, the major constraining factor for the parcel model is the surface layer temperature (specifically temperature at the first model grid point) which is a boundary layer property just like the gradient of the potential temperature that is used in the gradient method. This is especially true for the TKE (ECHAM) model which promotes very strong mixing inside the boundary layer and thus has similar properties of the surface layer and the mixed layer, as discussed in section. 2.3.2.

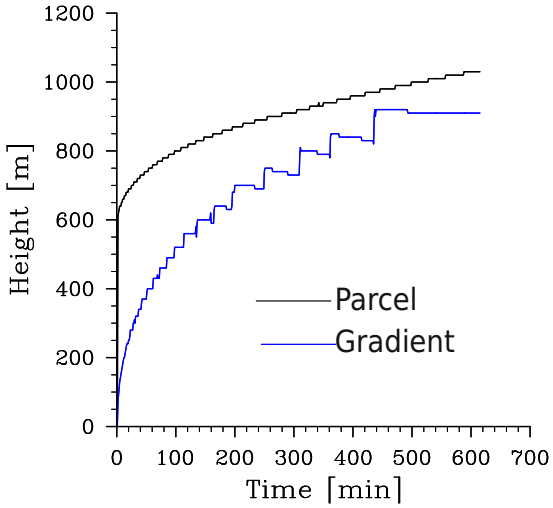

Figure 2.11: Boundary layer height growth with time

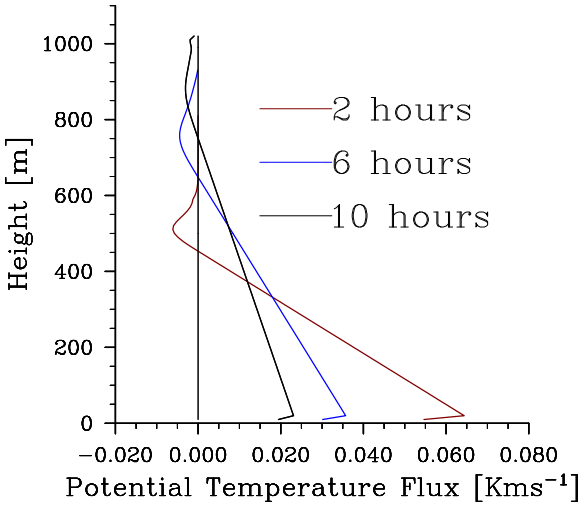

Figure 2.12: Flux profile

The thermodynamic and dynamic properties of the boundary layer behave more reasonably than for the case CBL1. This means that the profiles for potential temperature shows a slightly unstable layer near the surface, a well mixed layer and an entrainment zone at the top of the boundary layer. The entrainment zone is where warm air from the free troposphere is incorporated into the boundary layer. Its extent grows along with the growth of the boundary layer. The potential temperature flux has a linear profile inside the mixed layer and a negative flux near the top of the boundary layer (Fig.2.12). The magnitude of the flux at the top of the boundary layer is approximately one fifth of the magnitude of flux at the surface. As was discussed in Section. 2.3.3, the implementation of the Dirichlet boundary condition reduces the order of the model, i.e the error from the converged solution is more strongly dependent on the grid size. Hence the dependence of the solution on the grid size or on whether the grid is stretched or uniform is increased when compared to the case with flux boundary condition (Fig. 2.13). The convergence to the fine grid solution also becomes non-monotonic, hence approaching the exact solution is not possible using results (by Richardson extrapolation) from the coarser grids (except in the mixed layer and the surface layer where the behavior remains monotonic). Similar non-monotonicity can be noted for the shear layer (Fig. 2.14)

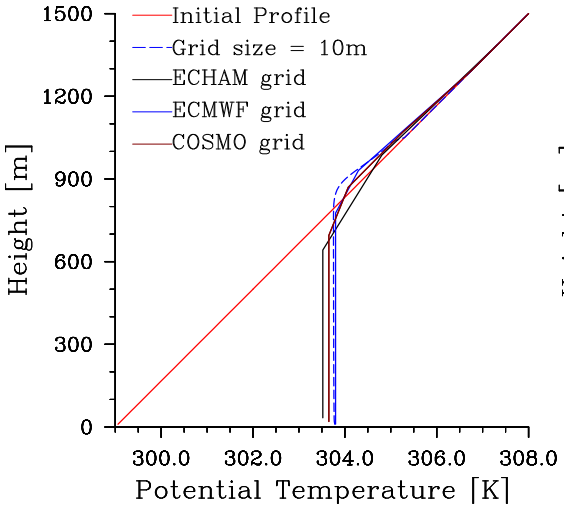

Figure 2.13: Dependence of the profile on the grids

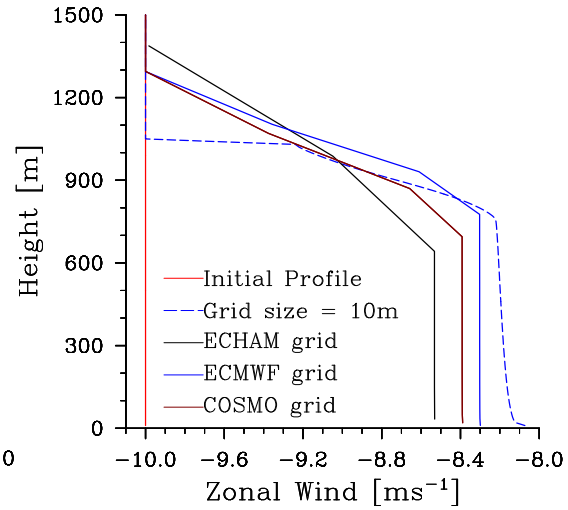

Figure 2.14: Dependence of the shear profile on the grids

2.3.5 Comparison between TKE (ECHAM) model and KPP

The K profile parameterization (KPP) model as developed by Troen and Mahrt (1986) has also been implemented in the single column alongside the TKE model to bring out the properties of a *non-local* model vis a vis a *local* model and help guiding us towards the development of the 2TKE model (which is done in the next Chapter). The KPP model is briefly described first and a comparison of the two models (KPP and TKE) is done next.

The boundary layer equation as solved in the KPP is given by Eq. 1.1 in Chapter 1. As done in the originial formulation, a profile for K (the eddy diffusivity/viscosity) is fitted according to LES data from Wyngaard (1984). The profile is a cubic function of a dimensionless number that represents the ratio of height above the surface to the boundary layer height, multiplied by a constant which is the product of a surface velocity scale and the boundary layer depth. Thus:

$$K_m = w_s h k \frac{z}{h}\left(1 - \frac{z}{h}\right)^2 \quad , \tag{2.33}$$

where k is the Von Kármán constant equal to 0.41. The value of K_h is K_m multiplied by the eddy Prandtl number, which for simplicity is set at a constant value of 2.5 throughout the boundary layer (Troen and Mahrt (1986)). Upon the calculation of eddy

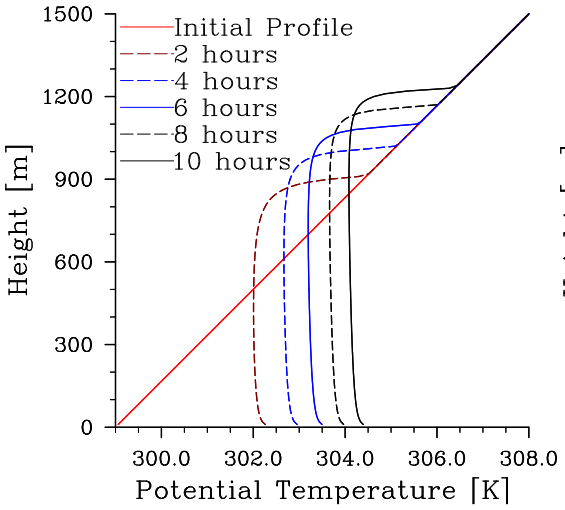

Figure 2.15: Growth of boundary layer for KPP

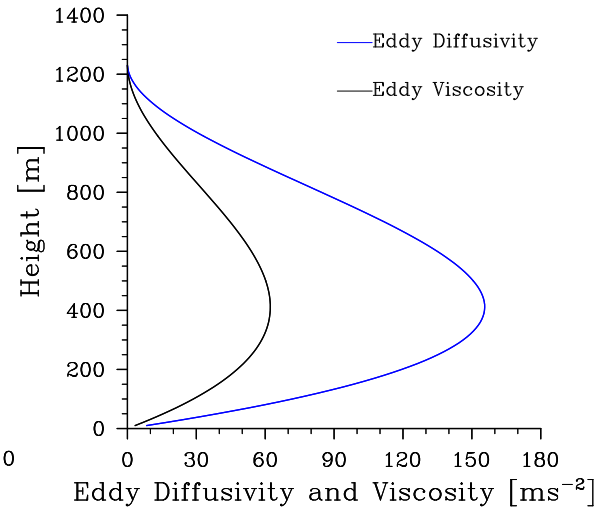

Figure 2.16: Profiles of eddy diffusivity and eddy viscosity for the KPP model

diffusivity/viscosity at each model level, the diffusion equation without the counter gradient term is solved. The counter-gradient term is neglected in the comparison between KPP and TKE models for two reasons. Firstly the value of the counter gradient term is widespread in literature (the scaling coefficient being 6.5 in Troen and Mahrt (1986), 8.5 in Holtslag and Bolville (1993), and 2 in Beljaars and P.Viterbo (1999)) and secondly without the counter-gradient term the comparison between the two models is conceptually simpler (that is, between two down gradient models, one *local* and the other *non-local*).

With this formulation we explore case CBL1 (constant surface flux) with the KPP and it shows a markedly different profile of the potential temperature in the boundary layer than with the TKE (ECHAM) model (Fig. 2.15). The KPP model simulations creates a clearly defined super-adiabatic (i.e unstable) layer near the surface, a well mixed layer and a very stable entrainment zone, which seems to be a representation of the convective boundary layer structure that is more in sync with observations and fine scale modeling data (see Stull (1988), for example).

The differences between the two models can be explained if we consider the profiles of the eddy diffusivity and viscosity for the two models, as shown in Fig. 2.5 and Fig. 2.16 (for the same initial and boundary conditions, that is for CBL1). Three

major differences can be identified. First is the difference of the values of diffusivity at the top of the boundary layer. This value, which is calculated at a half level below the calculated boundary layer height, is much higher for the KPP than the TKE (ECHAM) model (where the diffusivity is suppressed by the use of stability function). This means more entrainment of quiescent free tropospheric air into the boundary layer for the KPP. The dependence of this diffusivity value upon the vertical grid size leads to consequences that are discussed later. The second difference is the strong negative gradient of diffusivity in the entrainment zone for the KPP model which leads to the creation of a stable zone atop the boundary layer. This can be understood if the nonlinear diffusion equation (Eq. 2.1) is expanded as:

$$\frac{\partial\overline{\Theta}}{\partial t} = K\frac{\partial^2\overline{\Theta}}{\partial z^2} + \frac{\partial\overline{\Theta}}{\partial z}\frac{\partial K}{\partial z} \ . \tag{2.34}$$

The first part of the rhs is responsible for mixing while the second part of the rhs can be identified to make the profile more stable if the mixing is less while the gradient K_h is negative, which is the case for the KPP model in the entrainment zone. The third major difference is the structure of diffusivity near the surface which not only influences the surface thermodynamics but also that at the boundary layer top. Near the surface, the value of K_h for KPP is much smaller than that in the TKE model. Hence for the KPP model, the profile retains a super adiabatic zone (not well mixed) near the surface which means that air parcels heated from the surface will rise above the well mixed layer before merging with the sounding (free tropospheric profile that is above the boundary layer), hence creating the entrainment zone. The ratio between the encroachment height (height where the well mixed part of the profile is intersecting the sounding) and the height of the boundary layer is found out to be approximately $1 + 2\beta$, β being the ratio of the flux at the top and the bottom of the boundary layer (the ratio is found to be approximately -0.2 which is also in accordance with theory, Deardorff (1974)). This does not seem to be the case for the TKE model where the growth of the boundary layer is purely due to encroachment and so the encroachment height is the effective boundary layer height.

However, as can be seen in Fig. 2.17 and Fig. 2.18, the KPP shows a much higher spatial resolution dependence (the temporal resolution dependence is low for both the TKE and the KPP within a certain limit of temporal grid spacing) compared to the TKE model. This may severely hamper its usage for coarser grids. The major reason for this is the different length scales of mixing used at the top of the boundary layer for the different models (the flux is always calculated at half levels and the temperature at the model levels). This length scale increases for coarser grids (in the KPP) thus

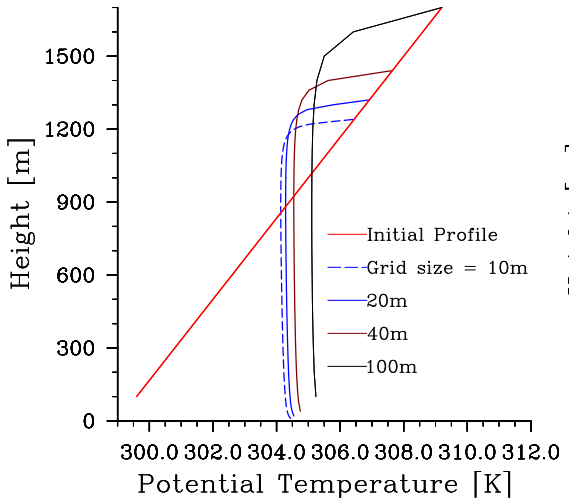

Figure 2.17: KPP dependence on spatial resolution

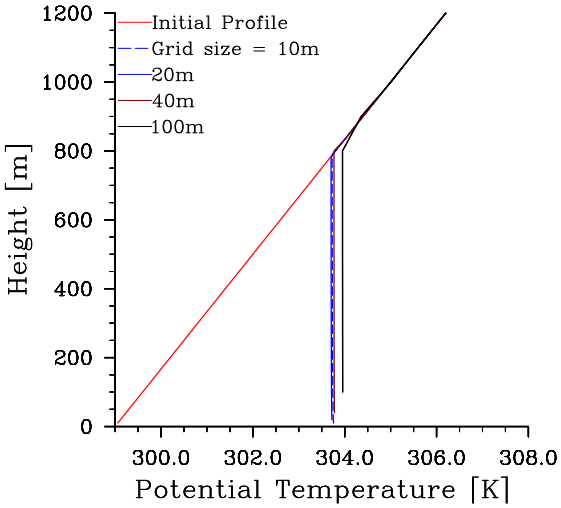

Figure 2.18: TKE dependence on spatial resolution

leading to more entrainment at the top of the boundary layer and hence faster boundary layer growths. As mentioned above, the TKE model suppresses all of this via the stability function, which on the one hand suppresses entrainment (thus, a less physical representation) and on the other leads to less grid dependence of the solutions (thus, a more consistent simulation irrespective of the vertical grid. Providing a physically accurate yet invariant (with grid sizes) representation of the dry convective boundary layer is one of the issues we tackle with the development of the 2TKE model (in Chapter 3).

2.3.6 Behavior in Stable boundary layer case

Next the TKE model is used to simulate the evolution of the shear driven stable boundary layer case SBL1. As expected (Section. 2.2.4), the boundary layer does not grow very fast unlike the convective case and stays fixed at a particular height (since the balance of turbulence production by shear and destruction by buoyancy sustains that height and there are no convective plumes causing entrainment) and there is inversion at the surface (Fig. 2.19).

The wind profile shows a similar initial growth and then assumes a reasonably constant profile (Fig. 2.20). Since the surface friction velocity and hence the Monin-

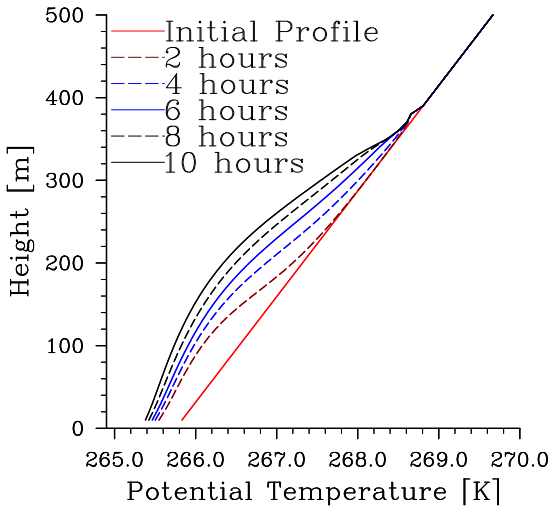

Figure 2.19: Stable boundary layer

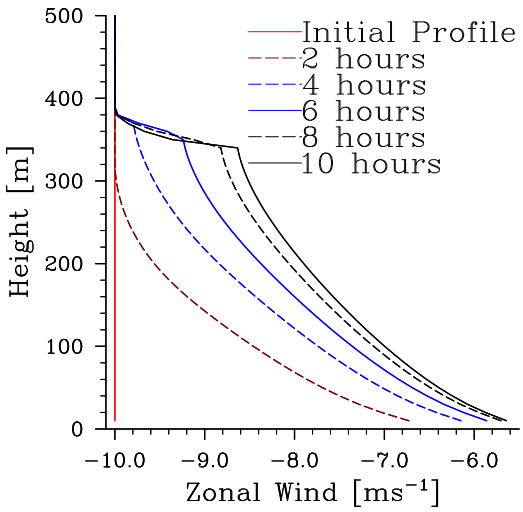

Figure 2.20: Zonal wind profile for stable boundary layer

Obukhov length scale (Eq. 2.15) is varying as the profile keeps changing in time, an average value is taken to evaluate a rough estimate of h_e (in Section. 2.2.4). The estimate is approximately 400 m, which is in good agreement with the profiles for the potential temperature and the wind profile. The relaxation time, i.e T_{relax} is approximately 5 hours, and in the profiles it can be observed that the boundary layer grows to approximately its steady state height near that time. The TKE model, thus fairs reasonable well for boundary layers which are governed more by *local* rather than *non-local* processes.

2.4 Conclusion

This chapter presents the theoretical and operational groundwork for the subsequent development and implementation of the 2TKE model. The single column setup we have developed has been explained first. This is a vertical grid, with the central-difference of second order or the Chapeau-function method used for the spatial discretization of the boundary-layer equations (the two methods are not found to give substantial differences in solutions). In time, the equations are solved semi-implicitly which means that the diffusivity (viscosity) that is used to solve for the potential temperature (wind velocity) is taken from the previous time step to solve for the current time step (the variables

being solved for, on the other hand, are taken at the current time step). The boundary conditions used are constant surface flux and constant surface temperature (surface fluxes being computed using surface similarity laws) and both convective and stable boundary layers have been simulated. Two boundary layer depth diagnostic methods which have been used: the gradient method used usually in large eddy simulations and the parcel method used usually in weather prediction/climate models, have been described. Finally to close the section, the test cases of convective and stable boundary layers, whose simulations have been used in this and the subsequent chapters to study the property of the numerical grid, the currently used turbulence models, as well as the new 2TKE model, have been described.

Having described the numerical setup, we turn our attention to the current boundary layer models. We start with the turbulence kinetic energy (TKE) model used in ECHAM. This model solves for a TKE at each grid point and computes the diffusivity/viscosity there as the product of a velocity scale (that is the square root of the TKE) and a length scale (that takes into account the distance from the surface and the thermodynamic stability at a grid point). To understand the model, we study the simulation of a dry convective boundary layer. From the evolution of the temperature and velocity profiles in time, it is noted that by the formulation of this model, the convective boundary layer is not well represented. The misrepresentation rises due to the inability of local-TKE-based-down-gradient formulation to accurately model the boundary-layer-depth scale plumes that dominate the convective boundary layer. However, the misrepresentation is reduced when a more realistic surface boundary condition is prescribed. The numerical properties of the grid and the TKE model are then explored and it is found that this model is reasonably convergent even upon the usage of coarse or stretched grids. The TKE model is then compared with a *non-local* KPP, in which the diffusivity/ viscosity is computed using the bulk properties of the boundary layer. It is found that though the KPP provides a much better representation of the convective boundary layer, its vertical grid dependence is higher than the TKE model. Finally, it is noted that, in contrast to convective boundary layers, in much more quiescent stable boundary layers where the turbulence is more governed by the local balance of shear production and buoyancy destruction, the TKE model provides a reasonably accurate representation.

These factors guide our development of the 2TKE model that is designed to represent the boundary layer consistently, have less dependence on the vertical grid and be applicable in both stable and convective scenarios (Chapter 3) as well as address the "grey-zone" problem (Chapter 4).

Chapter 3

The 2TKE scheme [1]

3.1 Introduction

In the last chapter, we presented the single column model we developed and also elaborated on the idea of *local* vs.*non-local* models of the planetary boundary layer as used in numerical weather prediction/climate applications. The local model we explored, the TKE (ECHAM), as is characteristic of *local* models, uses the properties inside the grid box at each height level to calculate a total turbulence kinetic energy (TKE) which is then used to prescribe the mixing at that level. The *non-local* model, the KPP, on the other hand used boundary layer-integrated parameters such as the the convective velocity, the boundary layer depth and a continuous shape function (which idealizes the variance of the vertical velocity in the convective boundary layer) to get the mixing coefficient. We also saw that near the surface another scale is implicitly used, which is the distance from the surface. In any case, all these models usually assume a single scale acting in any one part of the boundary layer. This chapter explains the detailed derivation and application of the novel 2TKE model, which, as mentioned in Chapter 1, uses the idea of two scales acting inside the boundary layer to develop a model that works both in the limits of very-large and very-small horizontal grid sizes. The idea developed is that such a model can be expected to perform well in the "grey-zone" (exploration of the "grey-zone" itself is presented in Chapter 4). The model is theoretically derived from large eddy simulation (LES) set of equations, which are designed to model fluid flows using small (compared to the inertial range of the flow) isotropic grids, such that it works well in the single column limit as well as converges back to the LES set if the horizontal grid size is very small.

[1] Parts of this Chapter has been submitted to Journal of Advances in Modeling Earth Systems for publication (Bhattacharya and Stevens, 2014)

The chapter is organized as follows: Section. 3.2 presents the major steps in the derivation of the 2TKE model, and attempts to justify the assumptions taken in closing the unresolved terms in the resulting equations. Comparison with the two currently used models (which make use of findings about the structure of the (clear and cloudy)boundary layer, from LES models and observations, for example Deardorff (1974) for the convective boundary layer and Finger and Wendling (1990) for Arctic stratus clouds, in their formulation) and which we discuss in the last Chapter: the TKE model as used in ECHAM (Brinkop and Roeckner (1995)) and the KPP (Troen and Mahrt (1986)), is done in Section. 3.3. The dynamics of how the two energies work together in different cases (buoyancy and shear driven) has also been explored. The treatment of entrainment mixing of the resolved potential temperature and wind velocities via small-scale energy and its effect of lessening the grid dependence associated with a poor resolution of the vertical structure of the PBL has also been looked into. Section. 3.4 provides the conclusion and states how such a model could be used in the "grey-zone" (we do that in detail in Chapter 4).

3.2 Model Derivation

As discussed in the introduction, it is desired that the model converges to a traditional LES representation in the limit that the grid spacing is much smaller than the depth, h, of the PBL. Hence we begin with the LES equation set for which the subgrid-scale fluxes are modeled using a small scale turbulence kinetic energy (Deardorff (1980)). These equations are then filtered over a large area, thus facilitating the Reynolds averaging assumptions, and yielding a modified set of Planetary Boundary Layer (PBL) equations. The averaging of the LES equations is performed in analogy to what is done in deriving the Reynolds averaged Navier Stokes (RANS) models, i.e., assuming that the energy containing eddies, whose scale is of order h, are much smaller than the horizontal grid spacing (eg. see Mellor and Yamada (1974)). The vertical grid is initially assumed to be on the order of what one finds in LES, but this assumption will later be relaxed. For this presentation only a dry incompressible fluid is considered. The PBL equations derived in this manner differ from typical PBL equations in one key aspect: instead of a single TKE, two energies remain: a large scale TKE that accounts for eddy sizes from the boundary layer scale to the vertical grid size and a small scale TKE which accounts for eddies which are subgrid to the vertical grid size. These equations need a closure assumption for the large scale average of the LES subgrid stresses as well as the Reynolds stresses arising from larger, but still subgrid, eddies. In both cases it is assumed, for simplicity, that a down gradient approximation is sufficient, using small scale TKE and large scale TKE respectively. The former

works on a length scale proportional to the vertical grid size as well as the depth of the inversion layer (since inside the inversion layer the small eddies entrain warmer air from free troposphere into the boundary layer). The latter on the other hand, works on the scale of the boundary layer height and hence is modeled in a *non-local* fashion with a K-profile, taking into account the free tropospheric stability as well as the fact that the small scale energy contributes to the mixing especially at the surface and the EZ. The sum of the large and the small scale energies is independent of the vertical grid size, and at the same time dissipation of large energy acts as a source of the small scale energy (energy cascade, Kolmogorov (1941)). These two constraints relate the dissipation scale of the large scale energy to that of the small scale energy (which is tied to the vertical grid size), and is found to enhance convergence properties of the model solutions at coarse vertical resolutions.

3.2.1 Derivation of new set of PBL equations

In order to simplify the subsequent presentation a few notational conventions as applicable to a generic variable ϕ of an unfiltered fluid field are first introduced. Solving for the fluid field in an LES model with grid size of some distance Δ (much less than the depth of the boundary layer) yields:

$$\phi = \Phi + \phi* \ , \tag{3.1}$$

where Φ is the LES resolved field, and $\phi*$ represents LES subgrid fluctuations. The LES volume average, from which the LES resolved field is derived, is assumed to satisfy the properties of a Reynolds average. Now the quantities on the LES grid, Φ, can be decomposed into an average over a large horizontal grid box typical of a current global NWP or climate model (this average is equivalent to the Reynolds average and will be referred to as the large scale average or the Reynolds average henceforth) and a Reynolds subgrid fluctuation:

$$\Phi = \overline{\Phi} + \Phi' \ . \tag{3.2}$$

The Reynolds average of the LES resolved field should in theory be identical to the Reynolds average of the unfiltered fluid field from which the LES resolved fields have been derived. Thus:

$$\overline{\Phi} = \overline{\phi} \ . \tag{3.3}$$

The above notational conventions have been used throughout this presentation.

Equations for LES filtered variables

The LES equations for the velocity vectors can be written as:

$$\frac{\partial U_i}{\partial t} = -U_k \frac{\partial U_i}{\partial x_k} - c_p \Theta_0 \frac{\partial P}{\partial x_i} + \frac{g\Theta''}{\Theta_0}\delta_{i3} + f_j(U_k - V_{g,k})\epsilon_{ikj} - \frac{\partial \tau_{ik}}{\partial x_k} \ . \tag{3.4}$$

Here tensor notation is used, so that U_i denotes the three components of the LES filtered velocity vector field, (U_1, U_2, U_3), alternatively (U, V, W). The independent spatial coordinates are given by $x_i = (x_1, x_2, x_3)$, alternatively (x, y, z). Repeated indices represent Einstein summation. The lhs represents the rate of change of velocity at each LES grid point. The terms on the rhs represent advection of specific momentum, the gradient of the ageostrophic pressure (P), a buoyancy term, the Coriolis acceleration and the divergence of LES subgrid stresses ($\tau_{ik} = \langle {u_i}^* {u_k}^* \rangle$) respectively. In the above the double prime is used in the definition of the buoyancy term to denote deviations form the horizontal averages, and angle brackets, just in this one instance for notational clarity, denotes averaging over the LES grid, so that $\Phi = \langle \phi \rangle$.

For potential temperature (Θ), in the absence of diabatic forcings, the evolution equation reads:

$$\frac{\partial \Theta}{\partial t} = -U_k \frac{\partial \Theta}{\partial x_k} - \frac{\partial \gamma_k}{\partial x_k} \ , \tag{3.5}$$

where γ_k represents the LES subgrid flux of potential temperature ($\gamma_k = \langle \Theta^* {u_k}^* \rangle$), not to be confused with the counter gradient term discussed in Chapter 1 and Chapter 2.

The LES subgrid TKE, here denoted by e, has an evolution equation:

$$\frac{\partial e}{\partial t} = -\frac{\partial (eU_k)}{\partial x_k} + \frac{\partial}{\partial x_k}\left(K_e \frac{\partial e}{\partial x_k} \right) - \tau_{ik}\frac{\partial U_i}{\partial x_k} + b - \frac{C_e}{l} e^{3/2} \ . \tag{3.6}$$

The terms on the rhs represent transport by advection, a diffusion term (with a diffusivity, K_e) that combines the effect of subgrid turbulence and pressure velocity covariances as a diffusion process of e, subgrid dissipation, buoyant production/destruction (b) and viscous dissipation (standard model following Kolmogorov (1941), with l being the dissipation length scale for $\overline{e}$ and C_e being a flow dependent constant) respectively.

Derivation of Reynolds averaged fields

Reynolds averaging of Eq. 3.4 yields:

$$\frac{\partial \overline{u_i}}{\partial t} = -\overline{u_k}\frac{\partial \overline{u_i}}{\partial x_k} - \frac{\partial T_{ik}}{\partial x_k} - c_p\Theta_0\frac{\partial \overline{p}}{\partial x_i} + \frac{g\overline{\Theta''}}{\Theta_0}\delta_{i3} + f_j(\overline{u_k} - V_{g,k})\epsilon_{ikj} - \frac{\partial \overline{\tau_{ik}}}{\partial x_k} \ , \tag{3.7}$$

where, T_{ij} represents the Reynolds subgrid stress

$$T_{ij} = \overline{U_i'U_j'} \ . \tag{3.8}$$

Because the double prime denotes differences from a horizontal average:

$$\overline{\Theta''} = 0 \ . \tag{3.9}$$

The Reynolds average of P as well as the advective (convective) tendency is resolved by the large scale model. Also in a PBL model for large scale applications, the vertical fluxes and gradients can be considered to be approximately an order of magnitude larger than the horizontal fluxes and gradients respectively. This allows us to neglect the horizontal fluxes in the derivation of the 2TKE model, although formally they should be retained to preserve the correct LES limit, which implies that the Lagrangian acceleration of the Reynolds averaged velocity can be described as follows:

$$\frac{D\overline{U_i}}{Dt} = \frac{\partial \overline{u_i}}{\partial t} + \overline{u_k}\frac{\partial \overline{u_i}}{\partial x_k} = -\frac{\partial T_{i3}}{\partial z} + f_j(\overline{u_k} - V_{g,k})\epsilon_{ikj} - \frac{\partial \overline{\tau_{i3}}}{\partial z} \ , \tag{3.10}$$

where D is defined implicitly as the advective derivative which follows the Reynolds averaged flow.

Similarly for Reynolds averaged potential temperature field, we solve for:

$$\frac{D\overline{\Theta}}{Dt} = -\frac{\partial \Gamma_3}{\partial z} - \frac{\partial \overline{\gamma_3}}{\partial z} \ , \tag{3.11}$$

where Γ_3 represents the Reynolds subgrid vertical potential temperature flux, i.e:

$$\Gamma_3 = \overline{\Theta' W'} \ . \tag{3.12}$$

The difference between Eq. 3.4 and Eq. 3.7, again considering only the vertical fluxes describes the deviations from the Reynolds averaged quantities, such that for the ac-

celeration:

$$\begin{aligned}\frac{\partial U_i'}{\partial t} = &-W'\frac{\partial \overline{u_i}}{\partial z} - \overline{w}\frac{\partial U_i'}{\partial z} - \frac{\partial (U_i'W' - \overline{U_i'W'})}{\partial z} \\ &- c_p\Theta_0\frac{\partial P'}{\partial x_i} + \frac{g\Theta''}{\Theta_0}\delta_{i3} + f_j U_k'\epsilon_{ikj} - \frac{\partial \tau_{i3}'}{\partial z} \ .\end{aligned} \tag{3.13}$$

Taking the Reynolds average of the inner product of the acceleration fluctuations with the velocity fluctuations and further assuming that the Coriolis terms can be neglected inside the boundary layer since hf/u_τ is small (f being the Coriolis parameter and u_τ, the surface friction velocity), yields an expression for E, the turbulence kinetic energy of eddies whose scales range from the vertical grid to the boundary layer depth (henceforth called the large scale TKE):

$$\begin{aligned}\frac{\partial E}{\partial t} = &-\overline{U'W'}\frac{\partial \overline{u}}{\partial z} - \overline{V'W'}\frac{\partial \overline{v}}{\partial z} - \overline{w}\frac{\partial E}{\partial z} - \frac{\partial}{\partial z}\overline{U_i'U_i'W'} \\ &- \frac{\partial \overline{\tau_{i3}'U_i'}}{\partial z} + \overline{\tau_{i3}'\frac{\partial U_i'}{\partial z}} + g\frac{\overline{W'\Theta''}}{\Theta_0} \ .\end{aligned} \tag{3.14}$$

Note that the pressure velocity covariances redistribute the energy among the components but do not contribute to the total energy (Rotta (1951)), and so play no explicit role in Eq. 3.14.

The evolution equation for LES subgrid TKE, e, has been given by Eq. 3.6. Partitioning the LES subgrid TKE (e), the subgrid stress (τ_{ij}) and the buoyant production (b) into a Reynolds averaged and a Reynolds subgrid part ($e = \overline{e} + e', \tau_{ij} = \overline{\tau_{ij}} + \tau_{ij}', b = \overline{b} + b'$) yields:

$$\begin{aligned}\frac{\partial(\overline{e}+e')}{\partial t} = &-\frac{\partial((\overline{e}+e')(\overline{u_k}+U_k'))}{\partial x_k} + \frac{\partial}{\partial x_k}\left(K_e\frac{\partial(\overline{e}+e')}{\partial x_k}\right) \\ &- (\overline{\tau_{ik}}+\tau_{ik}')\frac{\partial(\overline{u_i}+U_i')}{\partial x_k} + \overline{b} + b' - \frac{C_e}{l}(\overline{e}+e')^{3/2} \ .\end{aligned} \tag{3.15}$$

Applying Reynolds averaging again on Eq. 3.15, using the boundary layer approximation of neglecting the horizontal gradients with respect to the vertical gradients, we note that:

$$\overline{(\overline{e}+e')^{3/2}} = \overline{\overline{e}^{3/2}} + \frac{3}{2}\overline{\overline{e}^{1/2}e'} + \frac{3}{8}\overline{\overline{e}^{-1/2}e'^2} + H.O.T \approx \overline{e}^{3/2} + \frac{3}{8}\overline{e}^{-1/2}\overline{e'^2} \ , \tag{3.16}$$

wherein the approximation arises through the neglect of the higher order terms, denoted by $H.O.T.$. Substitution of Eq. 3.16 into Eq. 3.15, and applying the aforementioned approximations yields an equation for the evolution of the Reynolds averaged small-

scale TKE:

$$\begin{aligned}\frac{\partial \overline{e}}{\partial t} = &- \frac{\partial(\overline{e}\ \overline{w})}{\partial z} - \frac{\partial(\overline{e'W'})}{\partial z} + \frac{\partial}{\partial z}\left(K_e \frac{\partial \overline{e}}{\partial z}\right) - \overline{\tau_{i3}}\frac{\partial \overline{u_i}}{\partial z} \\ &- \overline{\tau'_{i3}\frac{\partial U'_i}{\partial z}} + \overline{b} - \frac{C_e}{l}\left(\overline{e}^{3/2} + \frac{3}{8}\overline{e}^{-1/2}\overline{e'^2}\right) .\end{aligned} \tag{3.17}$$

The mean vertical wind at the surface is assumed to be zero, i.e., only flat surfaces are considered. This, combined with incompressibility implies that $\overline{w}$ does not enter our set of PBL equations.

Eq. 3.10, Eq. 3.11, Eq. 3.14 and Eq. 3.17 thus represent the evolution equations for the horizontal wind components, the potential temperature, the large scale TKE , and Reynolds averaged LES subgrid TKE, which form the basis of the 2TKE model.

Closure for the subgrid variances

To close this modified set of boundary layer equations, we parameterize the LES subgrid covariances and use them to model for the triple covariance terms in the equations for E and $\overline{e}$. Similarly, we also parameterize the Reynolds subgrid covariances. For the most part this can be accomplished using standard approaches as described below.

Like the diffusion of $\overline{e}$, the LES subgrid stresses are related to the mean using a down gradient model thus defining the diffusivity, K_e (K_e as mentioned in Eq. 3.31, is proportional to the square root of $\overline{e}$). For example:

$$\tau_{13} = -K_e \frac{\partial U}{\partial z}. \tag{3.18}$$

Assuming that K_e is uniform over the LES domain as a first approximation (also implying that $\overline{e'^2}$ can be neglected in Eq. 3.17, since the horizontal variation of the e field has been neglected):

$$\overline{\tau'_{13}\frac{\partial U'}{\partial z}} = -K_e \overline{\frac{\partial U'}{\partial z}\frac{\partial U'}{\partial z}}, \tag{3.19}$$

which is always negative semi-definite, such that it is always a sink of E and a source for $\overline{e}$. Assuming, as the simplest case, that the Reynolds filter size is within the inertial subrange (though for example Wyngaard (2004) assume otherwise), this dissipation of E to $\overline{e}$ can be parameterized in the same manner as the dissipation of $\overline{e}$ itself, i.e.:

$$K_e \overline{\frac{\partial U'_i}{\partial z}\frac{\partial U'_i}{\partial z}} = \frac{C_E}{L} E^{3/2} . \tag{3.20}$$

From Kolgomorov theory, the constant of proportionality in the energy spectrum is the same throughout the inertial range:

$$C_e = C_E \ . \tag{3.21}$$

L (dissipation length scale for E) may be parameterized as the Blackadar length (Blackadar (1962)). As will be discussed later, this assumption can be relaxed based on the fact that the dissipation of E is a source of e according to the cascade of turbulence kinetic energy, but for now it is assumed that :

$$L = \frac{kz}{1 + \frac{kz}{\lambda}} \ , \tag{3.22}$$

with λ denoting the asymptotic mixing length (taken as 150 m in ECHAM). The dissipation and production length scale of e (i.e. l) on the other hand is taken to be proportional to the vertical grid size, Δz of the model,

$$l = L\frac{\Delta z}{h} \ . \tag{3.23}$$

The other term that needs to be parameterized is $\frac{\partial \overline{\tau'_{i3} U'_i}}{\partial z}$ which represents the diffusion of E by LES subgrid stresses. Here it is assumed that:

$$\frac{\partial \overline{\tau'_{i3} U'_i}}{\partial z} = \frac{\partial \overline{-K_e \frac{\partial U'_i}{\partial z} U'_i}}{\partial z} = -\frac{\partial}{\partial z}\left(K_e \frac{\partial E}{\partial z}\right) \ . \tag{3.24}$$

The factor of 2/3 is absorbed in the definition of K_e. Thus the diffusion of E by LES subgrid stresses is modeled as a diffusion process.

Similarly, the vertical transport of Reynolds averaged quantities by the Reynolds averaged vertical velocity is modeled as :

$$\overline{\Phi' W'} = -K_E \frac{\partial \overline{\Phi}}{\partial z} \ , \tag{3.25}$$

with K_E denoting the eddy viscosity of large (boundary layer scale) eddies. Thus the equation for the Reynolds averaged acceleration required by the large-scale model is :

$$\frac{D\overline{u}_i}{Dt} = \frac{\partial}{\partial z}\left(K_E \frac{\partial \overline{u_i}}{\partial z}\right) - f_j(\overline{u_k} - V_{g.k})\epsilon ijk + \frac{\partial}{\partial z}\left(\overline{K_e \frac{\partial u}{\partial z}}\right) \ . \tag{3.26}$$

It differs from the traditional form of this equation because the vertical mixing is parameterized using two energies, represented in K_E and K_e respectively. Closures

require the additional assumption that fluctuations in K_e do not correlate with fluctuations in $\partial u/\partial z$ across the grid-scale of the large-scale model. With this assumption we arrive at a closed set of PBL equations.

New set of PBL equations

Based on the above arguments the 2TKE model is as follows :

$$\frac{D\overline{u_i}}{Dt} = \frac{\partial}{\partial z}\left((K_E + K_e)\frac{\partial \overline{u_i}}{\partial z}\right) - f_j(\overline{u_k} - V_{g,k})\epsilon_{ijk} \tag{3.27}$$

$$\frac{D\overline{\Theta}}{Dt} = \frac{\partial}{\partial z}\left(P_r(K_E + K_e)\frac{\partial \overline{\Theta}}{\partial z}\right) \tag{3.28}$$

$$\begin{aligned}\frac{\partial E}{\partial t} &= K_E\left(\left(\frac{\partial \overline{u}}{\partial z}\right)^2 + \left(\frac{\partial \overline{v}}{\partial z}\right)^2\right) + \frac{\partial}{\partial z}\left(K_E\frac{\partial E}{\partial z}\right) \\ &\quad + \frac{\partial}{\partial z}\left(K_e\frac{\partial E}{\partial z}\right) - \frac{C_E}{L}E^{3/2} - \frac{gP_rK_E}{\Theta_0}\frac{\partial \overline{\Theta}}{\partial z}\end{aligned} \tag{3.29}$$

$$\begin{aligned}\frac{\partial \overline{e}}{\partial t} &= \frac{\partial}{\partial z}\left((K_E + K_e)\frac{\partial \overline{e}}{\partial z}\right) \\ &\quad + K_e\left(\left(\frac{\partial \overline{u}}{\partial z}\right)^2 + \left(\frac{\partial \overline{v}}{\partial z}\right)^2\right) + \frac{C_E}{L}E^{3/2} + \overline{b} - \frac{C_e}{l}\left(\overline{e}^{3/2}\right).\end{aligned} \tag{3.30}$$

In these equations the Prandtl number (P_r) i.e the ratio of the eddy diffusivity to the eddy viscosity, has been introduced. It is assumed to be similar for mixing by boundary layer scale and LES subgrid eddies. Thus the system consists of five governing equations instead of the usual four used in PBL modeling. The additional one is for Reynolds averaged LES subgrid TKE ($\overline{e}$). The governing equations for wind velocity and potential temperature, which we intend to solve, require two separate eddy viscosities (diffusivities), one for boundary layer scale eddies (K_E) and the other for smaller isotropic eddies (K_e). This differs from the normal approach to PBL modeling where in only a single eddy viscosity (diffusivity) which models the entire range of eddies within the boundary layer is acknowledged.

When this new set of PBL equations is reverted to the limit that the Reynolds average tends to an LES filter (the large scale energy containing eddies getting resolved, thus K_E tending to zero) this set resembles the LES equation set we started with, with one key difference: the original set modeled small scale subgrid horizontal fluxes alongside the vertical fluxes while this new derived set models only the vertical fluxes (this difference comes due to the boundary layer approximations we applied early on in our derivation of the PBL equations). This difference could and should be addressed

in a more general formulation of the approach, but because our focus is on the "grey-zone", wherein we continue to assume that these terms play a more minor role, we continue to neglect them here.

3.2.2 Closure of the 2TKE equations

The closure of the 2TKE equations requires a specification of the eddy diffusivities associated with the large and small scale TKEs, E and $\overline{e}$ respectively, as well as their dissipation. This section provides a presentation of the closure for each of these terms.

Modeling small eddy diffusivity

Mixing of the mean quantities, by small scale eddies for the SCM, is represented by K_e in the 2TKE model. It is modeled such that it plays a substantial part in mixing in the surface layer as well as in the entrainment zone for entraining the warmer air from above the boundary layer into the layer, following for instance, the theoretical arguments of J.P.Mellado et al. (2013). The diffusivity also physically incorporates the vertical grid size, and in so doing can help minimize some of the deleterious effects of insufficient vertical resolution.

Thus, K_e is modeled (similar to current large scale models) as:

$$K_e = l_{\text{emix}}\sqrt{\overline{e}}\ , \tag{3.31}$$

where l_{emix} represents the length scale of mixing via the smaller eddies. With l_{emix} proportional solely to the vertical grid size, E is doing most of the mixing throughout the boundary layer. To make this model more grid independent (i.e since if E performs most of the mixing especially at the boundary layer top with a K-profile, the solutions are very highly vertical grid dependent, as was shown in Chapter 2), we introduce another length scale for mixing by $\overline{e}$ of the resolved variables in their respective evolution equations, i.e in all the mixing terms in Eq.3.27-Eq.3.30: the depth of the inversion layer. This accounts for the fact that this layer is often unresolved in the mean, and thus this length scale specification allows $\overline{e}$ to account, as it should, for the mixing in this region. The idea is that the mixing which causes entrainment at the top of the boundary layer is done by the smaller eddies which includes some influence of the stability of the region. This is somewhat different from the EDMF formulation by Siebesma et al. (2007), wherein the *local* scheme works predominantly in the surface layer whereas the *non-local* scheme has the major influence in the ML and within the

entrainment zone (entrainment, in this view point, is done by larger eddies from surface penetrating the stable region above the ML). Thus, in our model l_{emix} is formulated as:

$$l_{\text{emix}} = \left[\frac{\kappa(h-z)}{1+\frac{\kappa(h-z)}{\Lambda}}\right]\frac{A}{\Delta z^{1/2}} \ . \tag{3.32}$$

The first part in the rhs represents the influence of the EZ in mixing by using a formulation following the Blackadar formulation for surface scales. Here, Λ is the depth of the entrainment zone and κ is the Von Kármán constant.

Although the small eddy length scale is formulated so as allow K_e to represent substantial part of the mixing in the entrainment zone, for very coarse grids, our experiments show that it results in too much mixing at the top of the boundary layer, leading to unrealistic growth of the boundary layer for coarser grids. Hence the second term is used as a numerical correction factor (A is a constant with dimensions of $m^{-1/2}$). This is justified because from the inertial range theory, $\overline{e}$ theoretically scales with $\Delta z^{2/3}$ and so the length scale should decrease such that the product does not increase unrealistically for coarse grids. Thus our formulation for l_{emix} includes a contribution from the EZ as well as the vertical grid size of the model.

Modeling large eddy diffusivity

The large eddy diffusivity is modeled such that the large scale fluxes and profiles are reasonably represented, especially for the simple case of a convective boundary layer with constant surface fluxes.

By definition, E depends on on the large scale features of the boundary layer, rather than the specific thermodynamic and dynamic state at each model level. Hence, E_1 is introduced as the vertical average of E (the boundary layer depth is calculated by the parcel) :

$$E_1(t) = \frac{1}{h(t)}\int_0^{h(t)} E(z,t)\mathrm{d}z \ . \tag{3.33}$$

The evolution equation for E_1 can be derived by integrating the evolution equation for E:

$$\frac{\mathrm{d}(hE_1(t))}{\mathrm{d}t} = \int_0^{h(t)} \frac{\partial E(z,t)}{\partial t}\mathrm{d}z + E(h,t)\frac{\mathrm{d}h(t)}{\mathrm{d}t} \ . \tag{3.34}$$

The integral in Eq. 3.34 can be estimated from the bulk properties of the boundary layer (assuming logarithmic and linear profiles for velocity and potential temperature

flux profiles respectively). The discretized equation thus becomes :

$$\begin{aligned}\frac{(hE_1)^{n+1}-(hE_1)^n}{\Delta t} &= \frac{0.4g(h^{n+1})\overline{w'\Theta'}_0}{\Theta_0}+(\overline{E'w'}_0-\overline{E'w'}_h)\\ &+\frac{w_c{u_\tau}^2}{\kappa}\left((ln\lambda-lnz_0)+\frac{\lambda^2-{z_0}^2}{2h^2}-\frac{2(\lambda-z_0)}{h}\right)\\ &-C_E{E_1}^{3/2}\left(\frac{ln(h^{n+1})-ln(z_0)}{\kappa}+\frac{h^{n+1}-z_0}{\lambda}\right)+E(h^{n+1})\frac{h^{n+1}-h^n}{\Delta t}\ ,\end{aligned}$$

where superscript denotes the time level, z_0 represents the surface roughness length and u_τ represents the surface friction velocity. The terms on the rhs represent the contributions from the integrated buoyancy flux profile (the surface flux creates E, while E mixes the warm air from the entrainment zone into the ML), the fluxes of E at the surface and the top of the boundary layer, the integrated momentum profile, the dissipation to $\overline{e}$ and the growth of the boundary layer height.

The introduction of the large-scale energy, E_1, facilitates the definition of a convective velocity scale defined as:

$$w_c=\sqrt{2E_1}\ . \tag{3.35}$$

After defining w_c, a profile is used to diagnose K_E, following the general approach of Troen and Mahrt (1986) :

$$K_E=\kappa w_c h\left(\frac{z}{h}\right)\left(1-\frac{z}{h}\right)^m, \tag{3.36}$$

such that the maximum of K_E is at a non-dimensional height corresponding to the approximate maximum of vertical velocity variance in a convective boundary layer, see for example Wyngaard (1984)). In the present implementation of the 2TKE model, this exponent is made to depend on the free tropospheric stability as well. Unlike other models, in this model K_e contributes to mixing too. And that influence has been incorporated in the exponent as well. The procedure is described next.

To explore the dependence of K_E on the free tropospheric stability (G), cases with constant surface flux and no shear as well as no K_e have been considered with different values of G. For the boundary layer height to be correctly predicted, for instance as compared to LES, the flux at the point of minimum buoyancy must be correctly predicted. This is because, in the absence of mass flux out of the boundary layer (by convection or large scale convergences), the boundary layer growth depends on the fluxes according to :

$$\frac{dh}{dt}=\frac{\overline{w'\theta'}_0-\overline{w'\theta'}_h}{Gh}, \tag{3.37}$$

as, for instance, shown by Deardorff (1974). Further it is assumed that the profile stability at the height of minimum buoyancy (approximately 0.93 of the non-dimensional height in our model, this result is similar to those obtained from LES studies of the dry convective boundary layer, for example by Mason (1989) and Moeng (1984)) is independent of the stability above the boundary layer. Thus if an exponent m_1 of the non-dimensional height in K_E is suited for a given free tropospheric stability, matching the value of K_E at 0.93 of the non-dimensional height gives a value of m_2 that can work for a different stability. This is shown below:

$$\kappa(Q_0 h_1)^{1/3} h_1 (.93)(.07)^{m_2} = \kappa(Q_0 h_2)^{1/3} h_2 (.93)(.07)^{m_1} \ , \tag{3.38}$$

where Q_0 is the bottom flux and h_1 and h_2 are the boundary layer heights for a initial stability of G_1 and G_2 respectively. Now, height of the boundary layer is inversely proportional to the square root of the stability. This implies:

$$(h_1)^{4/3}(.07)^{m_2} = (h_2)^{4/3}(.07)^{m_1} \ . \tag{3.39}$$

Now, height of the CBL is proportional to $G^{-1/2}$, which implies:

$$m_2 = m_1 + \frac{2}{3} ln \left(\frac{G_1}{G_2} \right) \ . \tag{3.40}$$

This revised exponent helps ensure that the large- and small TKE diffusivities work together to provide the correct representation of the growth of the convective boundary layer, irrespective of the degree of stratification of the layer into which the boundary layer is growing.

The exponent used in the shape function for K_E (m) is also modified to better account for the fact that K_e is doing mixing especially in the entrainment and surface layers. This can be done in a number of ways. Here it is done by matching the value of the total diffusivity at the height of maximum vertical velocity variance (at $h/3$) such that this value is same when both the energies contribute as to when only E is contributing to the mixing, thus :

$$l_{\text{emix}}|_{h/3} \sqrt{\overline{e}} + \kappa w_s h \frac{1}{3} \left(\frac{2}{3} \right)^{m_1} = \kappa w_s h \frac{1}{3} \left(\frac{2}{3} \right)^{m} \ . \tag{3.41}$$

At a height of $h/3$, l_{emix} can be approximated as:

$$l_{\text{emix}} = \frac{.5\kappa h}{4(1+\kappa)} \ . \tag{3.42}$$

And since $O(\overline{e})$ is approximately $O(E/10)$ (from our model simulations), or

$$\sqrt{\overline{e}} \approx \frac{w_s}{\sqrt{10}} \ , \tag{3.43}$$

it follows that:

$$\begin{aligned} \frac{3}{8\sqrt{10}(1+\kappa)} + \left(\frac{2}{3}\right)^{m_1} &= \left(\frac{2}{3}\right)^{m} \ ; \\ m_1 &= \frac{log\left(\frac{2}{3}\right)^m - \frac{3}{8\sqrt{10}(1+\kappa)}}{log(\frac{2}{3})} \ . \end{aligned} \tag{3.44}$$

This model for large eddy diffusivity helps to represent the fluxes as theory argues they should be and perform most of the mixing inside the mixed layer. Perhaps the most important quality of the profiles engineered in this manner is that it allows the small energy to perform substantial mixing at the surface and across the entrainment zone. The consequences of these choices are seen in the solutions for different test cases as shown in Section.4.

Modeling dissipation to get consistent energetics

Eq. 3.19 shows that the dissipation of E leads to a production of $\overline{e}$. This can be conceptualized in terms of the energy cascade in which large-scale turbulence energy cascades into smaller scales, and eventually gets dissipated via molecular viscosity. Not only are the two energies connected by the cascade, the sum of E and $\overline{e}$ should be constant irrespective of vertical grid size of the host single column model (Δz partitions the inertial range without changing the size or shape of its spectrum). Using these two constraints lead to a relation between the dissipation length scales of these two energies, which leads to consistent energetics as well as an improvement in the convergence properties of the model solutions at coarser grids.

We first write the evolution equations for the two energies in a symbolic form ($\mathcal{P}_g$ and $\mathcal{P}_l$ representing global and local production terms respectively):

$$\frac{dE}{dt} = \mathcal{P}_g(w_c, u_\tau) - C_E\frac{E^{3/2}}{L} \ ; \tag{3.45}$$

$$\frac{d\overline{e}}{dt} = \mathcal{P}_l\left(\frac{\partial\overline{u}}{\partial z}, \frac{\partial\overline{\Theta}}{\partial z}\right) + C_E\frac{E^{3/2}}{L} - C_e\frac{\overline{e}^{3/2}}{l} \ . \tag{3.46}$$

Assuming steady solutions allows one to neglect the time derivatives in Eq. 3.45- 3.46 safely for analysis. Given that the vertical grid size is substantially smaller than the

boundary layer height, implies that the local production of e in Eq. 3.46 may be neglected. This leads us to a dominant balance between the transfer of energy from E to e and the dissipation of e by viscosity:

$$C_E \frac{E^{3/2}}{L} \approx C_e \frac{\overline{e}^{3/2}}{l}. \tag{3.47}$$

Now since C_E and C_e are dependent on the flow and by similarity (Kolmogorov (1941)), the same, it implies :

$$\frac{E^{3/2}}{L} = \frac{\overline{e}^{3/2}}{l}. \tag{3.48}$$

Now, for all Δz the sum of E and e should be constant, since Δz is essentially partitioning the inertial sub-range into two parts. This implies:

$$\overline{e} + E = \mathcal{E} \ . \tag{3.49}$$

Eq. 3.48 and Eq. 3.49 imply that:

$$\overline{e}\left(1 + \frac{L^{2/3}}{l^{2/3}}\right) = \mathcal{E}, \tag{3.50}$$

$\mathcal{E}$ being a constant. Thus the length scale of dissipation of E to $\overline{e}$ (L) is related to the length scale of dissipation of $\overline{e}$ (l) which is proportional to Δz (Eq. 3.23), as follows.

$$L \ = \ l\left(\frac{\mathcal{E}}{\overline{e}}\right)^{3/2}\left(1 - \frac{\overline{e}}{\mathcal{E}}\right)^{3/2} \ . \tag{3.51}$$

If the dependence of $\overline{e}$ is neglected, then L becomes proportional to l, which makes it proportional to Δz. This however is unphysical. Therefore taking into account that e is proportional to $(\Delta z)^{2/3}$ while $\mathcal{E}$ is proportional to $h^{2/3}$, three different approximations to L can be formulated. The first one neglects the magnitude of e with respect to $\mathcal{E}$, the second takes a simple two term expansion of Eq. 3.51 while the third one takes four consecutive terms of the binomial expansion of the same):

$$L \ \approx \ \frac{hl}{\Delta z} \tag{3.52}$$

$$L \ \approx \ \frac{hl}{\Delta z} - l \tag{3.53}$$

$$L \ \approx \ l\left(\frac{h}{\Delta z} - \frac{3h^{1/3}}{2\Delta z^{1/3}} + \frac{3\Delta z^{1/3}}{8h^{1/3}} - \frac{\Delta z}{16h}\right) \tag{3.54}$$

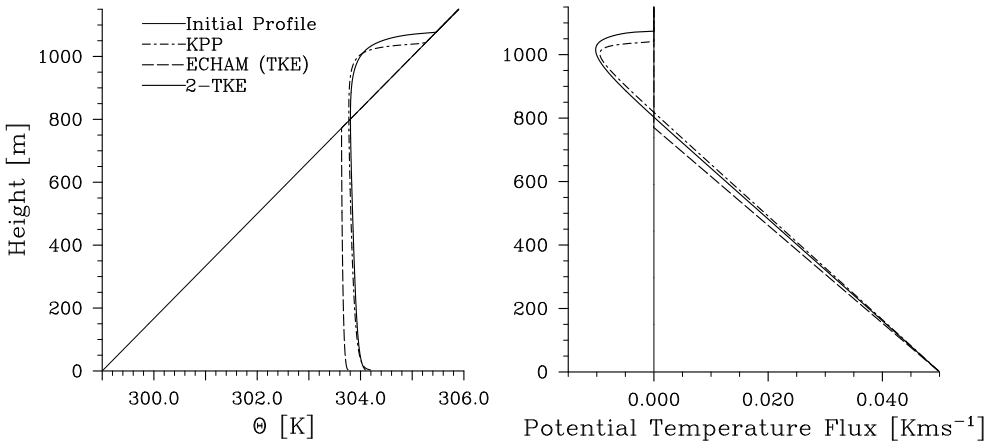

Figure 3.1: (a) Potential temperature profiles for different models after 10hrs, (b) corresponding flux profiles

Eq. 3.52 leads to independence of L from Δz, which was originally the case. Eq. 3.53 leads to :

$$L \approx l \left(\frac{h}{\Delta z} - 1 \right) \tag{3.55}$$

While the third option can be simplified to :

$$L \approx \frac{hl}{\Delta z} \left(1 - c \frac{\Delta z^{4/3}}{h} \right). \tag{3.56}$$

The constant c is a dimensional quantity which is necessary to make the second term inside the bracket in the rhs non-dimensional. This third option with reduction of the length scale of dissipation of E, by a term which has a slight superlinear exponent in Δz leads to a significant reduction of vertical grid dependency of the solutions and, as has been shown in Section. 3.3.2, consistent energetics across a range of grid sizes.

3.3 Solutions of the 2TKE model for idealized test cases

3.3.1 Physical Properties

To understand the general properties of the 2TKE model, it has been compared to a simple TKE scheme Brinkop and Roeckner (1995) implemented in ECHAM6 (Stevens

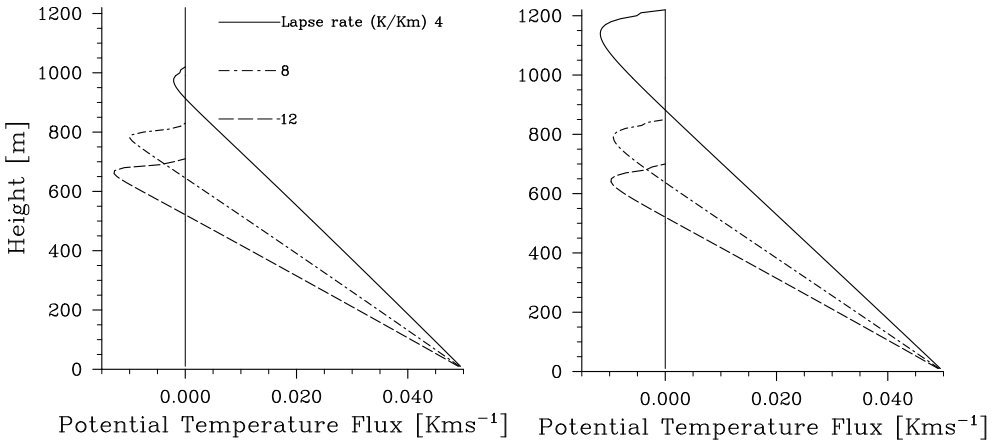

Figure 3.2: (a) Flux profiles for different tropospheric stabilities (without taking its influence on the large scale mixing), (b) Upon taking the influence of the tropospheric stability on the large scale mixing

et al., 2013), as well as the KPP Troen and Mahrt (1986) for the CBL1 case (Fig. 3.1). It is seen that the 2TKE scheme gives a more realistic representation of the temperature and the flux profile of the convective boundary layer as compared to the ECHAM scheme and preforms similarly to the KPP. Its main features are the presence of an unstable surface layer of around 15% of the boundary layer height, a well mixed layer (around 60%) and a stable EZ atop the ML. The ratio of the entrainment flux to the surface flux is governed by the boundary layer height diagnosis method (Eq. 3.37). Sensitivity of the rate of entrainment on the parameters of the parcel scheme (convective excess and critical bulk Richardson number (Ri_{cr}) for the KPP has been discussed in Beljaars and P.Viterbo (1999). As has been discussed in Beljaars and P.Viterbo (1999), in our model too it is observed that increasing the Ri_{cr} and/or the convective excess leads to an increase in the entrainment flux vis a vis the surface flux. The optimal value for the case of the convective boundary layer for Ri_{cr} (defined in Chapter 2) is found to be 0.3 and that for the coefficient D used in the excess parcel temperature excess (Eq. 2.12) is found to be 2. The structure of the convective boundary layer is well represented and the shape of the K-profile effectively determines it, as shown by Stevens (2000) and deviations from the solution are dissipated by the equation within a convective time scale.

The shape function (or K-profile) used in the present implementation of the 2TKE model is however different from that used in the standard KPP approach, in that the influence of the free tropospheric stability (lapse rate) in the exponent being used in

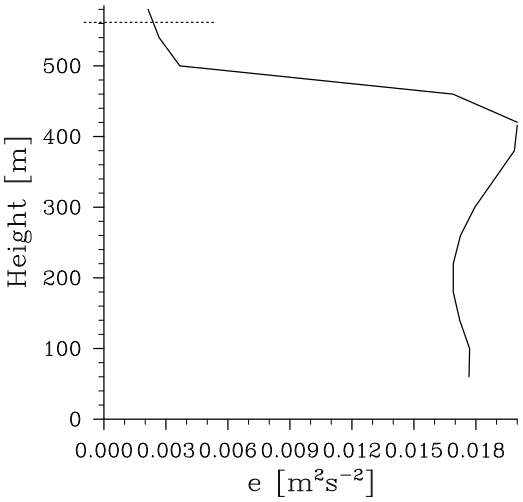

Figure 3.3: Vertical profile of e. The dashed line shows the boundary layer height.

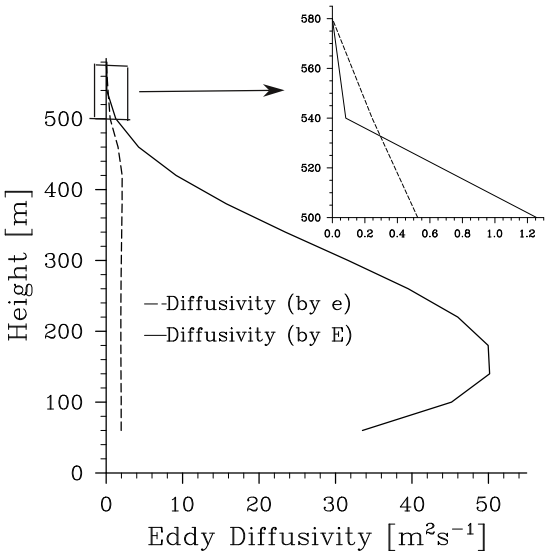

Figure 3.4: Diffusivity profiles. The inset zooms in near the top of the profiles and shows that near the boundary layer top, the small eddy diffusivity plays a dominant role compared to the large eddy diffusivity.

the shape function (Section. 3.2.2) is incorporated. This helps maintain the correct entrainment ratio and thus the boundary layer height irrespective of the stability of the free atmosphere into which the boundary layer deepens. The difference between the standard KPP approach and the approach adopted here can be observed in Fig. 3.2. These show the flux profiles for case CBL2 after 10 hours of simulation time for different tropospheric stabilities. In Fig. 3.2(a) which presents results from the case where the exponent m in Eq. 3.36 is fixed at the value of 2. For this case it is found that as the stability in the atmosphere increases, the boundary layer growth is not reduced compared to the theoretical value. Rather the entrainment rate is higher than what it should be. For lapse rate of 4 K Km^{-1} both the entrainment flux and the boundary layer depth are less than the theoretical value. So when the stability is increased, the increased entrainment rate (and thus boundary layer depth) is consistent with the progressively larger entrainment buoyancy flux. Taking into account the stability of the profiles (Fig. 3.2(b)) gives us the a better prediction of the entrainment to surface buoyancy flux ratio and consequently the growth of the boundary layer irrespective of the stability of the free atmosphere into which the boundary layer deepens.

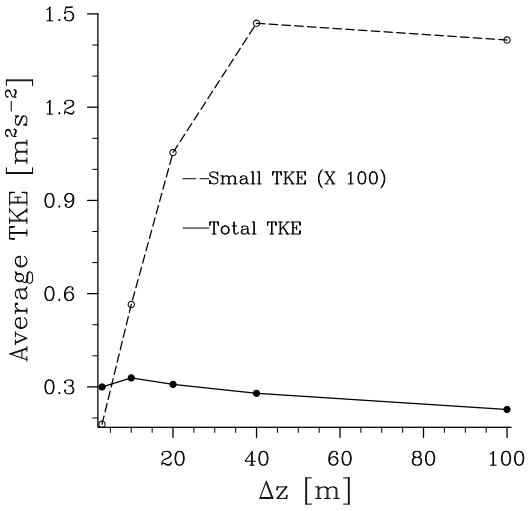

Figure 3.5: Relative contribution of the large and the small energies across a range of grid sizes

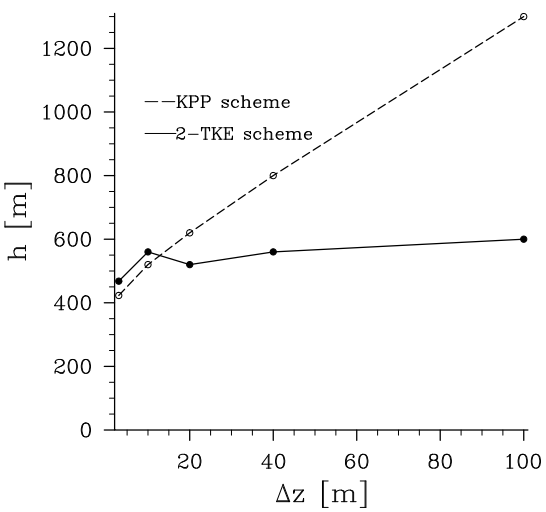

Figure 3.6: Boundary layer height predicted by the KPP and the 2-TKE model for a range of grid sizes

Another key aspect of the present implementation of the 2TKE model is its representation of mixing in the entrainment zone via two processes. One process is the local-mixing of warmer air from the free-troposphere into the entrainment-zone, and subsequently into the bulk of the boundary layer; and the other is associated with the downward-mixing by warm-thermals from the surface penetrating the inversion layer. Fig. 3.3 and Fig. 3.4 show the profile of $\overline{e}$ and the diffusivities through the boundary layer after 3 hrs for the case of a vertical grid size of 40 m (Case: CBL2). Mixing inside the ML is primarily carried out by E. On the other hand, in the surface and the entrainment-zone, e plays a substantial role compared to E, and this trend increases as either the top, or base, of the boundary layer is approached.

3.3.2 Numerical Properties

As discussed in Section. 3.2.2, the development of the 2TKE model has been guided by the desire to maintain a consistent-representation of the energetics irrespective of the vertical resolution. This means that E must decrease as the vertical-grid spacing becomes larger leading to a compensatory increase in e such that the vertical average (over h) of the sum of the two is approximately a constant. The ability of the model to meet this design constrain is demonstrated with the help of Fig. 3.5, which show

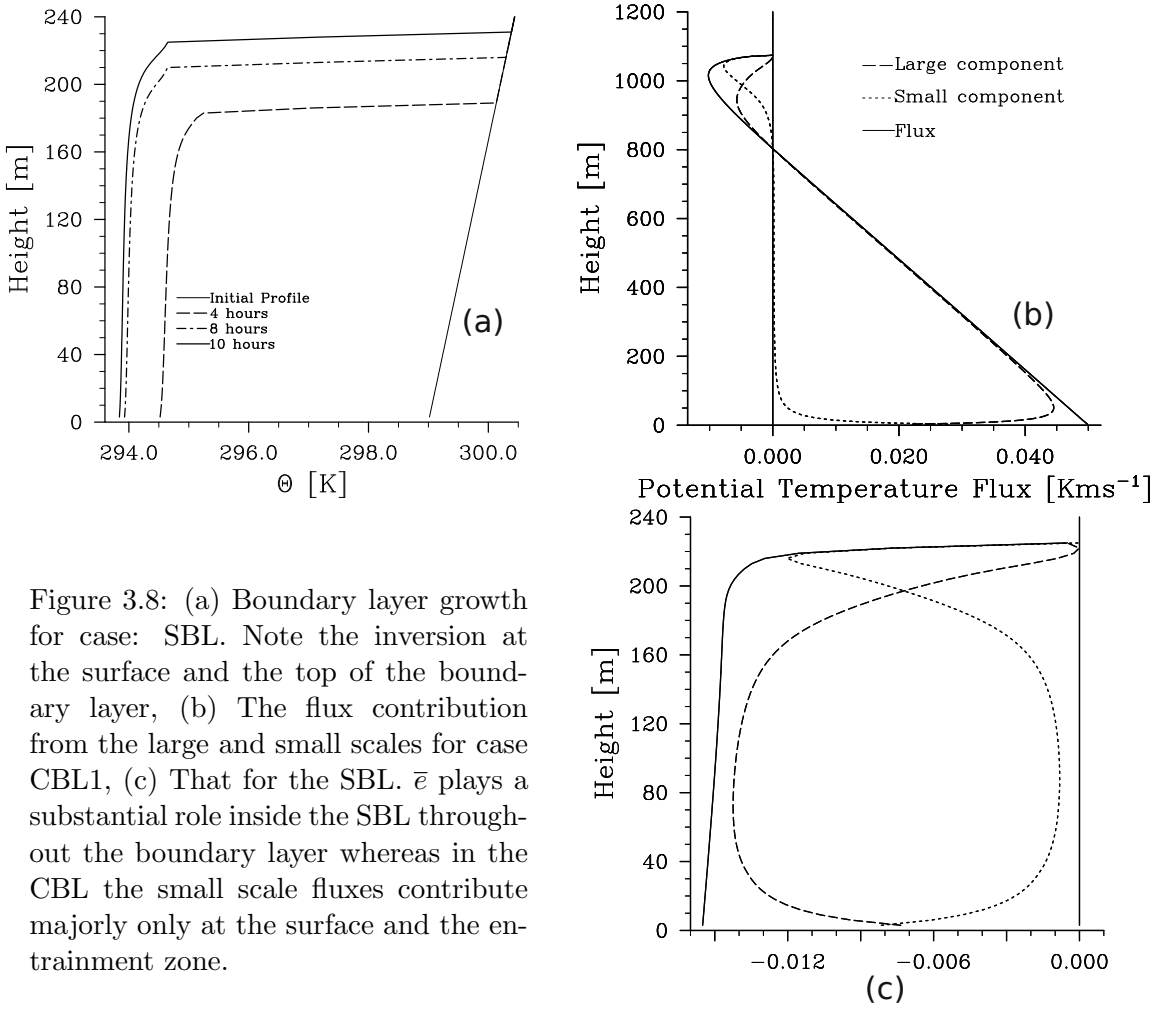

Figure 3.8: (a) Boundary layer growth for case: SBL. Note the inversion at the surface and the top of the boundary layer, (b) The flux contribution from the large and small scales for case CBL1, (c) That for the SBL. $\overline{e}$ plays a substantial role inside the SBL throughout the boundary layer whereas in the CBL the small scale fluxes contribute majorly only at the surface and the entrainment zone.

the vertically-averaged sum of the two TKEs as well as the vertically averaged $\overline{e}$ across a range of grid sizes. Till a certain grid size, the effect is observed clearly beyond which numerical effects reduce the sum of the two energies as a whole (the ratio of the averaged $\overline{e}$ to the total is seen to increase with increasing grid sizes nonetheless). By attempting to enforce a consistent representation of the distribution of energy in E and $\overline{e}$ and by allowing the small- scale energy to represent the entrainment processes, and in so doing compensate for numerical-artifacts arising from poor vertical-resolution, the model appears to perform more robustly on coarse vertical grids (Fig. 3.6 shows the boundary layer height after 3 hrs of model run for the KPP and the 2TKE scheme for a range of grid sizes).

3.3.3 Behavior across regimes

By using two TKEs it is possible to represent the evolution of the boundary layer more robustly in a large-scale model. In particular the use of the small TKE to model entrainment helps reduce grid-spacing dependencies. The advantageous use of large

TKE, on the other hand, has been demonstrated for the case of a convective boundary layer growing into layers of varying stability. To conclude this section we explore the stable- boundary-layer limit. In the stable boundary layer, the turbulence that sustains the boundary layer is generated by the balance of production via local-shear and destruction via local-buoyancy, the TKE model performs reasonably well as compared to the KPP, which has been designed more specifically for convective scenarios. The 2TKE model also performs well (Fig. 3.8(a), case SBL), with $\overline{e}$ doing relatively much more of the mixing in the bulk of the boundary layer as compared to a CBL. Thus, in a convective case where the boundary layer develops as a result of convective thermals driven by due to surface buoyancy, the large scale fluxes, represented by E, dominate the ML while the small scale fluxes play a significant role only at the surface and the entrainment zone (Fig. 3.8(b)). On the other hand, in the stable boundary layer case, the small grid scale fluxes, associated with the small scale energy, $\overline{e}$ play a much more significant role throughout the boundary layer (Fig. 3.8(c)).

3.4 Conclusions

This chapter presents a new boundary layer model, which we call the 2TKE model, that is developed based on the definition of two turbulence kinetic energies. Our approach is the division of scales in PBL turbulence into two parts: thermals that range from the boundary layer depth till the vertical-grid scale of the model and eddies that are subgrid to this vertical grid scale. The model is thus derived from the full set of LES equations with prescribed subgrid TKE and is shown to converge (modulo the treatment of the horizontal fluxes) to these equations in the limit when the grid spacing Δx is much less than the depth of the boundary layer. In the large-scale limit, we have tested the model for idealized cases in the single column setup (developed in the last Chapter) and it is found out that it represents the boundary layer as well as or better than models currently in use.

The major feature of the model is the usage of two energies: one represents the energy on scales smaller than Δz, called the small scale energy, $\overline{e}$ and the other over scales that range from $\min(h, \Delta x)$ to Δz, called the large scale energy, E. This assumes of course that $\Delta z \leq \Delta x$. We therefore formulate length scales over which these two energies mix and dissipate. The mixing length of the small scale energy has been defined in such a way that the small scale contributes substantially to the mixing inside the entrainment zone of the convective boundary layer. The mixing length of the large scale energy takes into account the boundary layer height, the free tropospheric

stability (both included in a shape function that roughly indicates the size of the largest eddy contributing to mixing at a given height) and the fact that in the entrainment zone, the small scale energy is responsible for much of the mixing. The dissipation and production length scale of small-energy is proportional to the vertical grid size of the model while that for the large-energy is defined in such a way that the total energy is consistently represented irrespective of the grid-size of the host model. These choices lead to a model of the boundary layer that behaves reasonably well across a range of vertical grid sizes. An extra advantage of the usage of two energies is the smooth transition of the representation of the boundary layer from convective to stable scenarios, with the small-scale energy contributing more in the stable scenario.

This model thus provides us a theoretical basis for approaching the "grey-zone" in which the small scale energy will continue to act, but the large scale energy will get progressively resolved as the horizontal grid size reduces. Having developed and tested this model, we implement this model in an LES model, the UCLA-LES so that we can approach the "grey-zone" with this model. This involves several challenges, principle ones being: how to blend the large energy in the "grey-zone" and how should the length scales of mixing, production and dissipation of the two energies behave in the "grey-zone" to provide consistent energetics as well as reasonable representation of the boundary layer in that regime. We discuss these issues in the next chapter.

Chapter 4

Blending functions in 2TKE model

4.1 Introduction

The previous chapter described the derivation of the 2TKE model, the major feature of the model being the usage of two turbulence kinetic energies working over two different ranges of scales: a large TKE (E) accounting for scales from the boundary layer depth, h, to the vertical grid scale, Δz, and a small TKE ($\overline{e}$) accounting for scales subgrid to Δz. It was also shown that although in the SCM limit (i.e $\Delta x >> h > \Delta z$, in general), E contributes the most to mixing except at the interfaces, in the usual large eddy simulation (LES) limit ($\Delta x \approx \Delta z < h$) the entirety of E is resolved and $\overline{e}$ converges to the Deardorff TKE (modulo the horizontal advection terms and the production due to horizontal gradients). This property guides our approach to modeling the intermediate scales, the so-called "terra-incognita" or "grey-zone" described in the previous chapter. "Grey-zone" implies $\Delta x \approx h$, which means a part of E has been resolved by the numerical mesh and the remaining part along with $\overline{e}$ remains subgrid. To explore this range of grid spacings we need a LES model, a 3-D model used usually to solve for a turbulent flow with $\Delta x \approx \Delta z$. We have used the UCLA-LES (Stevens (2013)), which is an LES model developed by Bjorn Stevens and others at the University of California in Los Angeles. At the end of this chapter, we arrive at the complete 2TKE model that can represent the boundary layer with fidelity irrespective of the grid paradigm it is being used in.

4.2 Procedure to approach the "grey-zone"

In this section we present an outline of the steps we take in the UCLA-LES setup to achieve a model that is scale adaptive. This involves developing an understanding of the current LES subgrid models and then implementing the 2TKE model in the UCLA-LES. Then simulations with the 2TKE model in the "grey-zone" are explored to guide its development into a scale adaptive model.

In the UCLA-LES, the default subgrid turbulence model is the Smagorinsky-Lilly model (Smagorinsky et al. (1965)), which assumes a production-dissipation balance of subgrid turbulence and uses the simplified balance obtained thus, to relate the subgrid scales to the resolved scales (Section. 4.3.2). The derivation of this simplified first-order closure from the generalized second moment equations, the simplifications involved and the flow-dependent constants used in the closure have been explained in details in the seminal work of **?**. The Deardorff model (Deardorff (1980)), to which our 2TKE model should converge to at fine numerical grids, on the other hand, solves prognostically for a subgrid LES TKE, which we call the Deardorff TKE, and uses that to prescribe the subgrid mixing of heat, momentum and scalars, assuming an eddy diffusivity that is a function of the Deardorff TKE. Therefore the Deardorff model has been implemented as a first step and the solutions have been compared to that from the Smagorinsky model to look into the factors that control the solutions from both the models (Section. 4.3.2). Since the 2TKE model converges to the Deardorff limit as $\Delta x \approx \Delta z$ (henceforth called the fine grid limit), implementing the Deardorff model is the first step to ensure that the 2TKE model works as expected in the fine grid limit. The next step was to implement the 2TKE model (Section. 4.4), building upon the Deardorff model, in the UCLA-LES. This involved solving for E using bulk properties of the boundary layer whose height, h, was determined using the gradient method (see for instance Sullivan et al. (1998)) and solving for $\overline{e}$ similar to the Deardorff TKE with a modified production term and contribution from E via a turbulence cascade. Note that in computing $\overline{e}$ similar to the computation of the Deardorff TKE, we implicitly take into account the horizontal advection and diffusion terms along side their vertical counterparts. These terms, which are insignificant in the large-grid-size limit, can be significant for fine grid sizes at which the 2TKE model should converge to the Deardorff model.

The implementation is then checked at two limits of horizontal grid sizes: the very large (henceforth called the SCM-limit) and the very small (the fine grid limit). In both these limits, we have benchmark solutions: in the SCM limit the benchmark solution is that from the 2TKE model in the stand alone setup we developed in the previous Chapter and in the fine grid limit, it is the solution from the Deardorff model to which

our 2TKE model solution should converge in theory. It is found that the solution from the 2TKE model implemented in UCLA-LES configured as an SCM ($\Delta x >> \Delta z$) matches that of the 2TKE model implemented in the stand alone setup, provided the boundary layer height diagnosis is the consistent for both the numerical setups. In the fine grid limit, the 2TKE model is found to behave similar to the Deardorff model provided the length scale of production and mixing of the small TKE is consistent with that of the Deardorff model. The above steps ensure the proper implementation of the 2TKE model in the UCLA-LES and also helps us determine the limits of the blending function approach we take in the "grey-zone". This means that the 2TKE model should ensure the following four conditions (Section. 4.5.1): a) In the SCM limit, E accounts for all the boundary layer scale eddies because none of them are resolved, while in the fine grid limit, $E = 0$ since all the boundary layer scale eddies are resolved. b) For a grid size, Δx, in the "grey-zone" the mixing length scale of E should represent only those "large" eddies that are still subgrid, c) $\overline{e}$ should ideally remain similar for all values of Δx, the only aspect that varies with the grid size being the ratio of the contributions from the resolved fields to that from E by cascade, d) in the fine grid limit, the length scale of mixing by $\overline{e}$ should match the length scale of mixing of the Deardorff TKE (in that limit).

Thus, in this chapter we take our 2TKE model forward, by taking into account the horizontal grid size into its formulation, in such a manner that the solutions from the model are grid independent. Current large scale PBL models do not use any information of the horizontal grid size in their formulation. As we shall see, the Deardorff model used in LES does use that information in a correct manner. This means that as the grid size is progressively reduced, so does the subgrid mixing. Therefore at the end of the Chapter, we compare our 2TKE model to the Deardorff model over range of grid sizes in the "grey-zone". Lesser dependence of our model solution (as compared to the Deardorff model) to the horizontal grid size allows us to conclude that our 2TKE model should outperform the current PBL models in an operational framework that is within the "grey-zone"

4.3 Brief Description of UCLA-LES

4.3.1 General

The UCLA-LES Version 3.2.1(Stevens (2013)) is a 3-D large eddy simulation model which solves for a turbulent atmospheric flow with the anelastic approximation (sound

waves, which are not of meteorological significance, are filtered out in this formulation). Variables being solved for include the three dimensional velocity field, the potential temperature field (liquid water potential temperature and total-water mixing ratio for moist flows), and any number of scalars (depending on the level of microphysical complexity for example). The pressure is solved diagnostically as a sum of a mean term (corresponding to the mean thermodynamic state) and a deviation to balance the mean vertical acceleration. The formulation is such that all length scales greater than a scale, Δ, that is proportional to the underlying numerical grid and much smaller than the inertial scale of the flow (i.e typically some fraction of the boundary layer depth, h, at least away from the boundaries) are resolved and scales smaller than Δ are modeled by a subgrid turbulence model. It is these subgrid turbulence models that interest us.

The simulations we perform aim at isolating the effect of the horizontal grid size and to use that information to guide the development of the 2TKE model in the "grey-zone". This implies that other numerical effects such as domain size and vertical grid size should not affect our simulations. Sensitivity studies have been performed and it is noted that for a dry convective boundary layer, if the simulation time is approximately of the order of 3 hours for fine horizontal grids, then a domain size greater than or equal to $4-5$ times the boundary layer depth in all three directions is enough for the solution to be independent of the domain size (similar results have been shown in de Roode et al. (2004)). For coarser horizontal grids approaching the the single column limit, the domain size is much larger and hence simulations till 10 hours have also been taken into consideration. This is because, in theory, even the mesoscale circulation that might have been generated is smaller than the domain size (de Roode et al. (2004)). The vertical grid size for all our simulations is less than 15 m and it is found that within that range the solutions are fairly independent of the vertical grid size (this has also been noted in the analysis of Sullivan and Patton (2011) and Tong et al. (1998)). Statistics used in this Chapter are computed over 10 minute intervals.

Fig. 4.1 illustrates the above points. The figure shows the mean temperature profile and subgrid TKE for four simulations described in Table. 4.1 after 3 hours of simulation time. The grid and the domain size in the two horizontal directions are the same. It can be noted from the figures that for simulations using grid size of less than 15 m and using domain size more than four times the boundary layer depth in the three directions, both the mean properties as well as the mean subgrid properties behave similar to each other

Having found that the all the above simulations lead to similar solutions, we choose Case:A above as our fine grid case (this has the minimum number of grid points and

Table 4.1: Grid sizes and domains of four cases which we use to show the domain and vertical grid size independence of the solutions (both mean as well as subgrid parts of the solution) within a certain grid size (nx and nz are the number of grid points in each of the horizontal direction and the vertical direction respectively).

Case name	$\Delta x, \Delta z$ [m]	nx, nz
A	$15, 15$	$132, 100$
B	$15, 10$	$132, 200$
C	$15, 5$	$132, 400$
D	$10, 10$	$132, 200$

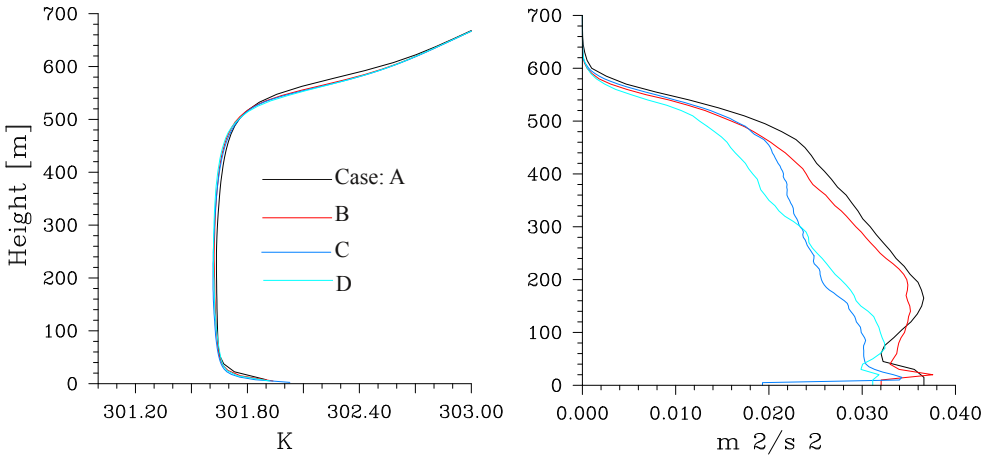

Figure 4.1: (a) Potential temperature after 3 hours of simulation for the four cases described in Table. 4.1. (b) The corresponding subgrid TKE.

hence the least computational expense among all the configurations). The details of the range of grid sizes and the corresponding grid points in each direction (which together gives the domain size) we explore in this chapter are presented in Table. 4.2

4.3.2 Subgrid turbulence models

The UCLA-LES models the subgrid fluxes of heat and momentum using the eddy diffusivity (viscosity) approach (notations used in this chapter have been described in Chapter 3). The ratio of the diffusivity to the viscosity is the eddy Prandtl number (P_{r}). Thus, for example:

$$\tau_{ij} = -\rho_0 K_m \left(\frac{\partial U_i}{\partial x_j} + \frac{\partial U_j}{\partial x_i} \right) , \tag{4.1}$$

Table 4.2: Range of grid sizes studied (the size of the domain is sufficient to not influence the solutions at least within the time of simulation.)

$\Delta x, \Delta z$ [m]	nx, nz
15, 15 (Fine grid)	132, 100
50, 10	28, 200
100, 10	28, 200
200, 10	28, 200
500, 10	12, 200
1000, 10	12, 200
2000, 10	12, 200
5000, 10	12, 200
10^4, 10	12, 200
10^5, 10 (SCM-like grid)	12, 200

K_m being the eddy viscosity. The key difference from the SCM is that the fluxes are tensors i.e both vertical and horizontal components are substantial. The LES model assumes that the eddy diffusivity/viscosity is isotropic and it is calculated as a product of a velocity and a length scale. The velocity scale is calculated differently for different subgrid turbulence models (here we consider the Smagorinsky and the Deardorff models), however the length scales are similar. The length scales for a grid box takes into account the grid sizes in three directions as well as the distance from the surface for that grid box. We now present a detailed formulation of these two subgrid models.

Smagorinsky model

The Smagorinsky model calculates the eddy viscosity as:

$$K_m = (C_s l_S)^2 S \sqrt{1 - \frac{Ri}{P_\mathrm{r}}}; Ri = \frac{S^2}{N^2} \ , \tag{4.2}$$

C_s being the Smagorinsky constant set at 0.2. Ri, the flux Richardson number, is the ratio of the local shear production and production (destruction) by local stability of the subgrid-turbulence kinetic energy. This assumes that the subgrid turbulence is stationary and steady and the production and dissipation of subgrid turbulence are in balance. The assumption allows us to solve for the subgrid TKE diagnostically (which reduces computational expense) based on local-flow-dependent variables (local, because to calculate the values at a grid point only information local to that grid point

is necessary) to calculate the eddy viscosity/diffusivity. For example, the local shear production term, that is given by:

$$S^2 = \frac{\partial U_i}{\partial x_j}\left(\frac{\partial U_i}{\partial x_j} + \frac{\partial U_j}{\partial x_i}\right) , \tag{4.3}$$

and the production (destruction) by ambient buoyancy, that is given by:

$$N^2 = \frac{g}{\Theta_0}\frac{\partial \Theta}{\partial z} . \tag{4.4}$$

are used to specify the subgrid-turbulence velocity scale. The length scale, l_S, on the other hand is given by:

$${l_S}^{-2} = (\Delta x \Delta y \Delta z)^{-2/3} + (z\kappa/C_s)^{-2} . \tag{4.5}$$

Thus, the Smagorinsky model essentially calculates K_m as a product of l_S, l_S S (which is a velocity scale) and other flow dependent non-dimensional local parameters. The length scale, l_S used above is similar to the one used in the Deardorff model, which we describe next, and which differs from the Smagorinsky approach in that it solves for the subrid TKE prognostically.

Deardorff model

The Deardorff model (Deardorff (1980)) is implemented in the LES such that its solution can be compared with that from the Smagorinsky model for simple dry convective boundary layer cases. The reason we do this is that the Samgorinsky model, as part of the UCLA-LES, has been benchmarked using various test cases and observations and if both these fine grid turbulence models converge for fine enough grids, then that should be the benchmark solution the 2TKE model should converge to in that limit of grid sizes (though that need not be the "exact" solution for the fluid flow, a point made by Clark et al. (1979)). More importantly, it allows us to gain an understanding of the controls of the behavior of the two subgrid models (something that has been done, for example, in smoke-cloud case by Stevens et al. (1999b)). How the length scales of mixing influence these two subgrid models in a CBL, which we discuss later in this section, has also been studied in Stevens et al. (1999a).

The Deardorff model calculates the velocity scale (to calculate the diffusivity) as the square root of subgrid TKE (e) which is prognostically calculated for each grid box using the subgrid TKE equation, Eq.3.6, in Chapter 3, Section. 3.2.1. The advection of e by the resolved velocity field is neglected in the current formulation since we

consider convective boundary layers with no shear or large-scale convergence. The remaining tendencies (contribution to the rate of change of e) are calculated in three steps: first the tendency due to shear-production and buoyancy-production/dissipation is calculated, next the tendency due to the horizontal diffusion is added to that and finally the vertical diffusion for e (combined with its dissipation to viscosity) is solved semi implicitly by solving a tridiagonal system of equations (similar to the procedure for solving for the diffusion of TKE in the ECHAM model in Chapter 2, Section. 2.3.1). Thus, symbolically:

$$\frac{de}{dt} = P_e \ + \ H_e \ + \ V_e \ , \tag{4.6}$$

where P_e represents the production by both shear and buoyancy, H_e represents the horizontal diffusion, and V_e, the vertical diffusion combined with the dissipation of e. These terms are modeled according to the procedure described in Deardorff (1980). Key features are: a) the length scale to compute P_e is a function of both the horizontal and the vertical grid sizes, b) the tendency due to H_e (with the eddy viscosity used as the diffusivity coefficient for e) is then added explicitly in time and finally c) the e computed using these two tendencies is used to solve for the diffusion equation and the tendency V_e is thus taken into account. The combined tendencies for each time step helps us to calculate the subgrid TKE for the next time step whose square root gives us the velocity scale.

Having computed the velocity scale, the eddy viscosity is calculated using the product of the velocity scale and the length scale, l_{De}. The formulation for the length scale, as given in Deardorff (1980), is l_S divided by a (universal for atmospheric flows) constant with modification at the top of the boundary layer. Thus:

$$l_{De} = MIN \left(.82 \ \frac{\sqrt{e}}{MAX(N,0)}, \frac{1}{\sqrt{(C_s^2(\Delta x \Delta y \Delta z)^{-2/3} + (z \ \kappa \ C_s)^{-2})}} \right) \ . \tag{4.7}$$

The first term on the rhs is the mixing length scale in the entrainment zone where the stability (N) is a large positive number (this term is a stability modification, much like the stability functions used in large-scale boundary-layer models). The second term on the rhs is a fraction of the Smagorinsky mixing length (l_S) and this is the mixing length in the surface layer and the mixed layer.

We show next that making the length scale (of mixing, production and dissipation of Deardorff TKE) same as the Smagorinsky length scale gives the same solutions for the Smagorinsky and the Deardorff models for fine grids. This helps define a benchmark solution to which our 2TKE model should converge in the limit of fine enough grids.

Solution of the simulation using the Smagorinsky subgrid model are compared to

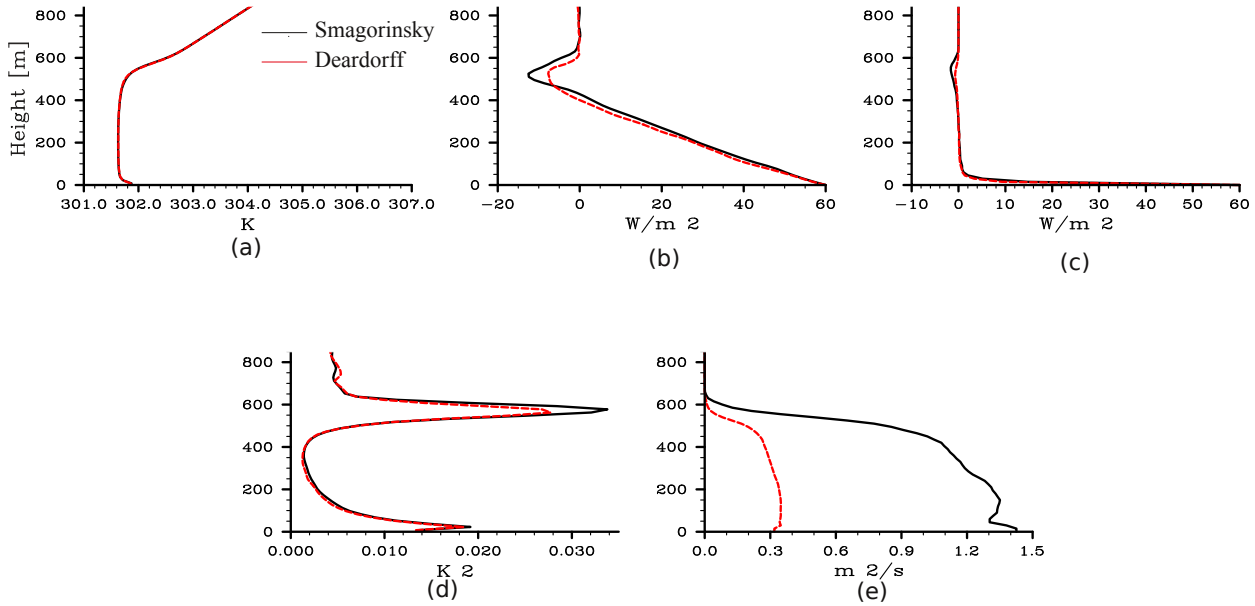

Figure 4.2: (a) Potential temperature profiles for Smagorinsky and Deardorff models after 3 hours. (b) The corresponding flux profiles, (c) subgrid contribution to the flux, (d) variances of the potential temperature, and (e) the eddy diffusivities.

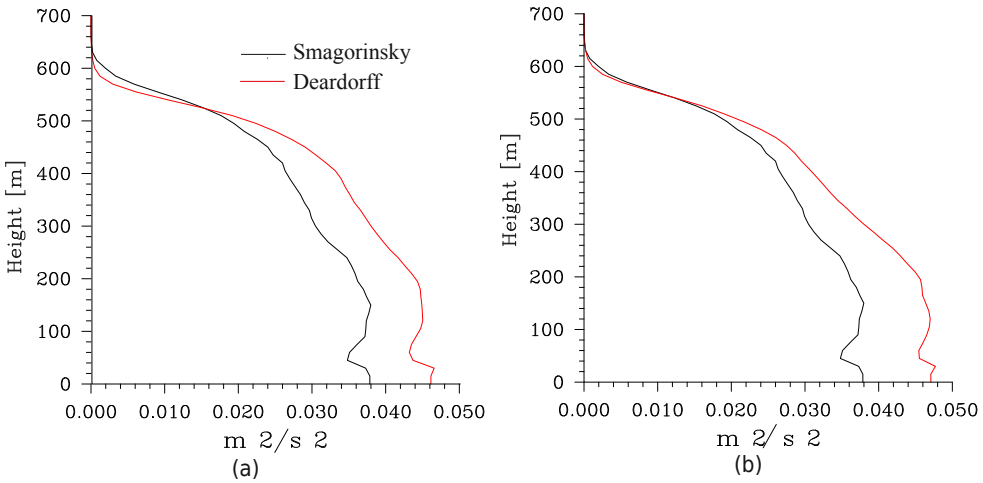

Figure 4.3: (a) Subgrid scale TKE. (b) Upon changing the dissipation of subgrid TKE for Deardorff model.

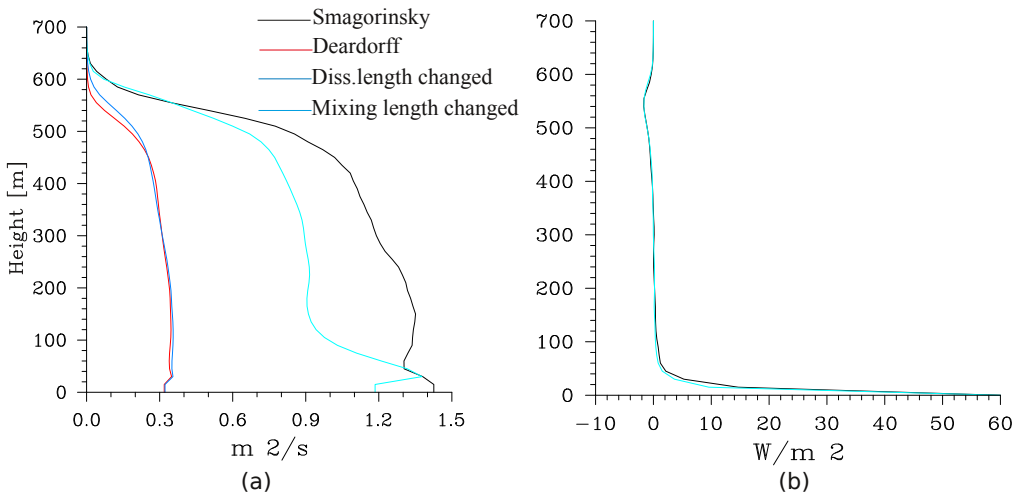

Figure 4.4: (a) Change in subgrid eddy diffusivity. How to approach the Smagorinsky subgrid diffusivity by changing the dissipation and mixing length of the Deardorff TKE. (b) The subgrid scale flux profile upon matching the diffusivitites.

solutions obtained using the Deardorff subgrid model for the dry convective boundary layer case CBL2 (described in Chapter 2). Fig. 4.2 shows the profiles of potential temperature, total heat flux, sub-grid heat flux, the variance of the potential temperature and the eddy diffusivities respectively for the two turbulence models after 3 hours of simulation time. The profiles of the potential temperature (Fig. 4.2(a)) nearly match for the two models and the variance (Fig. 4.2(d)) is relatively low and similar in magnitude and distribution (with height). This means that the temperature fields simulated by the two models are similar, except perhaps in the entrainment zone where the variance is large and slightly distinct in magnitude for the two models. However the total and the subgrid buoyancy fluxes (Fig. 4.2(b) and Fig. 4.2(c)) are smaller in the case of the Deardorff model as compared to the Smagorinsky model, especially near the entrainment zone.

The difference in the total flux can be attributed to the difference between the subgrid flux for the two models (the remaining flux being produced by the resolved scale motions which behave similarly for both subgrid models). The reason for this difference is seen in the diffusivity profiles (Fig. 4.2(e)), which shows that the Deardorff model calculates a smaller diffusivity compared to the Smagorinsky model, especially in the entrainment zone. Now the diffusivity, as mentioned before, is a function of the velocity scale and the length scale. The velocity scale is, directly in the case of Deardorff model and indirectly in the case of Smagorinsky model, related to the subgrid

turbulence kinetic energy (for the Smagorinsky model the subgrid TKE is calculated as part of post processing after the flow simulation). So the subgrid turbulence kinetic energy is compared in Fig. 4.3 (a), which shows that the values are very similar except in the entrainment zone. In the next paragraph we show that the lack of subgrid TKE in the entrainment zone is due to the modification of the Deardorff mixing length by stability correction (the first term in the rhs of Eq. 4.7.

Two steps have been adopted to get similar solutions from the Deardorff model and the Smagorinsky model: first is to remove the MIN function (that is, the stability correction) in the mixing length formulation (Eq. 4.7) which makes the length formulation uniform with height. This increases the subgrid TKE at the top to match that from the Smagorinsky model. The role of this stability correction, which we remove, for the Deardorff-model-simulated entrainment flux is discussed in details in Stevens et al. (1999b). It is good to stress that the removal is not done to achieve the "correct" solution, but rather to explore what controls the Deardorff model solution vis a vis the Smagorinsky solution

The second is to set the mixing length to the same as l_S. This is seen to reasonably match the diffusivities throughout. The first step and its impact on the subgrid TKE in shown in Fig. 4.3(b), while the impact of both the steps upon the eddy diffusivity is shown in Fig. 4.4(a). Getting the eddy diffusivitites similar to each other implies similar subgrid flux profiles (Fig. 4.4(b) and hence, by continuation, similar total flux profiles for both models. This influence of the mixing length scale on the Deardorff model, which we observe, vis a vis its relative non-importance on the Smagorinsky model has been expounded upon in detail by Stevens et al. (1999a). They find that the relative importance of the mixing length scale on the Deardorff model compared to the Smagorinsky model is because for the Deardorff model, in the entrainment zone there is a presence of "fossil" TKE, i.e TKE from unstable regions of the flow (regions below the entrainment zone). The Smagorinsky model that uses only a local balance of subgrid TKE does not take this "fossil" TKE into account and is thus relatively insensitive to the mixing length scale formulation. This also means that for the Deardorff model, a stronger inversion in the simulated flow, i.e. a closer proximity of unstable to stable flow regimes leads to more mixing length scale dependence of the flow, something which would be interesting to explore but we have not explored here since it does not directly correspond to our line of enquiry.

Thus in this section we implement the Deardorff model and understand its controls vis a vis the Smagorinsky model. This aids us in the implementation and exploration of 2TKE model in two ways. Firstly, the properties of the converged solution for fine

enough grids is established. The most important ones being the profile of the subgrid TKE in the boundary layer and the behavior of the eddy diffusivity, especially in the entrainment zone. These properties are shown to vary between different subgrid models, but not by a large amount. The controls on that variability have also been explored. It is important to note that none of the solutions can be considered to be the "exact" solution for the fluid flow (the very formulation of the subgrid models has some fallacies, see Clark et al. (1979)) however they can be considered to lie in the same ballpark as the actual solution and from the design of the formulation itself it is this LES solution that we want to achieve in the limit of fine enough grid.

Secondly, implementing the Deardorff model is the first step in implementing the 2TKE model. This is because the evolution equation for $\overline{e}$ in the 2TKE model is similar to the evolution equation for Deardorff subgrid TKE, by design. The only truly novel property of the 2TKE model is the presence of the large TKE, E and its capability to encapsulate the properties of subgrid but "large" eddies for any given horizontal grid size. The development and the properties of the 2TKE model in the "grey-zone" is the subject of the following sections.

4.4 Implementation of 2TKE in UCLA-LES and limits of the blending function

The 2TKE model is then implemented in the UCLA-LES, using the Deardorff TKE model as the back drop. The reader is reminded that the equation for small TKE, i.e $\overline{e}$ (Eq.3.30 in Chapter 3), in the 2TKE model is similar to the equation for the Deardorff TKE, with two key differences. First is a modified production term that incorporates only the vertical grid size (assuming the horizontal grid size is of the same order as the vertical grid size). This is because the "excess" energy due to the grid anisotropy, that is when the horizontal grid size is much larger than the vertical size, has already been taken into account in E. The second key difference in the budget equation of $\overline{e}$ as compared to that of the Deardorff TKE is the source or the cascade of energy from E.

Thus in the 2TKE implementation in the UCLA-LES, the tendency of $\overline{e}$ is calculated in four steps instead of the three for Deardorff TKE described in the previous section. Symbolically:

$$\frac{d\overline{e}}{dt} = P_{\overline{e}} \; + \; H_{\overline{e}} \; + \; V_{\overline{e}} + \; T_{\overline{e}} \; , \tag{4.8}$$

where $T_{\overline{e}}$ represents the turbulence cascade of energy from E to $\overline{e}$. The production by

shear and production/destruction of turbulence by buoyancy (that is, $P_{\overline{e}}$) is calculated first. This involves a delicacy because the production of Deardorff TKE considers the length scale of production, the same as the length scale of mixing, which is given by Eq.4.7. The length scale of production of $\overline{e}$ in the 2TKE model, on the other hand, is proportional to Δz, the boundary layer depth (h) and height from the surface (z) (see Eq. 3.23 in Chapter 3). Thus:

$$P_{\overline{e}} = P_e \, \frac{\kappa z}{h(1 + \frac{\kappa z}{150})} \left(\frac{\Delta z^{2/3}}{\Delta x^{1/3} \Delta y^{1/3}} \right) \, . \tag{4.9}$$

Eq. 4.9 effectively removes the influence of horizontal grid size on the production of $\overline{e}$. It is therefore seen to give a consistent production of $\overline{e}$ not only in the single column limit but also in the "grey-zone" as we shall present in Section. 4.5.1.

The second and the third tendency terms (horizontal and vertical diffusion of $\overline{e}$, that is $H_{\overline{e}}$ and $V_{\overline{e}}$ in Eq, 4.8) are treated similar to those of the Deardorff TKE described in the last section (H_e and V_e in Eq, 4.6). Finally, contribution from the large scale TKE ($T_{\overline{e}}$) is added as the fourth term in the tendency of $\overline{e}$ using the same procedure as done for the single column (the difference being that in the LES, e is a three-dimensional variable and E is a two-dimensional one defined at each x-y grid point, meaning that e at any height in the column has the contribution from E of that column, from the assumed cascade of kinetic energy from larger to smaller scales).

The Large-scale TKE, i.e. E, in each column, is calculated as described in Chapter 3 from the mean profiles of buoyancy flux and shear in the boundary layer, the depth of which (h) is calculated using the gradient method. The gradient method calculates h as the height at the maximum gradient of the potential temperature is reached (the average value over all the horizontal grid points is taken in UCLA-LES). Details of the gradient method of calculating the boundary layer height has been given in, for instance, Sullivan et al. (1998). Succinctly, boundary layer depth h at any horizontal grid point (x, y) is calculated as:

$$h(x, y) = z, \text{ where } \frac{\partial \Theta(x, y, z)}{\partial z} \text{ is maximum.} \tag{4.10}$$

It should be noted that the gradient formulation can simulate the horizontal heterogeneity of the boundary layer depth. This becomes progressively important as we enter the "grey-zone" from SCM-like grid sizes till the fine-grid limit. It is interesting to note that the other boundary layer depth diagnosis we discussed, the parcel formulation (described in Chapter. 2), does not have a clear extension in the "grey-zone". This is because the parcel method assumes that the parcels of air that merge with the

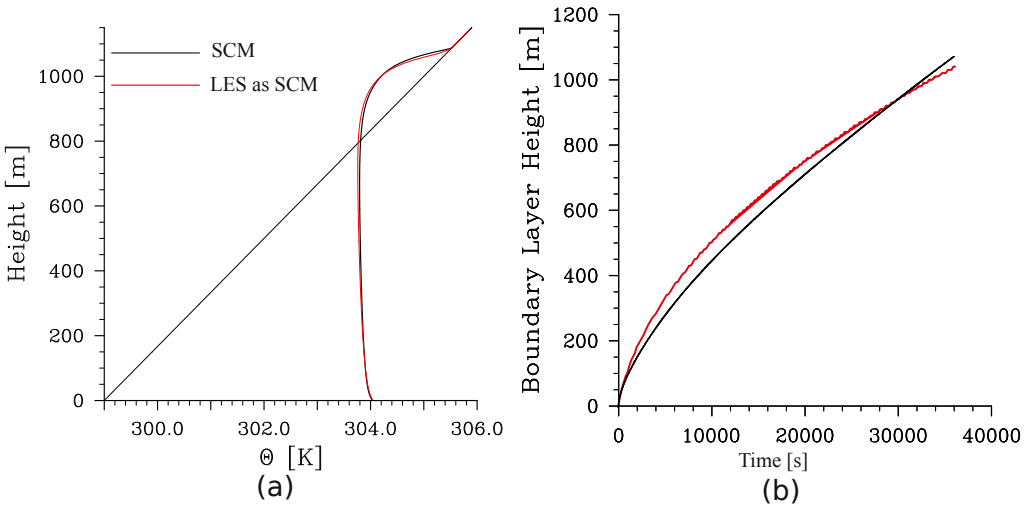

Figure 4.5: (a) Comparison of temperature profiles after 10 hours for case CBL2, in stand alone model and the UCLA-LES with a very large horizontal grid size, both with the 2TKE model as the subgrid model. (b) Growth of the boundary layer for the two models.

soundings to create the boundary layer have a velocity that is related to the surface flux. This relation works for large horizontal grid sizes, i.e when the entirety of the boundary layer processes are subgrid. In the "grey-zone", where the boundary layer is partially-resolved that is part of the parcel vertical-velocity is resolved-scale, this relation is unclear and hence the method is not applicable.

To ensure that the implementation of the 2TKE model in UCLA-LES is correct before looking into blending functions, the implementation is checked by comparing two limiting cases of $\Delta x/h$: in the SCM limit (i.e $\Delta x >> h$), the solution from the UCLA-LES is compared and found to be similar to solution from the 2TKE-implementation in the SCM we developed (in Chapter 3), provided the boundary layer height diagnosis is consistent. This SCM-limit is explored in Section. 4.4.1. In the other limit ($\Delta x < h$), which is the range in which LES is traditionally used, the 2TKE model has been compared with the Deardorff model. This fine-grid limit is inspected in Section. 4.4.2

4.4.1 LES model as a single column model

Under "SCM-like" grid spacing i.e $\Delta x = \Delta y = 100$ km, the 2TKE implementation is compared to the 2TKE implementation in the SCM which is described in Chapter 2, for

case CBL2, which is a pure CBL case with no shear. After 10 hours of simulation time, the temperature profiles and the boundary layer height diagnosed by the two models are compared, as shown in Fig. 4.5 (a) and (b) respectively, and found to be in reasonable agreement, barring minor differences which we attribute to differences in the numerical implementation. This gives us reasonable confidence that the implementation of the 2TKE model in the UCLA-LES has been performed correctly.

4.4.2 LES model with fine grid

In this limit, the solution of our 2TKE model is compared to the solution when the Smagorinsky and the Deardorff models are used for case CBL2 after 3 hours of simulation (statistics computed over 10 minute intervals). For the 2TKE model, E is resolved (hence, 0) at the fine grids and hence this condition is imposed. A more physical way of achieving this property (as well as getting E in the "grey-zone") is described in Section. 4.5.1. The comparison, Fig. 4.6(a) and (b), shows that the temperature and the subgrid flux profiles are, to a reassuring degree similar, the only difference being the subgrid TKE calculated (seen in Fig. 4.6(c)). This difference is reduced once the mixing length scale of $\overline{e}$ for the 2TKE model (l_{emix})is set the same as the Deardorff length scale (l_{De}) for fine grids (Fig. 4.6(d)). The mean solutions are still similar to each other as before the change of the mixing length, as shown in Fig. 4.6(e) that shows the boundary layer evolution in time. This leads us to the conclusion that for simulations employing the 2TKE model to be consistent with simulations based on the Deardorff subgrid model for fine grids, the major requirement is that the length scale used in mixing by $\overline{e}$ should match the Deardorff length scale at that limit.

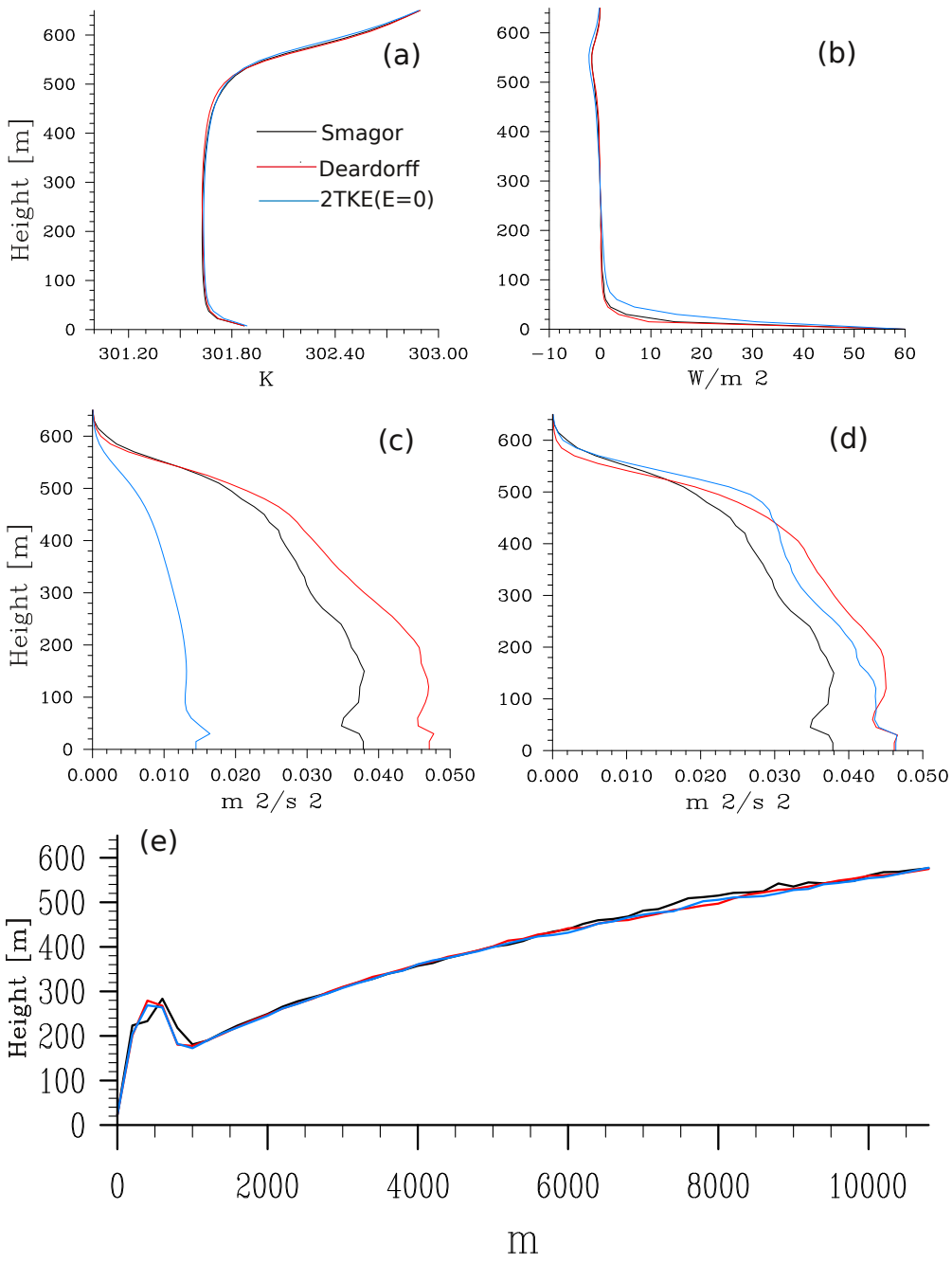

Figure 4.6: Comparison for fine isotropic grid of $\Delta x = \Delta y = \Delta z = 15$ m for Smagorinsky, Deardorff and 2TKE models (in the 2TKE model, E is set to zero) after 3 hours of simulation of (a) the temperature profile, and (b) the subgrid flux profiles. (c) The difference in the profiles can be explained by the different subgrid TKEs these models predict. (d) Upon setting the mixing length of $\overline{e}$ (l_{emix}) to be same as the Deardorff length (l_{De}), this difference is found to be mitigated. (e) The boundary layer depth diagnosed by the three models upon setting l_{emix} to l_{De} at fine grids.

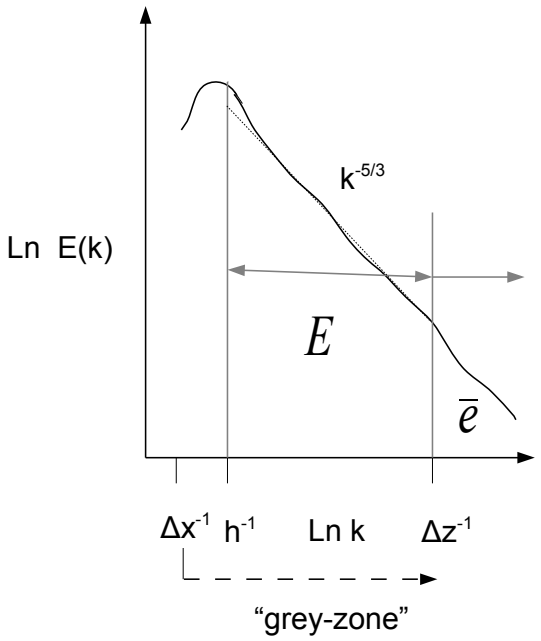

Figure 4.7: The theoretical spectrum of the Turbulence Kinetic Energy inside the boundary layer. When the horizontal grid size, Δx, of a model is similar in magnitude to h the model is in the "grey-zone".

4.5 Modeling the "Grey-zone"

Having demonstrated that the 2TKE model performs well in the two limits of grid sizes in the last section, the model is employed in the "grey-zone". This is done to explore ways to incorporate the horizontal grid size in its formulations in such a manner that properties of the two TKEs are well utilized and the model can generate boundary layer simulations that are independent of the horizontal grid size.

4.5.1 Blending function

"Grey-zone", as described in Section. 4.1, is the range of grid sizes where Δx is of the same order as h. Four key components of the behavior of the 2TKE model in the "grey-zone" can be identified:

- As the grid size of the setup reduces from the SCM-like sizes to smaller sizes, progressively more of E is resolved. This follows from the fact that with further and further size reduction an ever larger fraction of eddies generated by the

bulk profiles inside the boundary layer are resolved. This means tht only the "remaining" subgrid eddies needs to be modeled by E. Thus, in this intermediate range of grid sizes, the production terms of the evolution equation of E need to be multiplied by a continuous and monotonically decreasing function of the non-dimensional grid size, $\Delta x/h$. This function satisfies the property that all of the production of E (that is, the boundary layer integrated buoyancy and shear, Eq. 3.35 in Chapter 3) acts in SCM-like grid sizes while there is no production of E whatsoever for very fine grids. This function henceforth shall be called the blending function.

- The length scale of mixing by E (that is, l_{Emix}) should be blended accordingly, that is, the mixing length scale should only correspond to eddies that are still subgrid for a given grid size, not to *all* boundary layer eddies as is the case for the 2TKE model in the SCM-like grids. Thus the length scale of mixing by E at a non-dimensional grid size of $\Delta x/h$ is proportional to some power of the ratio of E at $\Delta x/h$ to E at SCM limit.

- The small scale TKE, $\overline{e}$, should be independent of the non-dimensional grid size in the range of grid sizes we explore, i.e from single-column-like grid sizes to grid sizes used typically in the LES (fine grid limit).

- The length scale of mixing by $\overline{e}$ (l_{emix}) should converge to the Deardorff mixing length, l_{De}, at small enough grid sizes. Henceforth this value of the Deardorff length is called $l_{De,fg}$ (Deardorff mixing length at fine grids)

Fig. 4.7, that shows the theoretical energy spectrum for a turbulent atmospheric flow, can be used to better visualize these properties. For example, it can be seen that $\overline{e}$ is the energy subgrid to Δz. Hence it should be independent of Δx. It can also be observed that when Δx is approximately equal to h, i.e. in "grey-zone", part of E is resolved and the remaining is subgrid. Thus, it is this subgrid part along with its length scale that needs to be modeled.

In the remainder of the section we present the choices we make to ensure that the above four characteristics are satisfied. The physical motivation behind the choices and how they guide the behavior of the 2TKE model in the "grey-zone" are expounded upon. The next subsection presents the results from the simulation of a dry CBL case, CBL2, in the "grey-zone" upon making those choices.

The source of E, as described in the last chapter, are the fluxes of momentum and buoyancy integrated throughout the boundary layer. In the LES, E is defined

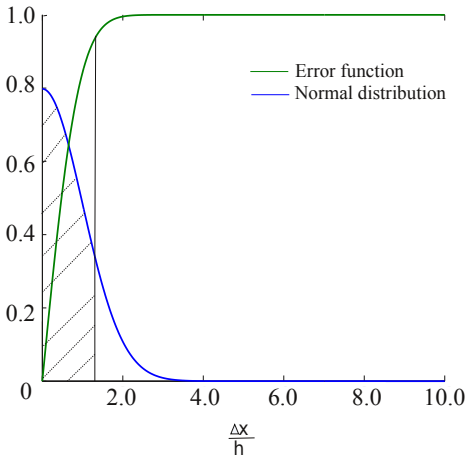

Figure 4.8: Double of the standard normal distribution that is used for the spectrum of the source terms of E. The integral from zero till a particular value (shaded by the dotted line) divided by the total area, which is 1, is the error function.

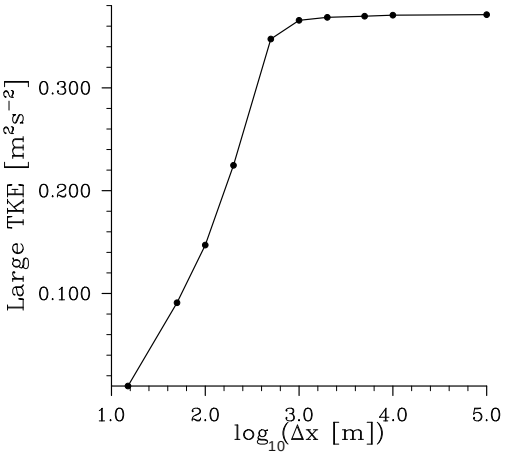

Figure 4.9: Large TKE, E, as a function of the logarithm of the horizontal grid size, Δx.

at each horizontal grid point and assumed to be a well-mixed quantity within the boundary layer (this assumption may come into question in the "grey-zone"). To get a continuous and monotonic function (of the horizontal grid size non-dimensionalized by h) for these source terms, we theorize that the fluxes are normally distributed as a function of scale (defined only for positive values of $\Delta x/h$ and the area under the curve from 0 to infinity integrates to 1). This has a dual advantage of assuming that, on the one hand the eddies are the result of stationary random process, and on the other hand in the spectral space (the Fourier transform of the normal distribution is also a normal distribution), the energy spectrum has a normal distribution which can approximately accommodate the $-5/3^{rd}$ law (Kolmogorov (1941)) usually assumed in the inertial sub-range of turbulence. This means that for a given non-dimensional grid size of $\Delta x/h$, the source terms can be represented as the source terms for SCM-like grid spacing (that is the full contribution) multiplied by $\mathrm{erf}(\Delta x/h)$, where $\mathrm{erf}(\Delta x/h)$ is the error function. The shape of the distribution and its integral, that is the error function, are shown in Fig. 4.8

$$f(\Delta x/h) = \mathrm{erf}(\Delta x/h) = \frac{2}{\sqrt{\pi}} \int_0^{\Delta x/h} e^{-t^2}\, \mathrm{d}t. \tag{4.11}$$

Thus the evolution equation for E becomes:

$$\begin{aligned}\frac{(hE)^{n+1}-(hE)^n}{\Delta t} &= \frac{0.4g(h^{n+1})\overline{w'\Theta'}_0}{\Theta_0}\, f(\Delta x/h) + (\overline{E'w'}_0 - \overline{E'w'}_h) \\ &+\frac{w_c {u_\tau}^2}{\kappa}\left((ln\lambda - lnz_0) + \frac{\lambda^2 - {z_0}^2}{2h^2} - \frac{2(\lambda - z_0)}{h}\right)\, f(\Delta x/h) \\ &-C_E {E_1}^{3/2}\left(\frac{ln(h^{n+1}) - ln(z_0)}{\kappa} + \frac{h^{n+1}-z_0}{\lambda}\right) + E(h^{n+1})\frac{h^{n+1}-h^n}{\Delta t},\end{aligned} \tag{4.12}$$

which is similar to Eq. 3.35 in Chapter 3 with the function $f(\Delta x/h)$ used to blend both the buoyancy and the shear source terms. $f(\Delta x/h)$ is used to encapsulate the effect of eddies that are still unresolved at a given grid size (but bigger in scale than the vertical grid size) and hence form the source of E. The rest of the eddies, which also contribute to E for very large horizontal grid sizes, have already been resolved in the "grey-zone". Thus $f(\Delta x/h)$ can be thought of as incorporating the fact that instead of averaging (of buoyancy or shear, i.e source terms of E) over a very large (ideally infinite) number of (small-sized) LES grid boxes we are averaging over a smaller number of LES grid boxes that correspond to any given Δx.

In the "grey-zone" a fraction of the boundary layer scale eddies gets resolved. This impacts not just E but also the length scale over which it performs mixing. To blend this length scale (l_{Emix}) we assume that the energy of eddies above a wave number k varies as $k^{-2/3}$ (a direct derivation from the $-5/3^{rd}$ law of inertial sub-range, see Pope (2000) for example). This allows us to blend l_{Emix} with $f^{3/2}$. It would be good to remind the reader that in the 2TKE model for SCM application, l_{Emix} is the boundary layer depth multiplied by a shape function (Eq. 3.36 in Chapter 3 Section. 3.2.2). In a similar fashion the contribution of the large eddies to mixing in the "grey-zone" can be written as:

$$K_E = \sqrt{E} l_{Emix} \frac{z}{h}\left(1 - \frac{z}{h}\right)^n \ , \tag{4.13}$$

which is similar to the equation for K_E used in the 2TKE model in SCM-like grids with the key differences that the E being used is a fraction of the E being used in SCM grids (source term has been blended by f) and the length scale of mixing by E, l_{Emix} is different from the boundary layer depth, h used in the SCM setup:

$$l_{Emix} = h f^{3/2}(\Delta x/h) \ , \tag{4.14}$$

the aforementioned shape function remaining the same. Upon making these choices in the blending of source terms and the mixing length of E, a number of simulations

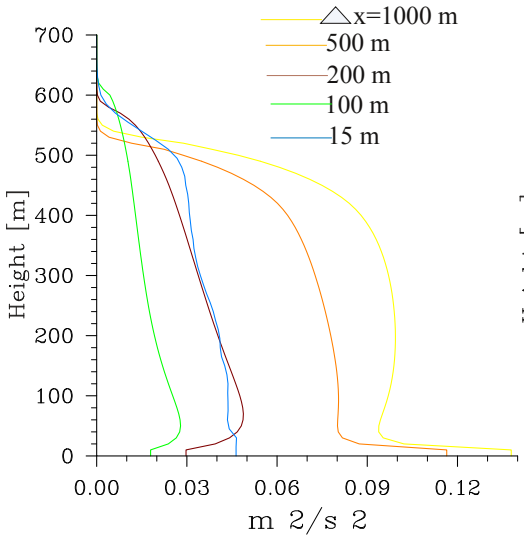

Figure 4.10: Small TKE profiles for different grid sizes.

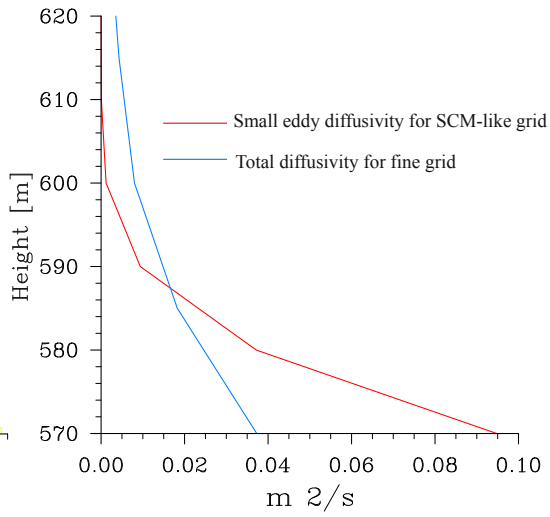

Figure 4.11: The total and the small eddy diffusivity (which are the same) at the top of the boundary layer for SCM-like grid size and the diffusivity for fine grid ($\Delta x = 15\ m$).

are performed using the 2TKE model in the "grey-zone". The detailed analysis of the results is done in Section. 4.5.2. In this section we would like to draw the attention of the reader to the behavior of E in the "grey-zone"(Fig. 4.9). The figure shows the horizontal-domain-averaged value of E after 3 hours of simulation. It can be noted E in the SCM-like grid spacing is similar to E obtained in the stand alone model (Fig. 3.5 in Chapter 3). With decreasing Δx, E reduces monotonically eventually going to 0 at the limit of fine grid.

The next constraint the 2TKE model should satisfy is the similarity of $\overline{e}$ irrespective of the horizontal grid size. We note that the production of $\overline{e}$ has two contributions: one from the resolved scales ($P_{\overline{e}}$ in Eq. 4.8) and the other via cascade from E ($T_{\overline{e}}$).

If we look into the nature of these two contributions to $\overline{e}$ we realize that in "grey-zone", with decreasing Δx, the contribution of the resolved scales to $\overline{e}$ increases. This can be inferred from the fact that since with finer grids more of the velocity is resolved, presumably the square of its differences across the vertical grid increases too, while the length scale of production, as shown in Eq. 4.9, remains constant since it depends on Δz, h and z. This means that decreasing Δx leads to increasing production by the resolved scales (that is, increasing $P_{\overline{e}}$ in Eq. 4.8). On the other hand, the contribution

of E to $\overline{e}$ via energy cascade reduces as more of E is resolved with decreasing grid size. The sum of these two should, in theory, be constant irrespective of Δx (also see Fig. 4.7).

This constraint can not be exactly satisfied by the 2TKE model, as shown in Fig. 4.10. The figure shows that for coarser grids $\overline{e}$ increases although the increase is certainly not drastic given the range of grid sizes we consider. This increase is due to the fact that, for example, in the SCM-like grids, though the contribution of resolved scales to $\overline{e}$ is less (compared to the contribution of the resolved scales in fine grids), the cascade from E is more than compensating. The same is the case for any coarser grid having higher value of $\overline{e}$ compared to finer grids (contribution from E is more than compensating). Changing the length scale of dissipation from E to $\overline{e}$ does not rectify this since the smaller fraction of E being transported is compensated by the larger value of E itself (since its dissipation has reduced) and hence the contribution from E to $\overline{e}$ remains similar in magnitude.

However the differences in $\overline{e}$ across grid sizes is not significant especially when the diffusivity contribution of $\overline{e}$ is considered. It is noted that K_e is significant, compared to either K_E (for coarse grids) or resolved mixing (for fine grids) only at the interfaces (surface layer and the entrainment zone). Only at the entrainment zone, does it contribution surpass that of both the K_E and the resolved scales for any grid size. Thus we compare K_e at the entrainment zone for the two limits of grid sizes, the very large and the very small (Fig. 4.11). Note that for the SCM-like grid size, at the top of the boundary layer K_e and $K_e + K_e$ are the same (the black and the red lines). The figure shows that this contribution is similar irrespective of the grid size. Therefore we conclude that the lack of exact similarity in $\overline{e}$ profiles does not affect the solution from the 2TKE model in the "grey-zone". This is also shown in Section. 4.5.2.

Fig. 4.10 and Fig. 4.6(d) also show that for fine grids $\overline{e}$ approaches Deardorff TKE which means that setting the length scale of mixing by $\overline{e}$ in fine grid to the same value as the mixing length scale of Deardorff TKE makes the diffusivities and hence the solutions to converge to the Deardorff solution. The method adopted for setting the length scale of mixing by $\overline{e}$ is a simple maximum function, i.e:

$$l_{\text{emix}} = MAX(l_{\text{emix}}, l_{De,fg}) \ . \tag{4.15}$$

This states that the mixing length of $\overline{e}$ is calculated by the usual method (that is by Eq. 3.32 in Chapter 3)as long as it is greater than the value of the Deardorff mixing length scale for fine grids, beyond which this Deardorff length is taken as the mixing length.

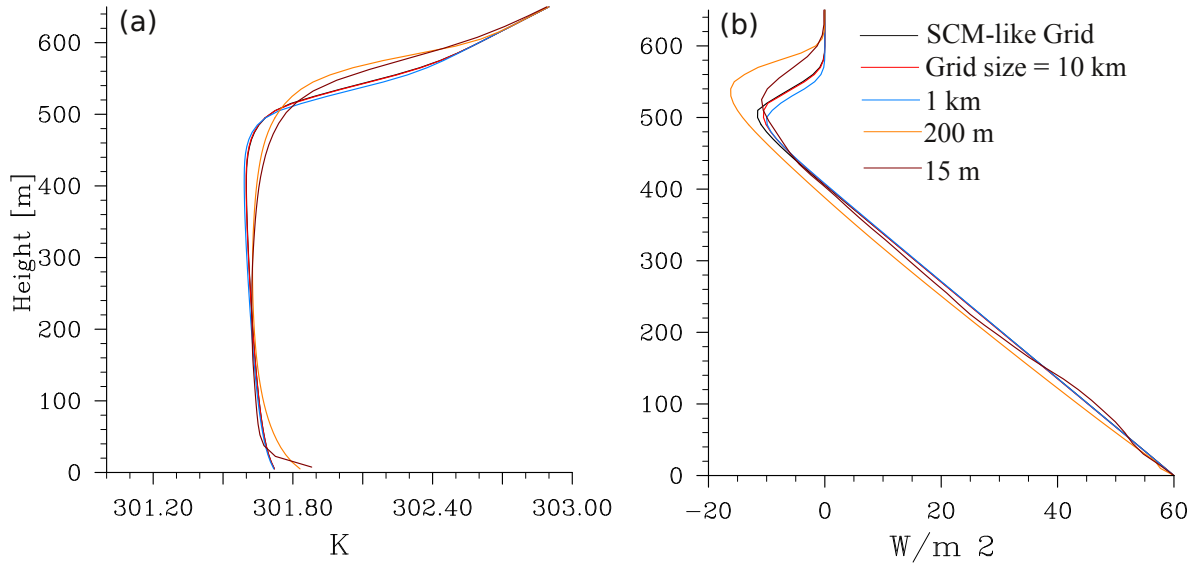

Figure 4.12: Behavior of the 2TKE model in the “grey-zone” for (a) potential temperature, and (b) total potential temperature flux.

4.5.2 Results

Having made the choices of blending functions in the last sections, in this section the major properties of simulations using the complete 2TKE model in the “grey-zone” are presented. Dry convective boundary layer Case2 is studied. Consistency of the mean properties of the boundary layer, such as the potential temperature and the total heat flux, across grid sizes is studied at first. Next, the mixing influence of the 2TKE model vis a vis that of the resolved flow, a property which varies across grid sizes, is looked into. Consistency in the energetics and similarity of the resolved flow irrespective of the grid size is what we would like to achieve. These properties are verified in the third part of this section. Finally the model is compared to the Deardorff model to bring out its scale-adaptive advantages compared to the Deardorff model (which has, as we shall argue, already a degree of scale adaptivity).

Fig. 4.12 elucidates on the mean behavior of the boundary layer simulations across grid sizes. Part (a) shows the temperature profile after 3 hours of simulation time (statistics computed over 10 minute time interval). It is observed that the mean temperature profiles are invariant with respect to the horizontal grid spacing which indicative of convergence. This is especially true considering the fact that with the

Deardorff TKE model Sullivan and Patton (2011) show that the solutions for slightly sheared DCBL have a bigger grid sensitivity. The range of grid sizes they consider is within $\Delta x = \Delta y = \Delta z = 5$ m limit on the one hand and $\Delta x = \Delta y = 160$ m and $\Delta z = 64$ m limit on the other, a range for horizontal grid sizes that is much narrower than the range we consider. Note that while for our simulations the vertical grid size was kept constant, Sullivan and Patton (2011) consider grids that are larger in all three directions. However we consider, as the authors of the paper do, that the vertical grid size for their coarse grid simulation still resolves the vertical structure of the entrainment zone at least in such a manner that its impact on the grid dependence of the solutions is not too large. This point is also made by Tong et al. (1998) who say that within a certain limit of Δz, the impact of 2-D isotropic filtering in the horizontal is similar to 3-D isotropic filtering. In the UCLA-LES too, we compare the 2TKE model to the Deardorff model which is discussed later in this section. Fig.Fig. 4.12(b) shows the corresponding flux profiles. The flux profiles have a shape that matches our expectation for a dry convective boundary layer (see for example Garratt (1992)): that is linear from the surface to approximately -0.2 of the surface flux at the height of minimum buoyancy and then back to neutral buoyancy above that height. The slight grid dependence of the profile is for grids in between 15 m and 200 m , something which can be explained by the behavior of the Deardorff model in that range (Sullivan and Patton (2011)). And as the grid gets coarser the behavior matches more that of the fine grid solution and remains reasonably consistent there (grid sizes of 1 km, 10 km and SCM-like).

Next we focus our attention to the behavior of the 2TKE model itself in the "grey-zone" (that is, the behavior of subgrid scales as the grid gets coarser from fine-grid onwards). Simulation with grid size of 100 m is added to our list of grid sizes to further explore this behavior. Fig. 4.13(a) shows the subgrid flux profiles. It can be noted that while for SCM-like grid sizes till about 1 km grid size, the majority of the heat flux is subgrid, when the grid size is 200 m or 100 m much of the flux is in the resolved scales (more so for 100 m). Note that the boundary layer depth is approximately 600 m for these simulations. Thus our results well corroborate the fact that we enter the "grey-zone" only when the horizontal grid size is of the order of a fraction of 600 m. Finally for fine resolution of 15 m, most of flux is resolved and the subgrid fluxes contribute only near the surface and the entrainment zone. To further understand the behavior of the 2TKE subgrid model we explore the subgrid diffusivity profiles that is computed by the model (Fig. 4.13(b)). From the figure it can be seen that with increasing resolution the subgrid diffusivity reduces and progressively more of the mixing is being carried out by the resolved scales, except at the very top of the boundary layer where the

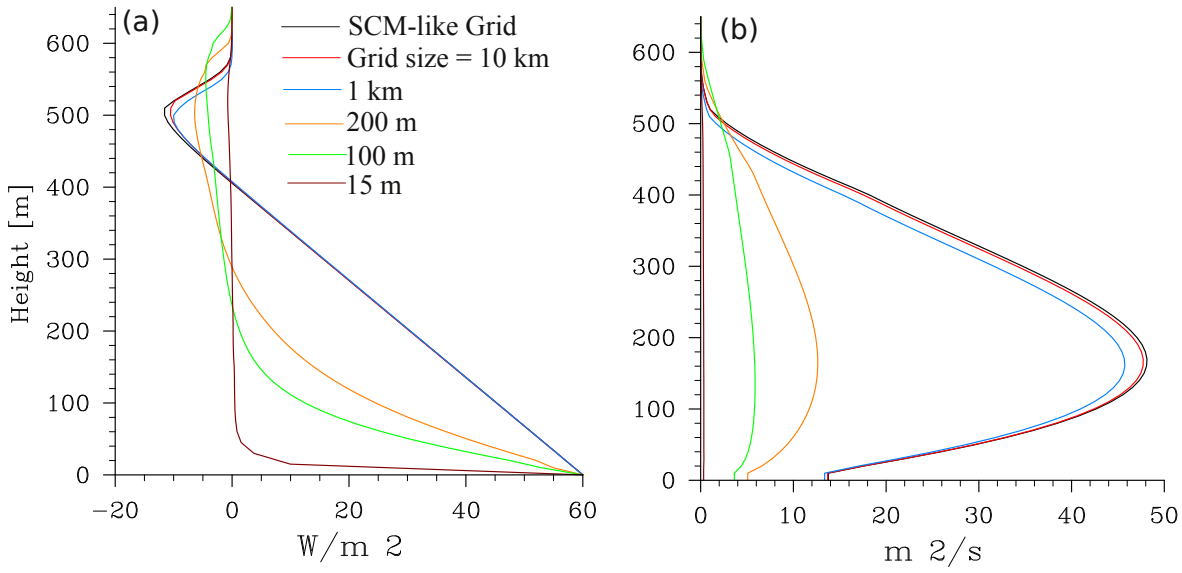

Figure 4.13: Behavior of the 2TKE model in the "grey-zone" for (a) subgrid potential temperature flux, and (b) subgrid eddy diffusivity.

subgrid scales may contribute even more in fine grid simulations than in coarse grid ones.

One of the main attributes of LES is the ability to accurately compute turbulence especially for fine enough grids. This allows us to study the behavior of the 2TKE model using the higher moments of resolved turbulent fields. Two major constraints the model needs to satisfy are: consistent energetics irrespective of grid sizes and convergent behavior of resolved scales of the simulated flow. These mean that the flow being simulated are similar, only the details of features to which they are resolved are different depending on the grid sizes.

Consistent energetics imply that the sum of E and the resolved TKE is the same irrespective of the grid size. Fig. 4.14, for example, shows the resolved variances, i.e for example in the vertical: the LES resolved portion of $\overline{W'W'}$ (notations described in Chapter 3), as the grid gets coarser. It can be observed that the resolved variances reduces as the LES grid gets coarser, which means that more of the eddies get subgrid and the difference between the computed fluid field and the domain averaged fluid field (equivalent to the Reynolds averaged fluid field) gets smaller. This also allows us to compute the sum of the resolved kinetic energy and the large TKE, E, and it can be seen that the sum is almost a constant over grid sizes, which means that as the grid

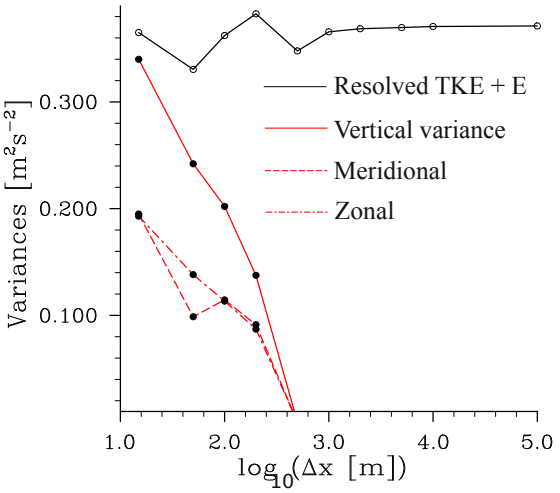

Figure 4.14: Resolved vertical, zonal and meridional variances as a function of the horizontal grid size. Also the resolved TKE added to large scale energy, E.

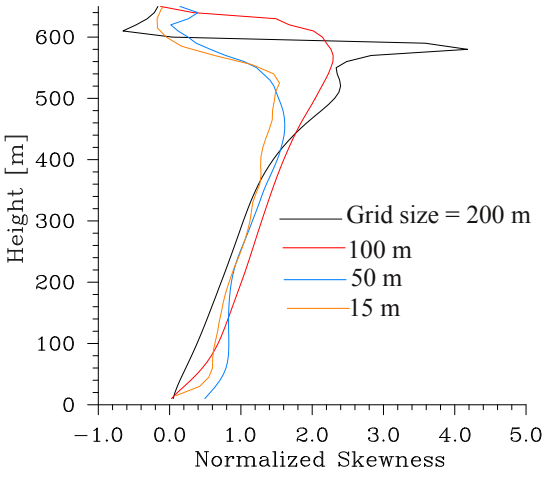

Figure 4.15: The resolved vertical skewness normalized by the 3/2 power of the vertical variance for grid sizes less than 200 m, i.e well within the "grey-zone".

gets coarser, E provides a reasonable approximation for the subgrid variances which are resolved in finer grids (and unresolved in coarser ones).

Convergent behavior of the resolved scales imply convergent boundary layer dynamics irrespective of the grid size. One way to study the resolved scales is to study the normalized resolved skewness of the vertical velocity. This is the resolved skewness divided by the 3/2 power of the resolved variance (that is LES resolved portion of $\overline{W'W'W'}$ divided by the 3/2 power of LES resolved portion of $\overline{W'W'}$). Fig. 4.15 shows this normalized resolved skewness of the vertical velocity for a range of Δx less than 200 m, i.e in the range where a substantial portion of the turbulent flow has been resolved. It can be observed that the resolved flows for fine enough grid sizes in the "grey-zone" are indeed similar to each other (if compared to results using the Deardorff subgrid model in Sullivan and Patton (2011)) except at the entrainment zone. In the entrainment zone the resolved moments are in any case low since the subgrid scales continue to play an important role there, as shown in Fig.4.13(a) for example. Thus the convergence of the resolved fields in the surface and mixed layer is definitive enough to point to the self-similar behavior of the 2TKE model in the "grey-zone".

Once the behavior of the 2TKE model in the "grey-zone" is understood, the model is compared with the Deardorff model in this range. This brings out the advantages

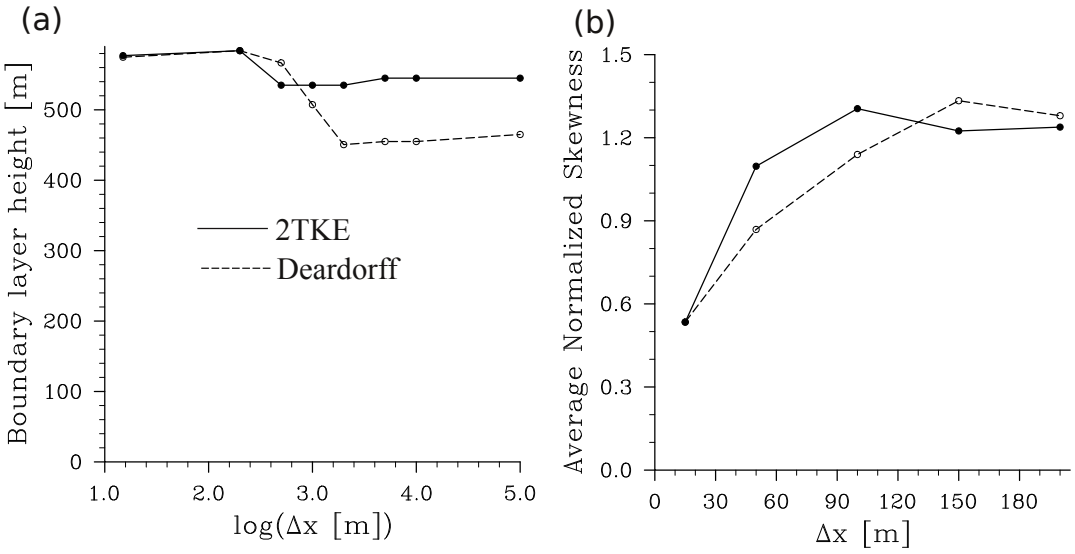

Figure 4.16: Comparison between the 2TKE model and the Deardorff model in the "grey-zone" for (a) Boundary layer height, (b) average normalized resolved skewness

of the 2TKE model compared to the current LES models in the "grey-zone". Two metrics are used to judge the relative merits of the two models (Sullivan and Patton (2011) provides justification for these two metrics as tools to study grid convergence): the predicted boundary layer depth and the normalized resolved skewness (discussed in last paragraph) averaged over the boundary layer depth. The boundary layer depth as diagnosed from the 2TKE model and from the Deardorff model after 3 hours of simulation time is compared in Fig. 4.16(a). It can be clearly observed that for the 2TKE model, the depth diagnosis is far less dependent on the horizontal grid size which gives us confidence in the 2TKE model. Finally the averaged resolved normalized skewness from the two models after 3 hours of simulation time is shown in Fig. 4.16(b). This shows two things: one, at the very fine grid the two subgrid models produce similar resolved scale dynamics (meaning the 2TKE model converges to the Deardorff model, which was a design consideration for the model) and two, beyond the very fine grid the dynamics are more similar to each other for the 2TKE model than for the Deardorff model. Thus it can be concluded that compared to the Deardorff model a better representation in the "grey-zone", at least for simple dry convective boundary layers, can be achieved by the 2TKE model.

The 2TKE model has been designed to provide a more scale adaptive representa-

tion of the planetary boundary layer compared to the current large scale models. As described in Section. 4.3.2, the Deardorff model, like the TKE model used in large scale modeling, solves for a TKE budget equation inside a grid box. Unlike the TKE model however, the Deardorff model uses a length scale (of mixing as well as production and dissipation of subgrid TKE) proportional to the grid sizes. This means decreasing horizontal grid size leads to reduced subgrid mixing compared to SCM-like setups, which indicates a degree of scale awareness (see also Beare (2014) which finds the same even for LES, with the much simpler in turbulence physics, Smagorinsky subgrid model). This scale awareness is lacking in any large scale boundary layer model (whether *local* or *non-local*) as was discussed in Chapter 1. Therefore since the 2TKE model performs better than even the Deardorff model in grid-convergence properties we could definitively state that it should behave better than the boundary layer models currently used in weather/climate modeling which use no explicit information of horizontal grid size in their formulation.

4.6 Conclusion

In the last chapter, we derived the 2TKE model from the LES set of equations with a Deardorff subgrid TKE keeping in mind that in theory the 2TKE model should converge to the LES model in the fine grid limit ($\Delta x \approx \Delta z < h$, at least for the CBL). We tested the model, however, only in the limit of $\Delta x >> h > \Delta z$, i.e in the single-column limit in our stand alone model. This Chapter presents the implementation of the 2TKE model in a large-eddy simulation model, the UCLA-LES, to explore its properties in the "grey-zone".

The first order of business was to explore the current LES subgrid models. The UCLA-LES uses the Smagorinsky subgrid turbulence model, that assumes a production-dissipation balance of the subgrid-turbulence-kinetic energy. This allows the usage of a truncated subgrid TKE equation to parameterize the influence of the subgrid turbulence on the resolved scales. Since the 2TKE model ideally converges to the full subgrid-TKE model (called the Deardorff TKE model) that solves prognostically for the turbulence kinetic energy inside each grid box in the limit of fine enough grids, implementation of the Deardorff model was done first in the UCLA-LES. This paved our path in two ways: first, in gaining an understanding of the limit of solutions the 2TKE model should approach in fine grids, and second, in the implementation process of the 2TKE model itself.

The small scale energy, $\overline{e}$, in the 2TKE implementation, is calculated similar to

the Deardorff TKE with modified production terms and a source from the large scale energy, E. E, on the other hand, is calculated using the bulk properties of the boundary layer, the depth, h, of which is determined using the gradient method. Having implemented the 2TKE model, it is tested in two limits of grid sizes. In the single column limit, it is compared with the 2TKE implementation in the stand alone model we developed in the last chapter and in the fine grid limit, it is compared with the Deardorff model. In both these limits, the solutions are similar to the benchmark solutions provided that in the small-scale limit the length scale of mixing by $\overline{e}$ converges to the Deardorff mixing length. The comparisons bring out the four constraints the 2TKE model is required to satisfy in the "grey-zone": one each for E, l_{Emix}, $\overline{e}$ and l_{emix} (at fine enough grid sizes). The first is to find a continuous and monotonic blending of the source terms in the evolution equation for E in the "grey-zone". This is done by assuming that the source of "large" eddies in the convective boundary layer (that is those that contribute to E) have an approximate normal distribution in the physical (as well as spectral) space. The length scale of mixing by E is blended according to the blending of E keeping in mind the $-5/3^{rd}$ law in the inertial subrange (the second constraint). $\overline{e}$ does not exactly satisfy the third constraint in that it is not completely independent of the horizontal grid size. However at the top of the boundary layer, where it is the most active compared to the other components of mixing, its values are similar irrespective of the underlying grid. And finally as mentioned above, at the limit of very fine grids, the mixing length of $\overline{e}$ is taken to be the Deardorff mixing length at those grids instead of the original formulation.

Having made these choices of blending in the "grey-zone", the solutions for convective boundary layer case CBL2 are compared for different grid sizes spanning the "grey-zone" and are found to be reasonably convergent. Similar growths of the boundary layer depth, consistent energetics and similar behavior of the higher moments of the resolved flow across grid sizes elucidate the point. Better behavior compared to the Deardorff model (that already uses knowledge of the horizontal grid size in its length scale formulation) suggests that the model should outperform the current large scale boundary layer models that use no information of the horizontal grid size upon which they are acting. Thus, in this chapter, we use a fine scale modeling framework and physically motivated reasoning to guide the development of the 2TKE model such that we can finally model the "grey-zone".

Chapter 5

Conclusion

In this thesis, I present a newly developed two Turbulence Kinetic Energy (2TKE) model that can be used to model the planetary boundary layer (PBL) in the "grey-zone" of numerical weather prediction/climate model grids. For the development of this model I went through six steps as mentioned in the Introduction to the thesis. In the summary section of this Chapter I present a succinct account of what I have learned in each of these steps and how they have contributed to the development of the 2TKE model. Since the first step involved developing the single column setup upon which I then implemented the TKE, the KPP and the 2TKE models, I present the knowledge gained from the first two steps together. I end with an outlook section where I talk about the future scope for the development of the model.

5.1 Summary

- **Implementing the *local* TKE (ECHAM) boundary layer model in the single column setup and exploring its physical and numerical properties as well as comparing it with the *non-local* K profile parameterization)**.

  Using the single column model, I find that the TKE (ECHAM) does not model the convective boundary layer (meaning mean potential temperature profile, the flux profile and the boundary layer depth) satisfactorily especially for a case with prescribed surface flux (a case for which we have the most theoretical knowledge). This misrepresentation is somewhat alleviated for a prescribed surface temperature (the surface flux is computed using surface layer similarity assumptions) and other more realistic boundary conditions. In comparison, the K-Profile Parameterization represents the convective boundary layer much more in accordance

with the theory. However, it shows a high dependence on the vertical grid size of the single column model, an issue that does not hinder the performance of the TKE(ECHAM) model very much. In the stable boundary layer, the TKE model performs reasonably well as compared to its performance in convective boundary layer, the reason being that the stable boundary layer dynamics is dominated by the local balance of shear production and buoyant suppression of turbulence, a mechanism that is well represented by the local TKE. The study shows that the new 2TKE model, along with dealing with the "grey-zone" problem, should also have the desirable properties of being independent of the vertical grid of the host model as well as being applicable for different regimes of atmospheric boundary layers found in nature (convective as well as stable).

- **Deriving the 2TKE model which is a set of PBL equations starting with the LES set of equations, applying the Reynolds averaging on it and then modeling the subgrid fluxes.**

  I develop the 2TKE model based on the idea that the boundary layer processes can be better represented if we consider two rather than a single scale (which is the case for current models, i.e the vertical grid size for *local* models and the boundary layer depth for the *non-local* models) of mixing explicitly within the boundary layer. The model is such that it is applicable both in the range of grid sizes of the current weather prediction/climate models (which is approximated by our single column model) as well as in the opposite extreme of very fine grid sizes of the LES model so that I can tune it with physical motivations to be applicable within the "grey-zone". Hence I derive a new set of boundary layer equations starting from the LES set of equations and apply the Reynolds filter, that is used to derive the usual large scale PBL equations, upon the LES equations. This new set of boundary layer equations include the equation for two distinct TKEs: one acting over the range from the boundary layer depth to the vertical grid size (the large TKE) and the other representing all eddies that are subgrid to the vertical grid size (the small TKE). Thus, these two TKEs represent the eddies that act in the two ranges of scales within the boundary layer. This implies that the large TKE acts predominantly when the boundary layer model is employed in a grid with very large horizontal grid spacing and this contribution to subgrid mixing progressively reduces as the grid size reduces in the "grey-zone". The small TKE, on the other hand, contributes similarly to mixing irrespective of the horizontal grid size. Moreover, these two TKEs are energetically linked via the turbulence cascade. This means that the large TKE, that is calculated using the bulk properties of the boundary layer (assumed to be a well mixed quantity),

dissipates into the small TKE . And the small TKE, that is calculated using the local variables defined in each grid box and the cascade from large TKE, dissipates into molecular viscosity i.e heat.

Upon derivation of the model set of equations, we need to provide closure for the unresolved terms. The two TKEs are used to parameterize the unresolved fluxes (which have, like the TKEs, two ranges of scales over which they mix) such that the large TKE acts upon a mixing length scale proportional to the boundary layer depth and the small TKE acts upon a length scale proportional to the vertical grid size and the depth of the entrainment zone. The dissipation length scales of these two energies are related in such a manner that consistent energetics can be maintained irrespective of the vertical grid size of the single column. If these equations are reverted back to the LES limit, it is noticed that they converge to the original set of LES equations I started from, modulo the horizontal fluxes which I neglected due to the boundary layer approximation. This concludes the derivation of the theoretical framework, which can then be applied to a single column (to bring out its properties) as well as be applied to an LES model to explore and modify the 2TKE model to model the "grey-zone" (which is done in Chapter 4).

- **Implementing the 2TKE model in the single column setup, comparing it with the TKE (ECHAM) model and the KPP and exploring its unique properties.**

  Upon derivation, I implement the 2TKE model into my stand alone setup and I demonstrate that the model can simulate both the convective and the stable boundary layer efficiently. In the convective boundary layers, the large TKE plays a predominant role throughout the boundary layer with the small TKE acting substantially only at the interfaces, i.e at the surface and the top of the boundary layer. In the stable boundary layers, the role of the small TKE is much more substantial throughout the boundary layer. Usage of the small TKE to model the entrainment zone fluxes is seen to help represent the boundary layer with physical realism irrespective of the vertical grid size (this was something lacking in both the TKE(ECHAM) model as well as the KPP). This favorable property of the 2TKE model has been observed in the diagnosed boundary layer depth, the temperature and the flux profiles as well as the sum of the large and the small TKEs across a wide range of vertical grid spacings.

- **Implementing the 2TKE model in the UCLA-LES (an LES model), and benchmarking the implementation by studying its properties in**

two limits: very large and very small horizontal grid sizes.

Having developed and tested the 2TKE model in a single column, I explore its applicability in the "grey-zone" by first implementing it in the UCLA-LES. The UCLA-LES is a three-dimensional fine scale model solving the anelastic set of fluid dynamical equations for a conserved buoyancy variable (which is the potential temperature for dry cases), momentum, scalars and pressure. The default subgrid turbulence model in the UCLA-LES is the Smagorinsky model that, assuming a production-dissipation balance of local subgrid turbulence kinetic energy, relates the fluxes (which are treated as tensors in fine scale modeling) to the local gradients using local shear and local buoyancy at each grid box. Since my model is developed keeping in mind that it converges to an LES model with a prognostic computation of subgrid TKE, I first implement the Deardorff TKE model in the UCLA-LES and explore the controls of its behavior vis a vis the benchmarked Smagorinsky model. This creates the groundwork for the implementation of the 2TKE model in the UCLA-LES which is done next. The small TKE of our 2TKE model is prognostically calculated similar to the Deardorff TKE with modified production term (to exclude information of the horizontal grid size and keep the source strictly dependent on the vertical grid size and the distance from the surface of a grid box) and the additional contribution from the large TKE. The large TKE is calculated, as for the single column case, using the bulk properties of the boundary layer. Upon implementation, the 2TKE model is checked in two opposite limits of horizontal grid sizes: in the large grid size limit with the 2TKE implementation in the single column and in the fine grid limit with Deardorff model solutions in the UCLA-LES. In the large grid size limit, the 2TKE model performs similarly for the UCLA-LES and the stand alone model provided the boundary layer height specification schemes are consistent in both setups. This is evidenced from the similar potential temperature profiles after a given simulation time as well as the evolution of the boundary layer depth with time. In the fine gird limit, the 2TKE model behaves similar to the Deardorff model with the large TKE being completely resolved, and hence nonexistent, and the small TKE, which is similar to the Deardorff TKE, working at the mixing length scale of the Deardorff model. Getting these two limits right, I then explore the "grey-zone".

- **Exploring the "grey-zone" with the 2TKE model by making physically motivated assumptions about the large and the small energies in the "grey-zone" thus getting a model that provides convergent results irrespective of the grid size.**

Now that I have my framework to approach the "grey-zone", i.e my 2TKE model, in the UCLA-LES I approach the "grey-zone" by making physically motivated assumptions on the two scales of TKEs in my model. I realize that in the "grey-zone", the model should satisfy four constraints. Firstly, the source terms contributing to the large TKE should reduce as the horizontal grid gets finer meaning the large TKE is getting progressively resolved. Secondly, the length scale of mixing by large TKE for a given grid size should depend on the amount of large TKE that is still unresolved at that grid size (that is, the length scale should take into account only those eddies that are unresolved at a given grid size, not the entirety of boundary layer scale eddies). Thirdly, the small TKE should be independent of the grid size. And finally at very fine grid sizes, the length scale of mixing by the small TKE should be the Deardorff mixing length at those grid sizes.

To satisfy the first constraint, I multiply the source terms for large TKE by a continuous and monotonic function (bounded by 0 and 1) of the non-dimensionalized horizontal grid size (the function is called the blending function). The formulation of the blending function assumes that the integrated (throughout the boundary layer) buoyancy and shear fluxes have a normal distribution in physical and hence, spectral space. This implies that the source terms (for large TKE) for a given horizontal grid size is a fraction of the source term in the limit of very large grid size, a fraction given by the error function. Thus for very large grid sizes the fraction is one and for very fine grids, akin to usual range of applicability of LES the fraction is zero. The length scale of mixing is blended with the power 3/2 of this fraction (or, function). This assumes that the subgrid TKE, at least in the range where the blending function is really important (i.e for grid sizes less than or of the order of the boundary layer depth), follows the $-5/3$ law of the inertial subrange of turbulence. Upon these blendings, it is found that the subgrid small TKE is reasonably independent of the grid size inside the "grey-zone" especially at the top of the boundary layer where its contribution vis a vis the other contributions (large TKE or the resolved mixing) is the most predominant. For grid sizes below a certain size, where the Deardorff model can be assumed to work well, the mixing length of small TKE, which essentially becomes the Deardorff TKE, is set to the Deardorff length.

I then use this complete 2TKE model with the blending to simulate the convective boundary layer for a range of horizontal grid sizes and I find a much more convergent behavior (compared to the Deardorff model) over the very large range of grid sizes I explore. This can be evidenced by the similar boundary layer growth rates, and the similar behavior of the resolved scales in the "grey-zone".

Consistent energetics is found to be maintained too, i.e the sum of the large TKE and the resolved kinetic energy is independent of the horizontal grid size. This favorable behavior of the 2TKE model compared to the Deardorff model (that already uses the horizontal grid size, in the right or scale-adaptive way, in its formulation) allows us to conclude that the 2TKE model definitely treats the boundary layer with much more credibility than the operational large scale models (none of these models are formulated keeping the horizontal grid size in mind) in the "grey-zone".

5.2 Outlook

The aim of scale-adaptive boundary-layer parameterizations is to represent the planetary boundary layer consistently, irrespective of the grid size of the numerical weather prediction/climate model which it is a part of. In this thesis, I take the crucial step of developing an idea which can be used to achieve that objective. However, further work needs to be done to fully realize the goal. I think the way forward requires a two pronged approach.

First, one should validate the scope and limitations of the physical assumptions I made to develop the model in conditions other than the one I studied most thoroughly and about which we have the most theoretical knowledge: a dry convective boundary layer with constant surface flux. For realistic boundary layers with diurnal cycle, moisture and the presence of clouds atop, observations and Direct Numerical Simulations can provide information about the various length scales and blendings we used, that is, about their applicability and behavior in different regimes.

The second approach is to implement this model in a weather prediction model/GCM and investigate how it performs operationally. This is far from trivial because the boundary layer model interacts with many other parameterizations in a GCM which can have varied effects upon its performance. Also the range of vertical grid sizes used operationally in GCMs can hardly, if at all, resolve the boundary layer top, i.e the entrainment zone. My model resolves much of this issue in the single column but this might be an interesting problem in an operational GCM in the "grey-zone". Keeping in mind all the limitations of the model, I still believe that the development of such simple models for idealized setups that represent the appropriate (to the best of our collective knowledge) physical mechanisms is an important step in the understanding as well as the development of the models of far greater complexity that we use to study nature.

List of Figures

List of Tables

Bibliography

Beare, R. J. (2014). A Length Scale Defining Partially-Resolved Boundary-Layer turbulence Simulations. *Boundary Layer Meteorology*, pages 39–55.

Beljaars, A. and P.Viterbo (1999). Role of the boundary layer in a numerical weather prediction model. In Holtslag, A. and P.G.Duynkerke, editors, *Clear and Cloudy Boundary Layers*. North holland Publishers.

Blackadar, A. K. (1962). The vertical Distribution of wind and turbulent exchange in a neutral atmosphere. *Journal of Geophysical Research*, 67(8):3095–3102.

Bretherton, C. S. and Park, S. (2009). A New Moist Turbulence Parameterization in the Community Atmosphere Model. *Journal of Climate*, 22(12):3422–3448.

Brinkop, S. and Roeckner, E. (1995). Sensitivity of a general circulation model to parameterizations of cloud-turbulence interactions in the atmospheric bpundary layer. *Tellus*, 47A:197–220.

Clark, R., Ferziger, J., and Reynolds, W. (1979). Evaluation of subgrid-scale models using an accurately simulated turbulent flow. *Journal of Fluid Mechanics*, pages 1–16.

Cuxart, J., Holtslag, a. a. M., Beare, R. J., Bazile, E., Beljaars, a., Cheng, a., Conangla, L., Ek, M., Freedman, F., Hamdi, R., Kerstein, a., Kitagawa, H., Lenderink, G., Lewellen, D., Mailhot, J., Mauritsen, T., Perov, V., Schayes, G., Steeneveld, G.-J., Svensson, G., Taylor, P., Weng, W., Wunsch, S., and Xu, K.-M. (2005). Single-Column Model Intercomparison for a Stably Stratified Atmospheric Boundary Layer. *Boundary-Layer Meteorology*, 118(2):273–303.

de Roode, S. R., Duynkerke, P. G., and Jonker, H. J. (2004). Large-Eddy Simulation : How Large is Large Enough ? *Journal of the Atmospheric Sciences*, 61:403–421.

Deardorff, J. (1974). Three-Dimensional Numerical Study of the Height and mean Structure of a heated Planetary Boundary layer. *Boundary-Layer Meteorology*, 7:81–106.

Deardorff, J. (1979). Structure of the Entrainment Zone Capping the Convective Atmospheric Boundary Layer. *Journal of the Atmospheric Sciences*, 36:424–436.

Deardorff, J. W. (1980). An atmospheric boundary layer capped by a deck of stratocumulus clouds is a common occurrence over cool portions of oceans and over land behind many cold fronts . Observationally , however , little is known about the structure of the turbulence in this. *Boundary-Layer Meteorology*, 18:495–527.

Dyer, A. (1974). A Review of Flux-profile Relationships. *Boundary-Layer Meteorology*, 7:363–372.

Ferziger, J. H. and Peric, M. (1996). *Computational Methods for Fluid Dynamics*. Springer.

Finger, J. and Wendling, P. (1990). Turbulence Structure of artctic stratus clouds derived from measurements and calculations. *Journal of the Atmospheric Sciences*, 47(11):1351–1373.

Garratt, J. (1992). *The atmospheric boundary layer*. Cambridge University Press.

Grenier, H. and Bretherton, C. S. (2001). A Moist PBL Parameterization for Large-Scale Models and Its Application to Subtropical Cloud-Topped Marine Boundary Layers. *Monthly Weather Review*, 129:357–377.

Högström, U. (1988). Non-Dimensional Wind And Temperature Profiles in the Atmospheric Surface Layer: A Re-Evaluation. *Boundary-Layer Meteorology*, 42:55–78.

Holtslag, A. and Bolville, B. (1993). Local versus Nonlocal Boundary-Layer Diffusion in a Global Climate Model. *Journal of Climate*, 6:1825–1842.

Honnert, R., Masson, V., and Couvreux, F. (2011). A Diagnostic for Evaluating the Representation of Turbulence in Atmospheric Models at the Kilometric Scale. *Journal of the Atmospheric Sciences*, 68(12):3112–3131.

J.P.Mellado, Stevens, B., and H.Schmidt (2013). Wind shear and buoyancy reversal at the stratocumulus top. *Journal of the Atmospheric Sciences*. in press.

Kolmogorov, A. (1941). The local structure of turbulence in incompressible viscous fluid for very large Reynolds numbers. *Proc. R. Soc. Lond.*, 434:9–13.

Large, W., Mcwilliams, J., and Doney, S. (1994). Oceanic Vertical Mixing : A Review And a Model With a Nonlocal Boundary Layer Parameterization. *Reviews of Geophysics*, 32(94):363–403.

Lock, A., Brown, A., Bush, M., and Martin, G. (2000). A New Boundary Layer Mixing Scheme . Part I : Scheme Description and Single-Column Model Tests. *Monthly Weather Review*, 128(1998):3187–3199.

Louis, J.-F. (1979). A Parametric model of vertical eddy fluxes in the atmosphere. *Boundary-Layer Meteorology*, 17:187–202.

Mason, P. (1989). Large Eddy Simulation of the Convective Atmospheric Boundary layer. *Journal of the Atmospheric Sciences*, 46(11).

Mellor, G. L. and Yamada, T. (1974). A hierarchy of Turbulence Closure Models for Planetary Boundary Layers.pdf. *Journal of the Atmospheric Sciences*, 31:1791–1805.

Mellor, G. L. and Yamada, T. (1982). Developement of turbulence closure model for Geophysical closure problems. *Reviews of Geophysics and Space Physics*, 20(4):851–875.

Moeng, C.-H. (1984). A Large Eddy Simulation Model for the Study of the Planetary Boundary-Layer Turbulence. *Journal of the Atmospheric Sciences*, 41(13).

Pope, S. B. (2000). *Turbulent Flows*. Cambridge University Press.

Roeckner, E. e. (2003). *The atmospheric general circulation model ECHAM5. Part1.*

Rotta, J. (1951). Statistische Theorie nichthomogener Turbulenz. *Zeitschrift für Physik*, 129(6):547–572.

Siebesma, A. P., Soares, P. M. M., and Teixeira, J. a. (2007). A Combined Eddy-Diffusivity Mass-Flux Approach for the Convective Boundary Layer. *Journal of the Atmospheric Sciences*, 64(4):1230–1248.

Smagorinsky, J., Manabe, S., and Holloway, J. (1965). Numerical results froma nine-level genral circulation model of the atmosphere. *Monthly Weather Review*, 93(12):727–768.

Stevens, B. (2000). Quasi-Steady Analysis of a PBL Model with an Eddy-Diffusivity Profile and Nonlocal Fluxes. *Monthly Weather Review*, 128:824–836.

Stevens, B. (2013). Introduction to UCLA-LES. Technical report.

Stevens, B., Moeng, C.-h., and Sullivan, P. P. (1999a). *IUTAM Symposium on Developments in Geophysical turbulence*, chapter Entrainment and Subgrid Length Scales in Large-Eddy Simulations of Atmospheric Boundary-Layer Flows. Springer.

Stevens, B., Moeng, C.-h., and Sullivan, P. P. (1999b). Large Eddy Simulations of Radiatively Driven Convection: Sensitivities to the Representation of Small Scales. *Journal of the Atmospheric Sciences*, 56:3963–3984.

Stull, R. B. (1988). *An Introduction to Boundary layer Meteorology*. Kluwer Academic Publishers.

Sullivan, P. P., Moeng, C.-H., Stevens, B., Lenschow, D. H., and Mayor, S. D. (1998). Structure of the Entrainment Zone Capping the Convective Atmospheric Boundary Layer. *Journal of the Atmospheric Sciences*, 55:3042–3064.

Sullivan, P. P. and Patton, E. G. (2011). The Effect of Mesh Resolution on Convective Boundary Layer Statistics and Structures Generated by Large-Eddy Simulation. *Journal of the Atmospheric Sciences*, 68(10):2395–2415.

Tong, C., Wyngaard, J. C., Khanna, S., and Brasseur, J. G. (1998). Resolvable- and Subgrid-Scale Measurement in the Atmospheric Surface Layer : Technique and Issues. *Journal of the Atmospheric Sciences*, 55:3114–3126.

Troen, I. and Mahrt, L. (1986). A Simple model of the Atmospheric Boundary Layer; Sensitivity to surface evaporation. *Boundary-Layer Meteorology*, 37(l):129–148.

Wyngaard, J. C. (1984). Towards Convective Boundary layer Parameterization: A Scalar Transport Module. *Journal of the Atmospheric Sciences*, 41(12):1959–1969.

Wyngaard, J. C. (1985). Structure of the Planetary Boundary Layer and Implication for its Modeling. *Journal of Climate and Applied Meteorology*, 24:1131–1142.

Wyngaard, J. C. (2004). Toward Numerical Modeling in the Terra Incognita. *Journal of the Atmospheric Sciences*, 61(14):1816–1826.

Zhang, D.-L. and Zheng, W.-Z. (2004). Diurnal Cycles of Surface Winds and Temperatures as Simulated by Five Boundary Layer Parameterizations. *Journal of Applied Meteorology*, 43:157–169.

List of Symbols

(U, V, W) Alternate notation for three components of LES filtered velocity vector field

β Ratio of flux at the top and at the bottom of the boundary layer

Δx Zonal or equivalently horizontal grid size of a model

$\Delta\Theta$ Surface temperature excess

Δz Vertical grid size of any numerical setup

γ Countergradient term

γ_k LES subgrid potential temperature flux in direction x_k

γ_c Growth constant for stable boundary layer

κ Von Kármán constant

Λ Depth of interfacial layer (Chapter.3)

Λ Differential equation set (Chapter.2)

λ Asymptotic mixing length

$\Lambda_{m,h}$ Lengthscale for TKE model

$\mathcal{P}_g$ Combined production term for E

$\mathcal{P}_l$ Combined production term for $\overline{e}$

$\overline{e}$ Reynolds average of LES subgrid TKE

Φ Generic variable

$\phi*$ LES subgrid fluctuation

ϕ_h Solution for grid size of h

τ_{ik} LES subgrid stress

Θ Potential temperature

b Buoyancy production/ destruction of LES subgrid TKE

C_e Flow dependent dissipation constant for LES subgrid TKE

C_s Smagorinsky constant

C_ϕ Surface transfer coefficient

E Large TKE

e LES subgrid TKE, alternatively Deardorff TKE

E_1 Boundary layer average of E

f Coriolis Parameter

G Free tropospheric stability

H Higher order terms

h Bpundary layer height

h Heat

h_e Equilibrium boundary layer height (Stable boundary layer)

i Height level of model

K Diffusivity/Viscosity

K_E Diffusivity by E

K_e Diffusivity of LES TKE/ Also diffusivity by LES TKE

K_h Eddy Diffusivity

K_m Eddy viscosity

L Dissipation length scale for large TKE, i.e E

l Dissipation length scale of LES subgrid TKE

l_{emix} Mixing length scale of $\overline{e}$

L_h Discretized set of equations for grid size of h

$l_{Deardorff,finegrid}$ Deardorff mixing length for fine grids

$l_{Deardorff}$ Mixing length scale for Deardorff TKE

l_{Emix} Mixing length of E in the “grey-zone“

L_{MO} Monin Obukhov length

l_{Smagor} Mixing length scale in Smagorinsky scheme

M Number of model levels

m Exponent of non-dimensional height in K_E

m Momentum

n Time level of model integration

N_2 Buoyancy production/ dissipation of LES subgrid TKE

P_r Eddy Prandtl number

r_e Grid expansion ratio

Ri_{cr} Critical Richardson number

Ri_B Bulk Richardson number

S_2 Shear production of LES subgrid TKE

T_{relax} Relaxation time scale (Stable boundary layer)

T_ij Reynolds subgrid stress

U Zonal Wind

U_i Three components of LES filtered velocity vector field

u_τ Surface friction velocity

V Meridional Wind

V_g Meridional Geostrophic Wind

V_i Wind speed at first model level

w Vertical wind velocity

w_c Convective velocity scale

w_s Surface velocity scale

w_s Surface velocity scale

x_i Three directions in space

z_0 Surface roughness length

${\epsilon_h}^d$ Discretization error for grid size of h

ϕ' Reynolds subgrid fluctuation

τ_h Truncation error for grid size of h

Acknowledgements

First of all I would like to thank Bjorn Stevens for advising me during this journey. I learned a lot from the immense body of knowledge as well as the quick wit of Bjorn. My thanks goes to Cathy Hohenegger for providing compassionate support whenever I needed it. I also appreciate her calm and balanced view on the thesis, something I often lacked because of being too familiar with it. I am grateful to Axel Seifert for always thinking of my project from a different perspective than me and hence giving me valuable ideas on how to make the research broader and with more depth.

I would like to thank all the members of Hans Ertel Research Zentrum group at Max Planck Institute for Meteorology for valuable discussions and help whenever needed. Special thanks are due to Mirjana Sakradzija, Malte Reick, Vera Schemann, Linda Schlemmer and "former" members Thijs Heus and Bart Van Stratum. Support, help and encouragement also came from many other members of the Atmosphere department.

The acknowledgment would be incomplete without thanking the International Max Planck Research School and specifically: Antje Weitz, Cornelia Kampmann and Wiebke Böhem who do a great job at running the school.

I will not thank my family since in my mind it will be like a fruit thanking the fruit tree: they *are* the same process and share the same destiny. And hence it is meaningless to thank or receive thanks from them.

A lot has and can be said about friends or friendship. Truth is, friends often do save you from your own self. I can only mention a few names here but the actual number of people whose, often unbeknownst to their own selves, support I should acknowledge is quite a bit larger. Thanks to Suvarchal Kumar Cheedela for always bringing cheer to the lives of people around you. Thanks are also due to Max Popp, Fabio Cresto Aleina, Davide Zanchettin and Dr. Daniel Goll: four completely divergent personalities whose friendships made life and my stay in Hamburg quite a bit interesting. Thanks Rohit Ghosh and Pawlok Dass for, at the very least, speaking Bengali!

Thanks to Angela Cheska Siongco. Smart, slightly neurotic, and kind to a fault, you make life more beautiful.

Finally thanks to three thinkers I owe a lot to: Swami Vivekananda, Alan Watts and Thich Nhat Hanh. You show through your lives that it *is* possible to live with freedom of thought and action irrespective of the conditions someone is in. That, to me, is quite something to aspire to.

Eidesstattliche Versicherung

Declaration on oath

Hiermit erkläre ich an Eides Statt, dass ich die vorliegende Dissertationsschrift selbst verfasst und keine anderen als die angegebenen Quellen und Hilfsmittel benutzt habe.

I hereby declare, on oath, that I have written the present dissertation by my own and have not used other than the acknowledged resources and aids.

Hamburg, den

Die gesamten Veröffentlichungen in der Publikationsreihe des MPI-M
„Berichte zur Erdsystemforschung“,
„Reports on Earth System Science“,
ISSN 1614-1199

sind über die Internetseiten des Max-Planck-Instituts für Meteorologie erhältlich:

http://www.mpimet.mpg.de/wissenschaft/publikationen.html



ISSN 1614-1199